UNIVERSITY OF NAPLES FEDERICO II

Doctorate School of Earth, Environmental and Resource Sciences

Doctoral thesis in Stratigraphy and Structural Geology

(XXXI Cycle)

SEQUENCE STRATIGRAPHIC CONTROLS ON RESERVOIR-SCALE MECHANICAL STRATIGRAPHY OF SHALLOW-WATER CARBONATES

Supervisor

Prof. Alessandro Iannace

Ph.D. Student

Francesco Vinci

Ph.D. Coordinator

Prof. Maurizio Fedi

Academic Year 2017-2018

Abstract

Studies on mechanical stratigraphy of shallow-water carbonates have shown that the distribution of fractures can be controlled by depositional facies, sedimentary cycles/sequences, and diagenesis. Understanding the role of these sedimentary controls is therefore crucial in the characterization of matrix-tight reservoirs, where fractures may represent the main conduits for fluid flow. Nonetheless, the relation between fracture distribution and sedimentary controls is not always investigated at scales that are relevant to reservoir and fluid-flow characterization.

In this dissertation, is provided a solution to this problem by integrating sequence stratigraphic analysis with the multi-scale fracture characterization of two carbonate platform exposures outcropping in the Sorrento Peninsula (southern Italy). These outcrops represent the surface analogue of subsurface hydrocarbon reservoirs of the Basilicata region (southern Italy), and consist of nearly vertical cliffs (hundreds of meters wide and high) exposing shallow-water limestones and dolostones, crossed by several sub-vertical fractures ranging in height from few centimetres up to few tens of metres. Due to the partial inaccessibility of this cliff, field measures have been combined with remote sensing on virtual outcrop models. The study allowed to identify the key control exerted by sedimentary sequences on the thickness of mechanical units and the position of their boundaries, which implies that sequence stratigraphy can be used to predict the distribution of large-scale fractures.

The applicability of this concept has been tested on a subsurface dataset from the Basilicata region. Performing a sequence stratigraphic analysis on image logs calibrated with core data, the main mechanical boundaries were predicted in a portion of fractured stratigraphic units.

The thickness of predicted mechanical units showed a clear relation to the distribution of fractures. Indeed, in the investigated stratigraphic interval, an increase in the mean thickness of mechanical units corresponds to an increase in the mean spacing of fractures, of a comparable order of a magnitude.

The main outcome of this study is the proposal of a new approach to estimate large-scale fracture intensity in carbonate reservoirs, based on the evaluation of the thickness of mechanical units through sequence stratigraphy.

Index

1 INTRODUCTION

1.1 Fractured carbonate reservoirs

Characterization of fractured carbonate reservoirs is a major challenge in petroleum production since they are inherently heterogeneous, with respect to both matrix and fracture properties. This heterogeneity is expressed at various scales, from the pore to the basin, and can result not only in large variations in productivity between wells belonging to the same oil-field, but also within a single well, where a large part of the production could come from a short but intensely fractured interval (Bratton et al., 2006; Narr et al., 2006; Spence et al., 2014; Wennberg et al., 2016).

An understanding of the spatial distribution of fractures is then essential to predict fluid-flow, particularly in low porosity reservoirs (tight), whose production is strictly dependent upon porosity and permeability of the fracture network. Within this network, major through-going fractures, spanning from few meters to several tens of meters in height, can represent important conduits for fluid migration (Dean and Lo, 1988; Odling et al., 1999; Aydin, 2000; Bourne et al., 2001; Gauthier et al., 2002; Guerriero et al., 2013, 2015, Bisdom et al., 2016, 2017a). However, the 3D distribution of fractures in the subsurface is not easily predictable using only well or seismic data, which are often incomplete or biased by a too low resolution (Narr, 1996; Angerer et al., 2003; Peacock, 2006; Li et al., 2018).

For this reason, the study of an outcrop analogue can help in understanding the key controls on fracture distribution and in building a reservoir model (Antonellini and Mollema, 2000; Sharp et al., 2006; Agosta et al., 2010; Storti et al., 2011; Vitale et al., 2012; Bisdom et al., 2014; Richard et al., 2014; Hardebol et al., 2015; Zambrano et al., 2016; Panza et al., 2016; Corradetti et al., 2018; Massaro et al., 2018; Volatili et al., 2019). Decades of work on outcrop

analogues highlighted the influence of stratigraphic layering on fracture occurrence, and this led to introducing the concept of mechanical stratigraphy, a discipline that subdivides sedimentary beds into units defined by mechanical or fracture network properties (Corbett et al., 1987; Gross et al., 1995; Bertotti et al., 2007; Laubach et al., 2009).

An early result of these studies is the well-documented linear relationship between fracture spacing and bed thickness in sedimentary rocks (Price, 1966; McQuillan, 1973; Ladeira and Price, 1981; Huang and Angelier, 1989; Narr and Suppe, 1991; Gross, 1993; Gross et al., 1995; Bai et al., 2000). This relationship tends to be verified where the bedding surface represents a low-cohesion surface that can inhibit fracture propagation across it (Pollard and Aydin, 1988; Gross et al., 1995; Cooke et al., 2006), and therefore there is a correspondence between sedimentary beds and mechanical units.

However, this condition is not always fulfilled in carbonate rocks, which are a material intrinsically heterogeneous. This led some authors to explore another research path, focused on the links between sedimentary facies, diagenesis and the fracturing patterns (Wennberg et al., 2006; Lézin et al., 2009; Larsen et al., 2010; Ortega et al., 2010; Barbier et al., 2012; Rustichelli et al., 2013; Lavenu et al., 2014). These studies showed that stratigraphic architecture can be a primary controlling factor on fracture development as it dictates the distribution and variability of sedimentary facies, which influences the style, intensity and location of fractures. Therefore, integrating the study of structural deformation in a sequence stratigraphic framework, can maximize the predictability of fracture distribution (Underwood et al., 2003; Di Naccio et al., 2005; Morettini et al., 2005; Zahm et al., 2010).

In any case, any dependence of the fracture network attributes on the occurrence of stratigraphic discontinuities requires that studies of fracture dimensions in analogues of

naturally fractured reservoirs are addressed at the scale of the considered stratigraphic discontinuity (Ortega et al., 2006). Because of difficulty to access vertical exposures, most of previous analogue studies, have been limited to the examination of spatial distribution and dimensional properties of fractures at relatively small length scales. How large through-going fractures are distributed within thick mechanical carbonate units, and where they arrest, remain poorly understood. As it shown in this dissertation, the most recent remote-sensing technologies, such as the photogrammetry-derived Virtual Outcrop Models, can contribute to solve this issue.

1.2 Digital survey techniques: Virtual Outcrop Models

The use of multi-view photogrammetry in building Virtual Outcrop Models (VOMs) represents an increasingly accessible source of high-quality, low-cost geological data (Favalli et al., 2012; Westoby et al., 2012; Bemis et al., 2014; Tavani et al., 2014; Reitman et al., 2015), as well as an affordable and reliable alternative to LiDAR (light detection and ranging) for the three-dimensional representation of geological outcrops (Adams and Chandler, 2002; Harwin and Lucieer, 2012; James and Robson, 2012; Cawood et al., 2017).

These detailed 3D reconstructions of outcrop geology are obtained by means of randomly distributed digital photographs pointing at the same scene, and can be applied to a broad range of studies, including sedimentology and stratigraphy (Pringle et al., 2001; Hodgetts et al., 2004; Chesley et al., 2017), geomorphology and engineering geology (Haneberg, 2008; Sturzenegger and Stead, 2009; Firpo et al., 2011; Mancini et al., 2013; Massironi et al., 2013; Clapuyt et al., 2016), reservoir modeling (Pringle et al., 2001; Buckley et al., 2010; Casini et al., 2016; Bisdom et al., 2017b; Massaro et al., 2018), and structural geology (Bistacchi et al., 2011, 2015; Vasuki et al., 2014; Thiele et al., 2015; Tavani et al., 2016a; Vollgger and Cruden, 2016; Corradetti et al., 2017a, 2017b; Gao et al., 2017; Menegoni et al., 2018).

In particular, the increasing availability of Unmanned Aerial Vehicles (UAVs, commonly referred as drones) equipped with digital photo-cameras , has made VOMs nowadays widely used in the characterization of fractured outcrops, since they allow for the collection of large volumes of fracture data from reservoir-scale outcrops, in some cases not accessible with traditional field techniques (Casini et al., 2016; Seers and Hodgetts, 2016; Bisdom et al., 2017b; Corradetti et al., 2018; Massaro et al., 2018).

The extraction and analysis of such a big amount of data can be a time-consuming step of the interpretation workflow. For this reason, several Authors developed software packages dedicated to (semi-)automatic mapping of structural discontinuities (e.g. Monsen et al., 2011; Lato and Vöge, 2012). However, even if (semi-)automatic mapping can show good results in terms of fracture size and orientation, do not ensure the extraction of the maximum available information from the VOMs. This makes preferable, for some purposes (e.g. for mechanical stratigraphy studies, Casini et al. 2016), the manual picking of the discontinuities.

Another way to optimize the interpretation workflow, is analyzing the extracted fracture data with software packages for the structural analysis. Even if some valuable tools are currently available (e.g. see Hardebol and Bertotti, 2013; Zeeb et al., 2013; Healy et al., 2017), their scope is generally restricted to datasets acquired on flat 2D surfaces oriented roughly perpendicular to fractures, a condition which has the big disadvantage of forcing the interpretation of the 3D nature of the fracture array into a 2D plane (Minisini et al., 2014), that implies significant errors when structures oriented oblique to the outcrop surface are studied.

A robust workflow allowing the extraction and quantification of structural data from VOMs with a complex topography is still lacking. Contributing to solve this issue is one of the aims of this study.

1.3 Scope of the work

In this dissertation, the results obtained from integrating sequence stratigraphic analysis with the multi-scale fracture characterization of two carbonate platform exposures outcropping in the Sorrento Peninsula (southern Italy) are presented. These outcrops represent the surface analogue of subsurface hydrocarbon reservoirs of the Basilicata region (southern Italy), and consist of nearly vertical cliffs (hundreds of meters wide and high) exposing shallow-water limestones and dolostones, crossed by several sub-vertical fractures ranging in height from few centimetres up to few tens of metres. For studying these partially inaccessible cliffs, a cutting-edge workflow combining remote sensing and VOMs with geological fieldwork has been developed.

The purpose of the study was to better understand the role of sedimentological features (e.g. bed-thickness, lithology, textures, bed boundaries) on the vertical continuity of reservoir-scale cluster of fractures (e.g. through-going fractures) and to use these insights to develop predictive tools for subsurface fracture distribution. The study allowed to identify the key control exerted by sedimentary sequences on the thickness of mechanical units and the position of their boundaries, suggesting that sequence stratigraphy can be used to predict the distribution of large-scale fractures in shallow-water carbonates.

The applicability of this concept has been tested on a subsurface dataset from the Basilicata region. Performing a sequence stratigraphic analysis on image logs calibrated with core data, the main mechanical boundaries were predicted in a portion of fractured stratigraphic units. The thickness of predicted mechanical units showed a clear relation to the distribution of fractures. Indeed, in the investigated stratigraphic interval, an increase in the mean thickness

of mechanical units corresponds to an increase in the mean spacing of fractures, of a comparable order of a magnitude.

The main outcome of this study is the proposal of a new approach to estimate large-scale fracture intensity in carbonate reservoirs, based on the evaluation of the thickness of mechanical units through sequence stratigraphy.

2 GEOLOGICAL SETTING

2.1 The Southern Apennines

The Southern Apennines are a fold and thrust belt consisting of a stack of several Mesozoic thrust sheets which, together with their Tertiary cover, overlay the buried Apulian shallow-water carbonates (see Cello and Mazzoli, 1999 for a review). From top to bottom, the tectonic units consist of ocean-derived successions, namely the Ligurian Accretionary Complex (Ciarcia et al., 2011; Vitale et al., 2011), shallow-water carbonates of the Apennine Carbonate Platform and basinal sediments of the Lagonegro-Molise units (Figure 1).

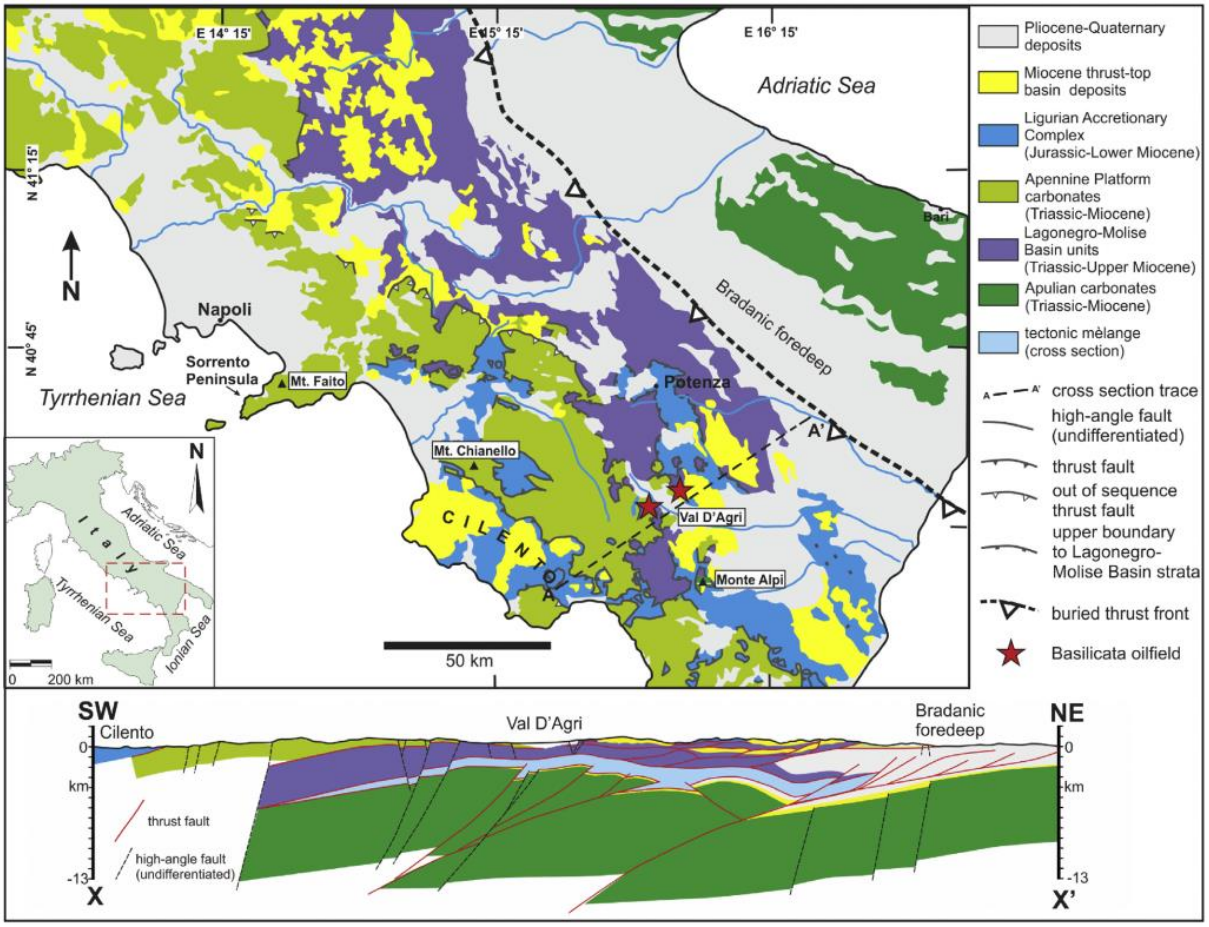

Figure 1 Structural framework of southern Italy and regional cross-section with main localities cited in the text (from Giorgioni et al., 2016, after Vitale et al., 2012).

During the Cretaceous, these units were part of the isolated platforms and basins system developed on the Adria passive margin (Ogniben, 1969; D'Argenio et al., 1975; Mostardini and

Merlini, 1986; Zappaterra, 1994; Bosellini, 2004; Patacca and Scandone, 2007). Starting from the Late Cretaceous the system started to be progressively incorporated in the Apennines belt as a result of the collision between the Eurasian and the Afro-Adriatic continental margins (Malinverno and Ryan, 1986; Dewey et al., 1989; Patacca and Scandone, 1989; Oldow et al., 1993; Mazzoli and Helman, 1994; Shiner et al., 2004; Vitale and Ciarcia, 2013).

The carbonate succession presently exposed at Mt. Faito (Figure 2) was originally part of the western sector of the Apennine Carbonate Platform. Nowadays it forms an ENE-WSW ridge, the Lattari Mts. of the Sorrento Peninsula (Figure 3), mainly made of Upper Triassic to Upper Cretaceous shallow-water limestones and dolostones (De Castro, 1962; Robson, 1987; Iannace, 1993; Carannante et al., 2000; Iannace et al., 2011), unconformably covered by Miocene foredeep and wedge-top siliciclastic sediments. The whole sedimentary pile is locally covered by Quaternary pyroclastic deposits.

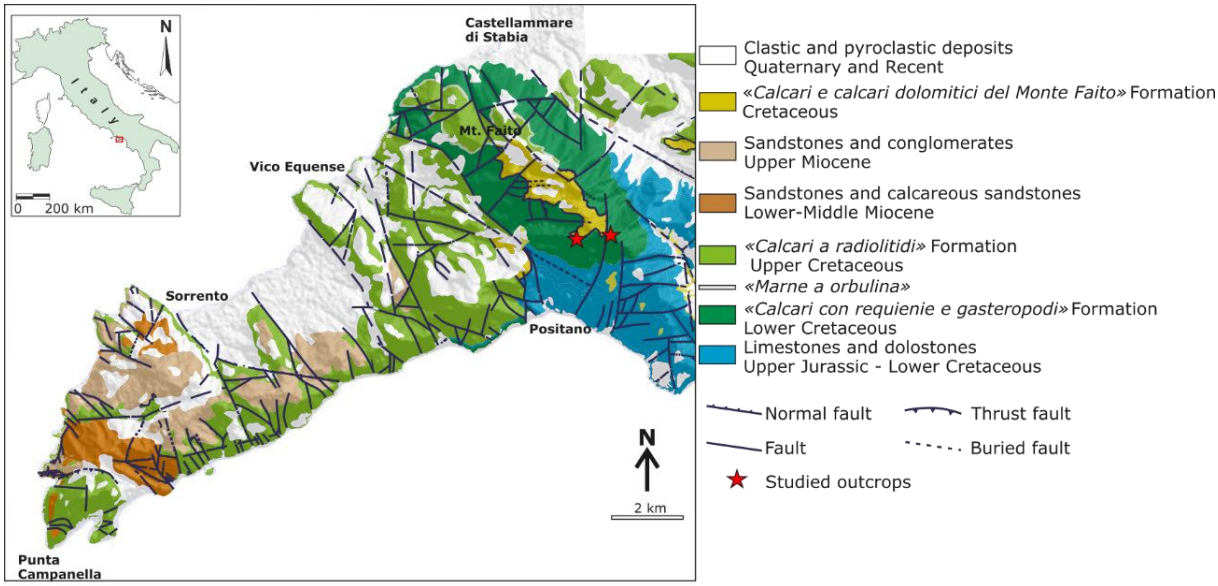

Figure 2 Geological map of the Sorrento Peninsula; after ISPRA (2016), modified.

The Early Cretaceous interval has been the object of detailed cyclo-stratigraphic investigations (D'Argenio et al., 1999, 2004, Raspini, 2001, 2012; Amodio et al., 2013; Graziano and Raspini,

2015; Amodio and Weissert, 2017). These Authors found that the stacking pattern of the mainly lagoonal succession is controlled by Milankovitch-type periodicity. The formation of very small intraplatform basins was formerly suggested by the presence of rich fossil fish *lagerstätten* fish (Bravi and De Castro, 1995), and has been fully documented by Tavani et al., (2013) and Iannace et al., (2014) who described syn-sedimentary faults, soft-sediment deformation and breccias during the Albian.

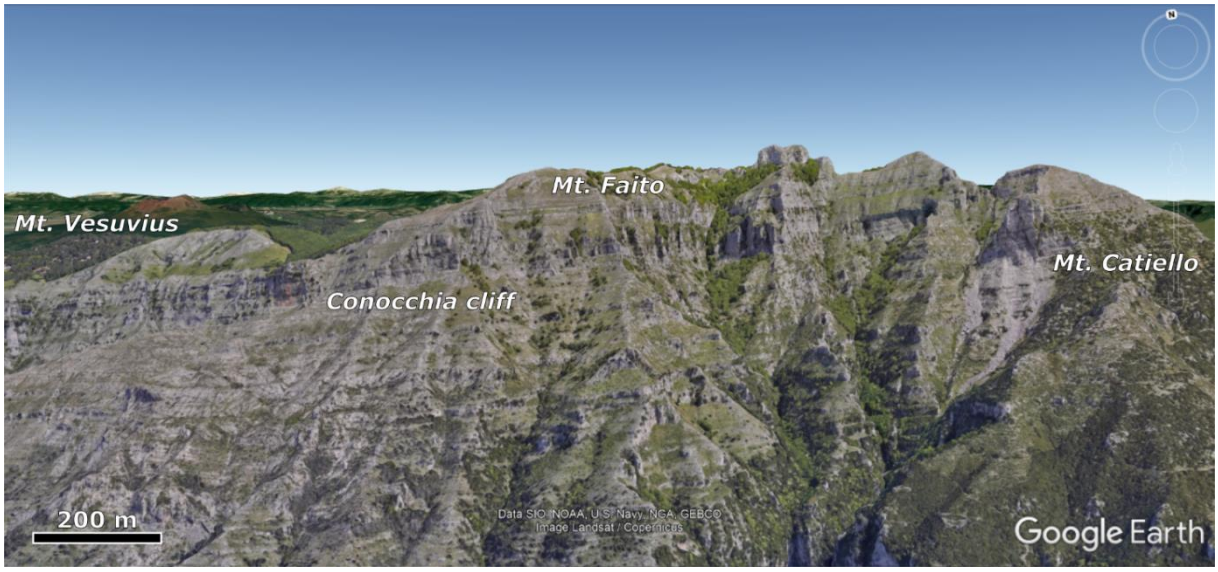

Figure 3 Satellite image showing location of the outcrops cited in the text.

2.2 The Apennine Platform carbonate as field analogues for the Basilicata reservoirs

The largest oil fields of Italy, Val d'Agri and Tempa Rossa (Bertello et al., 2010), are hosted by Cretaceous platform carbonates of the buried Apulian Platform in the subsurface of Basilicata (Shiner et al., 2004). Because of the low permeability of their reservoirs, these oil fields are most successfully explored in the highly fractured structures of the thrust belt (Bertello et al., 2010). The upper part of the reservoir is made up of Upper Cretaceous rudist limestones while the lower part consists of Barremian-Cenomanian interlayered limestones and dolostones (Bertello et al., 2010). Although belonging to a different paleogeographic domain (i.e. the Apennine Platform), the Cretaceous shallow-water carbonates of the Mt. Faito area are very similar in terms of lithology, facies, and rock texture to the coeval carbonates of the Apulian Platform (Figure 4), which constitute the thick reservoir interval of the Basilicata oil fields (Bertello et al., 2010).

In particular, the Albian-Turonian interlayered limestones and dolostones succesion outcropping at Mt. Faito is the best available surface analogue for the lower part of the reservoir, which is made of interlayered limestones and dolostones as well (Bertello et al., 2010; Iannace et al., 2014). For this reason, surface analogues of the Apennine Platform have been successfully used not only for investigating facies distribution and petrophysical parameters, but also for studying the fracture network attributes and their relations with lithology and textural parameters, provided that the different tectonic evolution and burial conditions experienced by the Apennine and Apulian Platform were taken into account

(Guerriero et al., 2010; Iannace et al., 2014; Giorgioni et al., 2016; Vinci et al., 2017; Corradetti et al., 2018; Massaro et al., 2018).

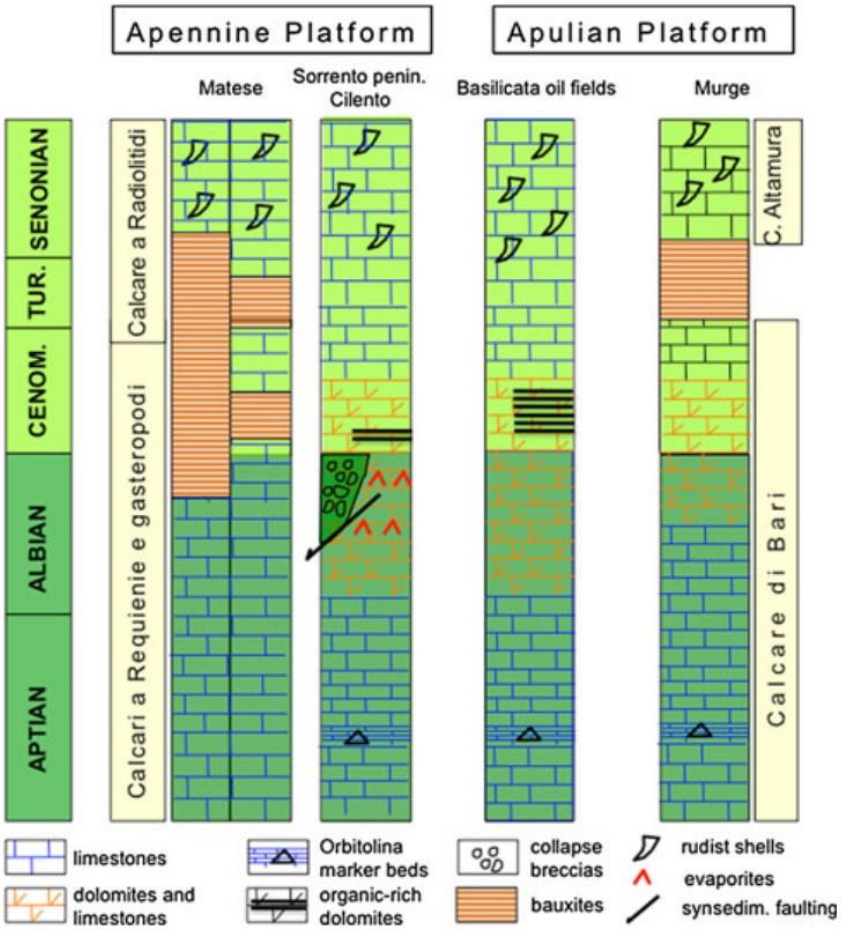

Figure 4 Synoptic view of the main stratigraphic units of the Aptian to Senonian outcrop successions of the Apennine and Apulian Carbonate Platforms (with lithostratigraphic nomenclature) compared with those of the Cretaceous reservoir in the Basilicata oil-fields (From Iannace et al. 2014).

2.3 Stratigraphy of the Mt. Faito area

A detailed study of the stratigraphy, facies and dolomitized bodies of the Lower Cretaceous platform carbonates of Mt. Faito area was performed by Vinci et al. (2017). The Authors investigated a sedimentary succession 466 m thick, made up of middle Berriasian to lower Aptian shallow water carbonates. The succession is part of the "Calcari con Requienie and Gasteropodi" Formation (Requienid and Gastropod Limestones Formation) (Figure 2) and has been informally subdivided into three intervals, namely A, B and C, on the basis of dolomitization intensity (Figure 5). The lowermost interval A and the uppermost interval C consist of limestones with minor dolomites whereas interval B is completely dolomitized. General characters of the three intervals are given below.

2.3.1 Interval A (middle Berriasian – lower Hauterivian).

This interval, about 203 m thick, is mainly calcareous, but becomes progressively more dolomitized from its middle part to the top. Bed thickness ranges from 10 to 200 cm and averages approximately 54 cm. The sedimentary facies organization is dominated by single-bed elementary cycles. Thicker beds consist of up to five amalgamated elementary cycles. Each cycle usually starts with a thin basal interval of peloidal intraclastic packstone-grainstone, interpreted as a reworked transgressive lag deposit, followed by ostracodal mudstone-wackestone deposited in a low-energy lagoon with restricted circulation, occasionally with charophyte remains, pointing to more brackish condition. The top of the cycle is generally represented by a thin reddened or brownish dolomitic interval capped by an undulated and/or nodular surface, linked to an emersion surface. Commonly, dolomite occurs as scattered

crystals in the calcareous micrite. This facies succession, characterized by a subtidal facies directly overlain by a subaerial exposure surface, without the interposition of intertidal facies, has been interpreted as a diagenetic cycle (*sensu* Hardie et al., 1986) formed in an inner platform setting. Dolomite becomes more abundant in the upper part of this interval, but it is generally restricted to the upper part of beds, where it makes a dolomitic cap diffusing downward into limestone. Thin, mm- to cm-thick, silicified crusts can occur at the top of the elementary cycles, either associated to dolomite cap or as a distinct feature on top of limestone strata. These silicified crusts are peculiar of the Interval A, and have been interpreted as the result of diagenetic replacement of former evaporites (Folk and Pittman, 1971; Heaney, 1995; Chafetz and Zhang, 1998).

2.3.2 Interval B (upper Hauterivian – lower Barremian).

This interval, about 91-m thick, is completely dolomitized and is made of an alternation of yellowish and greyish dolostone strata, sometimes with mm-thin marly interlayers. The bed thickness ranges from 10 cm to 120 cm, the mean value is 51 cm. Dolostone strata are laterally continuous and can be either massive or thinly subdivided in cm-thick levels by bed-parallel stylolites. Beds with these diagenetic heterogeneities are more prone to be weathered and can form recessive intervals. Generally, Coarse dolomite (Cdol) is present at the base of beds whereas the top consists of darker, Fine-Medium dolomite (FMdol) caps, often associated with plane-parallel to wavy lamination of probable microbial origin, fenestrae and sheet cracks. The presence of microbial laminae and fenestrae associated with sheet cracks suggest deposition in the intertidal to supratidal zone (Demicco and Hardie, 1995; Flügel, 2004). The

Cdol at the base of the beds preserves ghosts of a more grainy precursor facies, which could represent a basal transgressive lag at the base of a shallowing-upward peritidal cycle.

2.3.3 Interval C (upper Barremian – lower Aptian,).

This interval, about 172-m thick, is mainly calcareous. The dolomitization intensity is still fairly high in the lower half, but it gradually decreases upward. Bed thickness ranges from 5 to 150 cm; the mean value is 41 cm.

Interval C consists of shallowing-upward peritidal cycles. Cycles generally start with a thick foraminiferal-rich limestone basal interval, grading upward into a laminated stromatolitic interval, made of FMdol, capped by a slightly argillaceous brownish dolomite. In many instances the dolomitization intensity decreases gradually from the top toward the base of the bed. In the partially dolomitized strata, there is often a reticulate structure, infiltrating downward from brownish dolomite cap at the top of the beds, which is interpreted as due to selective dolomitization of root-related structures. Dolomite crystals can be also concentrated in bed-parallel dolomite seams, due to pressure solution (Tavani et al, 2016). The limestone interval at the base of the beds consists of foraminiferal wackestone to packstone-grainstone, or of intra-bioclastic floatstone-rudstone. These facies were deposited in a normal-marine subtidal lagoon. The laminated stromatolitic facies are indicative of a tidal flat environment. The slightly argillaceous dolomitic cap is interpreted as formed during subaerial exposure, in agreement with the interpretation of the reticular structures as selectively dolomitized root casts.

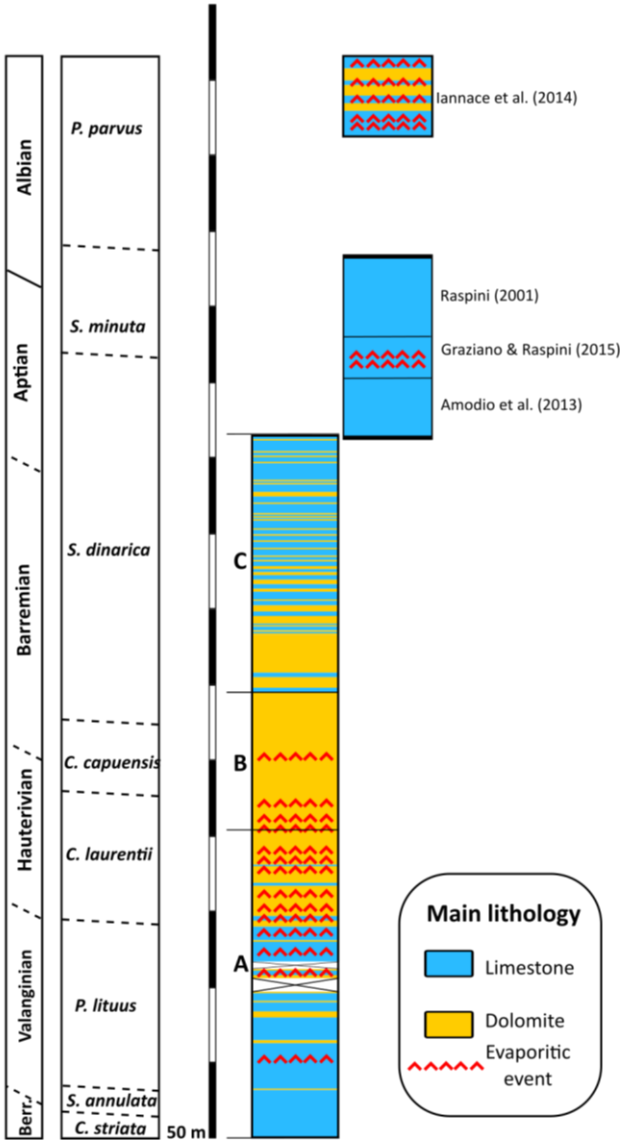

Figure 5 Stratigraphic distribution of early dolomite and evaporites in the Lower Cretaceous shallow-water carbonates of Mt. Faito; The age model is based on the biozones of De Castro (1991). Data of the Aptian-Albian interval from Raspini (2001), Amodio et al. (2013), Iannace et al. (2014), Graziano and Raspini (2015). From Vinci et al. (2017).

3 MATERIAL AND METHODS

3.1 Field Dataset

The field dataset presented in this work was acquired during three distinct surveys on the southwest slope of Mt. Faito (Figure 2) aimed at reconstructing the stratigraphy of the area and observe fracture distribution at the outcrop scale. During the first survey, measurements and sampling at a centimeter scale were made along the slope at the western flank of the Conocchia cliff. In this way, a 127-m-thick stratigraphic and stratimetric section was reconstructed. Collected evidences and correlations with the regional stratigraphy showed that the investigated sedimentary succession is made up of upper Barremian to lower Aptian shallow-water carbonates, it is part of the "Calcari con Requienie and Gasteropodi" Formation (Requienid and Gastropod Limestones Formation) (ISPRA, 2016) and corresponds to the interval C of the stratigraphic subdivision made by Vinci et al. (2017) for Lower Cretaceous carbonates of Mt. Faito area.

The second survey, focused on the structural setting of the area, was performed along the slope at the western flank of the Conocchia cliff and in some adjacent exposures. This allowed to observe fracture distribution and the behavior of mechanical boundaries at the outcrop scale.

Finally, the third survey was made along the slope at the eastern flank of the Mt. Catiello peak. Field observations combined with the analysis of satellite image available on the web (i.e. Google Earth) allowed to correlate the succession exposed at Mt. Catiello with the succession exposed at the Conocchia cliff. These observations showed that the exposed sedimentary succession is made up of Barremian to lower Aptian shallow-water carbonates, that it is part of the "Calcari con Requienie and Gasteropodi" Formation (Requienid and Gastropod

Limestones Formation) (ISPRA, 2016) and corresponds to the upper part of the interval B and the whole interval C of the stratigraphic subdivision made by Vinci et al. (2017) for the Lower Cretaceous carbonates of Mt. Faito.

3.1.1 Petrography

Field data analysis was integrated with microfacies analysis and petrographic description of >130 thin-sections. Thin sections were examined under transmitted light with an optical microscope. Dolomite texture classification was referred to Sibley and Gregg (1987) and Warren (2000). Dolomite crystal size was classified according to petrophysical classes of Lucia (1995) as fine-medium (<20 µm to 100 µm) (FMdol) or coarse (>100 µm) (Cdol).

3.2 3D Virtual Outcrop Model Dataset

A large part of the data used in this study were acquired by remote sensing using Virtual Outcrop Models (VOMs). A VOM is a digital 3D representation of the outcrop topography in the form of xyz point clouds or textured polygonal meshes (see Corradetti, 2016 for a review). VOMs are traditionally obtained by high precision Terrestrial Laser Scanner (TLS) surveys (Richet et al., 2011) and, more recently, also by Structure from Motion (SfM) photogrammetric techniques (Westoby et al., 2012), or by a combination of both. Even if, especially in geology, TLS is the most acknowledged technique, TLS surveys have a few intrinsic limitations (Wilkinson et al., 2016), such as the weight of the field equipment, the need of scanning from multiple field-based positions and long acquisition time. These limitations make TLS unsuitable in certain remote area, like those investigated in the present study, where data acquisition cannot be conducted from the ground level. Unlike TLS, SfM photogrammetry is a technique that allows the reconstruction of a 3D object through the analysis of multiple images of the same scene taken from different points of view (Remondino and El-Hakim, 2006). What makes this technique highly versatile, is the possibility of acquiring the images needed for the model building by means of Unmanned Aerial Vehicles (UAVs), commonly referred as drones, equipped with digital photo-camera. This combination allowed to overcome the logistic issues that were typical of TLS surveys and widened the applications of SfM photogrammetry for Earth Science, which is gaining much popularity in recent years.

Three VOMs were analyzed in the present study. The models were all built using SfM photogrammetry, with images acquired by means of UAV equipped with a digital photo-camera. Two out of three VOMs represent the Conocchia cliff while the third model represents

the Mt. Catiello peak. The two models of the Conocchia cliff were acquired in different phases of the research project, with the older model (already presented by Corradetti, 2016) characterized by a larger coverage of the outcrop but a minor resolution, and the new model focused on a restricted portion of the outcrop but with a very high resolution. Detailed technical information about the used models are given in Table 1.

	Conocchia cliff - Old Survey (Corradetti, 2016)	**Conocchia cliff - New Survey (This study)**	**Mt. Catiello - (This study)**
Photo-camera	Sony Nex-7 (24Mpx)	Sony Alpha 7r (36Mpx)	Sony Alpha 7r (36Mpx)
Photo number	105	96	173
Point cloud	~12.4 x 10^6 points	~30.1 x 10^6 points	~23.8 x 10^6 points
Triangular mesh	~11.1 x 10^6 triangles	~13.9 x 10^6 triangles	~44.5 x 10^6 triangles
Model surface	~4.69 x 10^4 m^2	~5.18 x 10^3 m^2	~3.93 x 10^4 m^2
Model resolution	~10 cm	~4 cm	~4 cm

Table 1 Technical details of the VOMs

3.2.1 Building a photogrammetry-derived VOM

The photogrammetric method is an estimative (i.e. indirect) technique through which the metric data of a 3D object (shape, position and size) are obtained by estimating the spatial coordinates of each point in the photographs (Remondino and El-Hakim, 2006). Since each photograph contains only 2D coordinates, at least two overlapping images taken from different points of view are needed to estimate the 3D coordinates of points. This operation can be accomplished using the algorithms of Structure from Motion, which by matching and analyzing the 2D coordinates of pixels in different images, estimate the location of any point of the VOM (Ullman, 1979; Grün et al., 2004; Szeliski, 2010).

SfM algorithms are nowadays implemented in several software packages (see Tavani et al., 2014 for a review) that, for a given set of partially overlapping images, can automatically

detect a suite of common points in each image pairs and also recognize the camera parameters for each photo. This allows to extract the 3D coordinates of each point recognized in at least two photos, and to create a point-cloud representing the surfaces of the objects captured within the scene (Grün et al., 2004; Favalli et al., 2012; Tavani et al., 2014). The overlapping photos should be taken from multiple points of view, using the same camera with the same focal length, in order to minimize the source of errors. In this way, each portion of a scene is represented by a similar pixel pattern in the different photos, ensuring and maximizing the recognition of points by the SfM algorithms and, therefore, allowing for the creation of denser point-clouds (Tavani et al., 2014).

The photogrammetry package chosen for this study is Agisoft PhotoScan, a software characterized by a user-friendly nature, by the availability of academic licensing and by tools allowing for the export of results in OpenPlot.

The first step of the workflow for the creation of a VOM is uploading the selected photos in PhotoScan (Figure 6) and proceeding with a preliminary photo-masking operation. This consists in defining areas that will not be involved in the 3D reconstruction, such as vegetated areas or the sky. Even if photo-masking is not a compulsory operation, is recommended to obtain a faster reconstruction of the model (Tavani et al., 2014). Subsequently, the photo-alignment command tries to recognize the position of the same points in the different overlapping photos, allowing to compute relative position and orientation of photos and, therefore, to create the point-cloud (Figure 6d). At the end of this step, the software reports which photos have been aligned and which not. A bad alignment can be recognized by checking the presence of unrealistic or wrong photos positioning and/or the presence of unrealistic geometries of the point cloud. The next step, the “Building geometries”,

triangulates the point-cloud obtained in the previous phase of the workflow and returns a mesh made up of irregular triangles (Figure 6e). After that, the "Build texture" command reconstructs a texture map that will be draped onto the triangular mesh, generating as a result a photorealistic virtual model. The final step is the georeferentiation of the model, which consists in the re-orientation and re-scaling of the 3D model by recognizing in the model at least three point of known position. At this point, the model is ready to be exported as a wavefront OBJ format and used to extract geological features with OpenPlot.

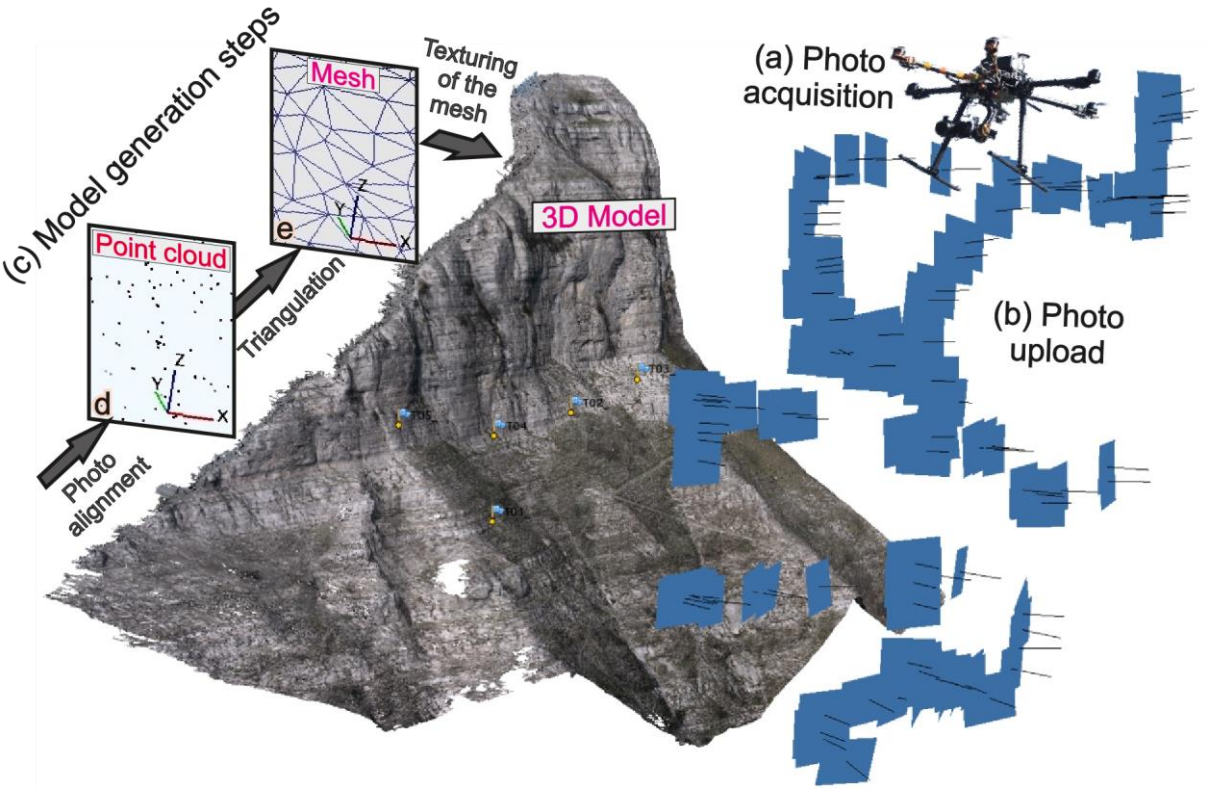

Figure 6 Workflow for the generation of the Virtual Outcrop Models. Photographs were acquired by means of an UAV (a) and the uploaded in PhotoScan (b). The workflow of Photoscan (c) went through the steps of photo alignment, building of the geometry and building of the texture.

3.2.2 Extracting geological information with OpenPlot

The VOM built with Agisoft Photoscan can be imported as a wavefront mesh in OpenPlot, a multiplatform (Linux, Mac OS and Windows) and open source software for geostructural data

analysis (Tavani et al., 2011, 2014). The software has a 3D environment which allows visualizing and manipulating the imported mesh. Morevoer, it allows using several drawing tools to extract geological information from the VOM. One of these tools is “draw-polyline” (Figure 7), that allows digitizing a polyline by clicking point-by-point directly on the VOM (Figure 7b), along the intersection between a geological surface of interest (such as bedding, fractures, faults, etc.) and the outcrop topography (Hodgetts et al., 2004). During digitization, the moment of inertia of the picked points is computed (Fernández, 2005). This allows OpenPlot to compute and store a best-fit plane of the polyline (Figure 7c), together with its strike and dip (Tavani et al., 2014), so that the newly created planar polygons can be treated as a structural object, filtered, analyzed, plotted and more (Tavani et al., 2011).

Finally, the polygons created in OpenPlot can be projected on a panel along a selected direction (i.e. onto a perpendicular panel). The projected features can be saved in .svg format, an XML-based vector image format, and hence can be opened with any vector drawing software.

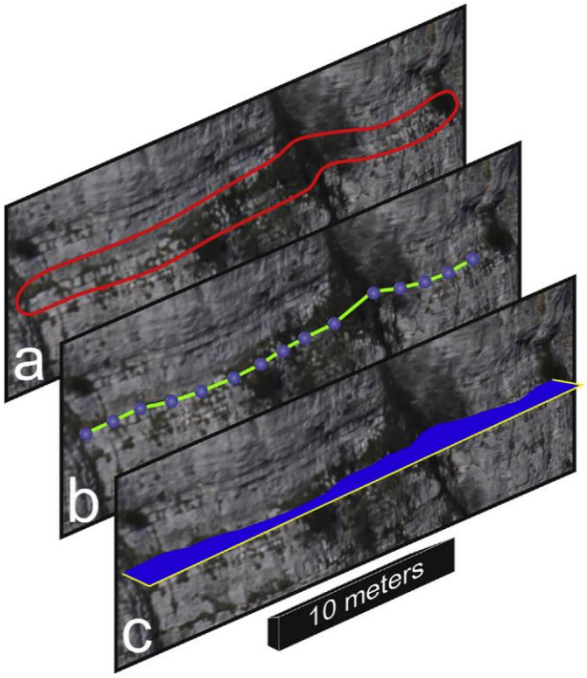

Figure 7 Fracture digitization process. (a) Once a geological surface is recognized in the model, a polyline is drawn (b), picking point-by-point, over the textured mesh. (c) During digitization, the moment of inertia of the picked points is computed, allowing the software to draw a best-fit plane for the digitized polyline (from Corradetti et al., 2018).

3.2.3 Fracture pattern quantification with FracPaQ

The structural data extracted with OpenPlot can be quantitatively analyzed with FracPaQ, an open-source, cross-platform and freely available MATLAB™ toolbox designed to quantify fracture patterns in two dimensions (Healy et al., 2017). The toolbox comprises a suite of MATLAB™scripts based on previously published quantitative methods for the analysis of fracture attributes: orientations, lengths, intensity, density and connectivity.

There are two main type of input data accepted by FracPaQ: tab-delimited (.ascii) text files of fracture trace nodes ("node file") and graphical image files of fracture traces ("image file"). However, supplying a node file of specific (x,y) coordinate pairs of every node along every fracture trace is the most robust way of entering data into FracPaQ. This type of input file is the one selected for this study, and it can be easily obtained from a .svg file containing a layer with fracture traces saved as 'line' or 'polyline' in a vector graphics software. The .svg files are one of the standard file outputs produced by OpenPlot, and this makes the integration of the two software a smooth process.

Once that the .svg file is imported in FracPaQ, a C-shell script included within the software source code can be used to extract the (x,y) fracture-trace coordinates from the .svg input file and write them into a tab-delimited text file. If the input file is valid, FracPaQ builds a MATLAB™ struct array of fracture *traces* (1 per fracture in the input file) composed of one or more *segments* delimited by *nodes*. In FracPaQ, then, a fracture trace is a continuous line composed of one or more straight fracture segments.

After the conversion of the .svg file in .ascii format, the software can be used to perform spacing analysis of fractures. In particular, one of the main focus of this study was the production of spatial density maps of fractures and, using the results, to define the mechanical

stratigraphy of the studied outcrops. FracPaQ provides two measures of spatial density calculated from the input 2D fracture data (Healy et al., 2017). Fracture intensity, labelled P21 by Dershowitz and Herda (1992), has units of m^{-1} and is defined as the total length of fracture in a given area (hence units of $m/m^2 = m^{-1}$). Fracture density, labelled P20 by Dershowitz and Herda (1992), has units of m^{-2} and is defined as the number of fractures per unit area. These parameters are estimated from the fracture pattern using the circular scan window method of Mauldon et al. (2001). According to this method, fracture intensity is estimated as $n/4r$, where n is the number of fractures intersecting the perimeter of a circle of radius r (Figure 8a); while fracture density is estimated as $m/2\pi r^2$, where m is the number of fractures terminating within a circle of radius r (Figure 8b). FracPaQ generates a 2D grid of evenly spaced circular scan windows to fit within the fracture trace map area, where the scan circle diameter is defined as 0.99 of the grid spacing in x and y to avoid overlapping scan circles. This grid of values is then contoured using the standard MATLAB triangulation function to produce the maps of estimated fracture intensity (P21) and estimated fracture density (P20). The number of circles can be selected by the user, considering that the optimum number of scan circles is variable and depends on the specific attributes of the fracture pattern (Rohrbaugh et al., 2002).

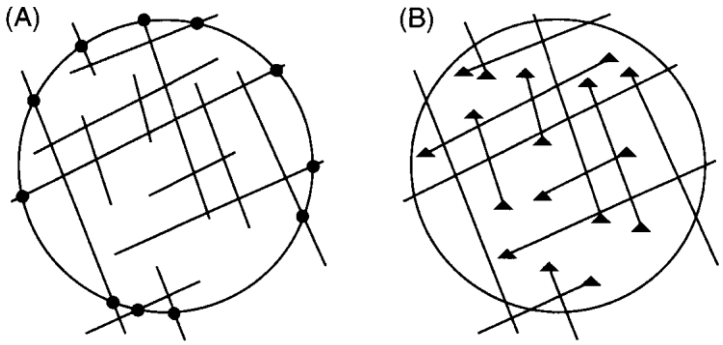

Figure 8 Fracture trace pattern with circular estimators. (A) Solid dots are intersection points (n) between fractures and circle. (B) Triangles are fracture endpoints (m) in the circular window. From Rohrbaugh et al. (2002).

3.3 Subsurface Dataset

[Testo non disponibile in quanto relativo a dati protetti da segreto industriale]

4 RESULTS

4.1 Stratigraphy and facies interpretation

4.1.1 The Conocchia cliff

Field observations and measurements were made along the slope at the western flank of the Conocchia cliff (Figure 10). The investigated sedimentary succession is 127-m-thick (Figure 11) and is made up of upper Barremian to lower Aptian shallow-water carbonates. It is part of the "Calcari con Requenie and Gasteropodi" Formation (Requienid and Gastropod Limestones Formation) (ISPRA, 2016) and corresponds to the interval C of the stratigraphic subdivision made by Vinci et al. (2017) for Lower Cretaceous carbonates of Mt. Faito. Field observations and thin-section analysis of textures and sedimentary features, allowed to recognize a total of 8 lithofacies grouped in 4 lithofacies associations, which suggest a shallow-marine depositional environment ranging from open marine to restricted lagoon and coastal settings. Detailed description of lithofacies and their association are given in Table 2. In the following sections are described the general characters of the interval.

Figure 9 View of the lower part of the stratigraphic succession outcropping on the Conocchia cliff. Note the alternance of thicker grey limestone beds and thinner brownish dolostone beds. Geologists in the upper right corner are for scale

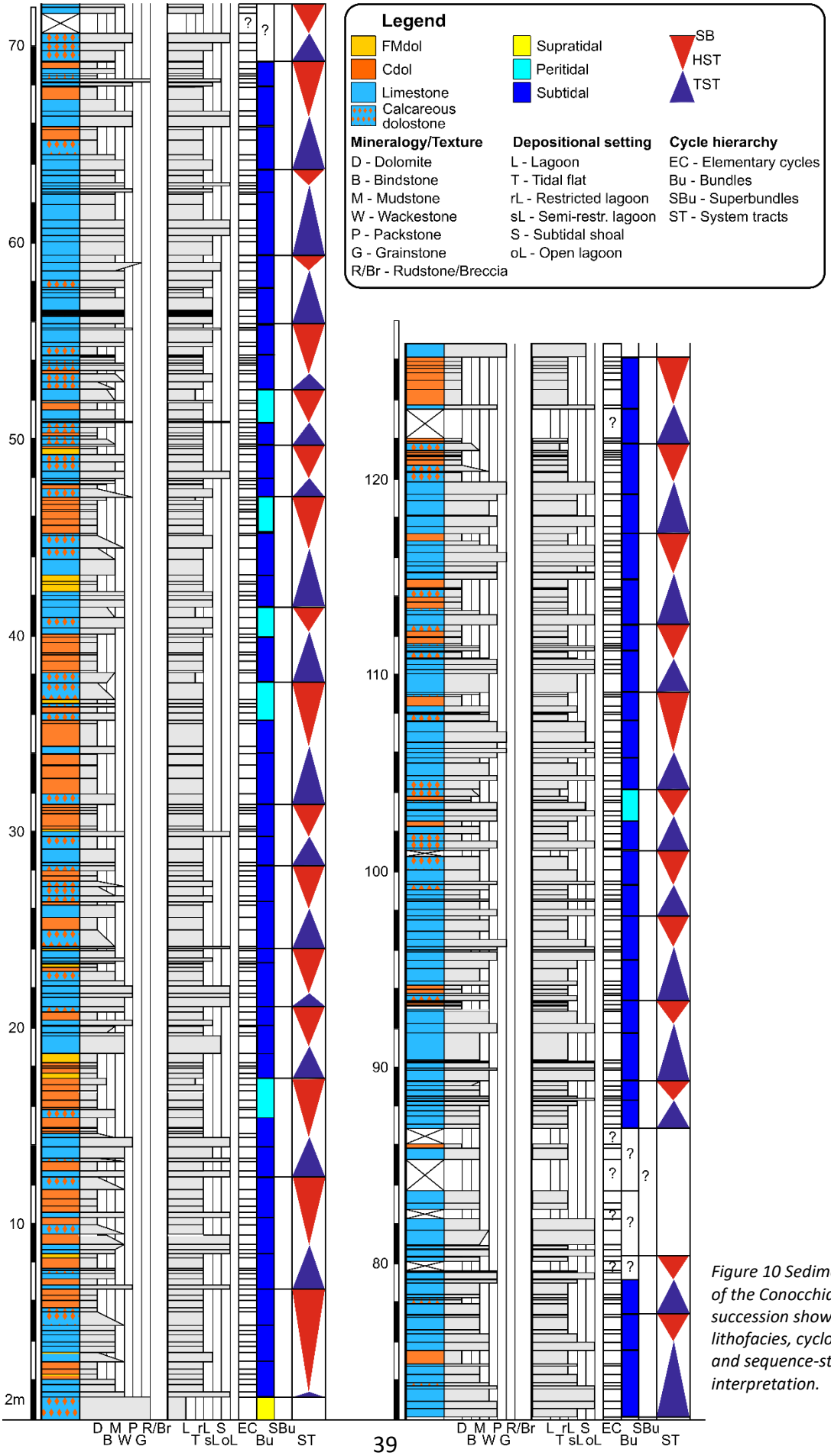

Figure 10 Sedimentologic log of the Conocchia cliff succession showing lithofacies, cyclostratigraphic and sequence-stratigraphic interpretation.

Lithofacies	Textures	Skeletal and non-skeletal components	Sedimentary structures	Environmental interpretation
Dolomitic breccia (A)	Clast-supported or matrix-supported breccia	Intraclasts (va), black pebbles (c)	Chaotic and unsorted	Supratidal environment - subaerial exposure
Microbial and fenestral laminated bindstone (B1)	Bindstone alternating with laminar of lithofacies M W	Intraclasts (c), peloids (c)	Lamination (microbial), fenestrae, mudcracks, sheetcracks	Tidal flat
Ostracodal mudstone-wackstone (B2)	Mudstone-wackestone	Ostracods (va, disarticulated valves), small micrite intraclasts (a), reddish micrite intraclasts (c), peloids (r), *Favreina salevensis* (r), benthic foraminifers (small miliolids, textularids, valvulinids) (r), gastropods (r), sponge spicules (r)	Very faint parallel lamination (mechanical)	Restricted marine subtidal lagoon
Miliolid-ostracode-algal wackestone-packstone (B3)	Wackestone-Packstone	Benthic foraminifers (a), ostracodes (a), calcareous algae (a), gastropods (c), small-sized oncoids (c), micritic intraclasts (c), peloids (c). Reduced diversity of biota	Very faint parallel lamination (mechanical)	Semi-restricted shallow-subtidal lagoon
Peloidal intraclastic packstone-grainstone (C1)	Packstone-grainstone	Peloids (va), small micrite intraclats (a), small benthic foraminifers (low diversity assemblages, including textularids, miliolids) (a), ostracods (c), *Favreina salevensis* (c), dasyclads (c).	Parallel lamination (mechanical)	Open lagoon with migrating sandbars
Foraminiferal wackestone and packstone-grainstone (C2)	Wackestone Packestone-grainstone	Benthic foraminifers (high diversity assemblages) (a), micrite intraclasts (a), peloids (a), *Favreina saelevensis*(a), bivalve fragments (a), gastropod fragments (a), dasyclads (a), *Lithocodium/Bacinella* nodules (c), echinoderm debris (c), ostracods (c), sponge spicules (c)	Parallel lamination (mechanical), bioturbation	Normal marine open lagoon
Fine-medium crystaline dolomite - FMdol (D1)	Planar-e to planar-s mosaics	Dolomite crystals (10-80 µm)	Relics of sedimentary and microbial lamination, fenestrae	Early diagenetic replacement of calcareous facies
Coarse crystalline dolomite - Cdol (D2)	Planar-e to nonplanar-a mosaics	Dolomite crystals (80-250 µm)	Relics of faint sedimentary lamination, filled vugs	Early diagenetic replacement of calcareous facies

va very abundant, *a* abundant, *c* common, *r* rare

Dolomite texture classification according to Sibley and Gregg (1987)

Table 2 Synoptic description of the lithofacies of the Lower Cretaceous shallow-water carbonates of the Conocchia cliff

The stratigraphic succession outcropping on the Conocchia cliff (Figure 10) is mainly made up of gray limestones with frequent brownish dolomite caps, organized in beds bounded by discontinuity surfaces due to erosion or, more frequently, to emersion.

Bed thickness ranges from 4 to 160 cm, with a mean value of 31 cm. The succession starts with a m-thick dolomitic breccia level, made up of matrix-supported intraclasts, with both matrix and clasts dolomitized. This lithofacies could be interpreted as a solution-collapse breccia caused by the dissolution of evaporitic layers interbedded with dolostone beds (Assereto and Kendall, 1977; Eliassen and Talbot, 2005). However, this interpretation is not fully supported because in the investigated area there are no evidences of precipitation of primary evaporitic layers. On the other hand, considering that the clasts of the breccia level are monomictic, angular, heterometric and matrix-supported, and then show evidences of in-situ formation, this lithofacies could alternatively interpreted as the product of brecciation of dolomitic beds during a prolonged sub-aerial exposure. The succession continues with an about 50-meter-thick interval with a fairly high dolomitization intensity. The dominant lithofacies is the ostracodal mudstone-wackestone (Figure 12a), sometimes capped by partly to completely dolomitized microbial and fenestral laminated bindstone, suggesting that the depositional environment was a subtidal lagoon with restricted circulation, occasionally passing to a tidal flat. Several levels of miliolid-ostracode-algal wackestone-packstone (Figures 12b-d) and of foraminiferal wackestone or packstone-grainstone are interbedded to the restricted lagoon lithofacies, pointing to a sporadic emplacement of semi-restricted to normal circulation conditions within a lagoon. The following stratigraphic interval, about 40-m-thick, is characterized by a pronounced decrease of the dolomitization intensity. The lithofacies exhibit higher variability and the presence of semi-restricted to open lagoon facies (Figures 13a-d) is more frequent respect to the previous interval. This facies shift is coupled with the occurrence

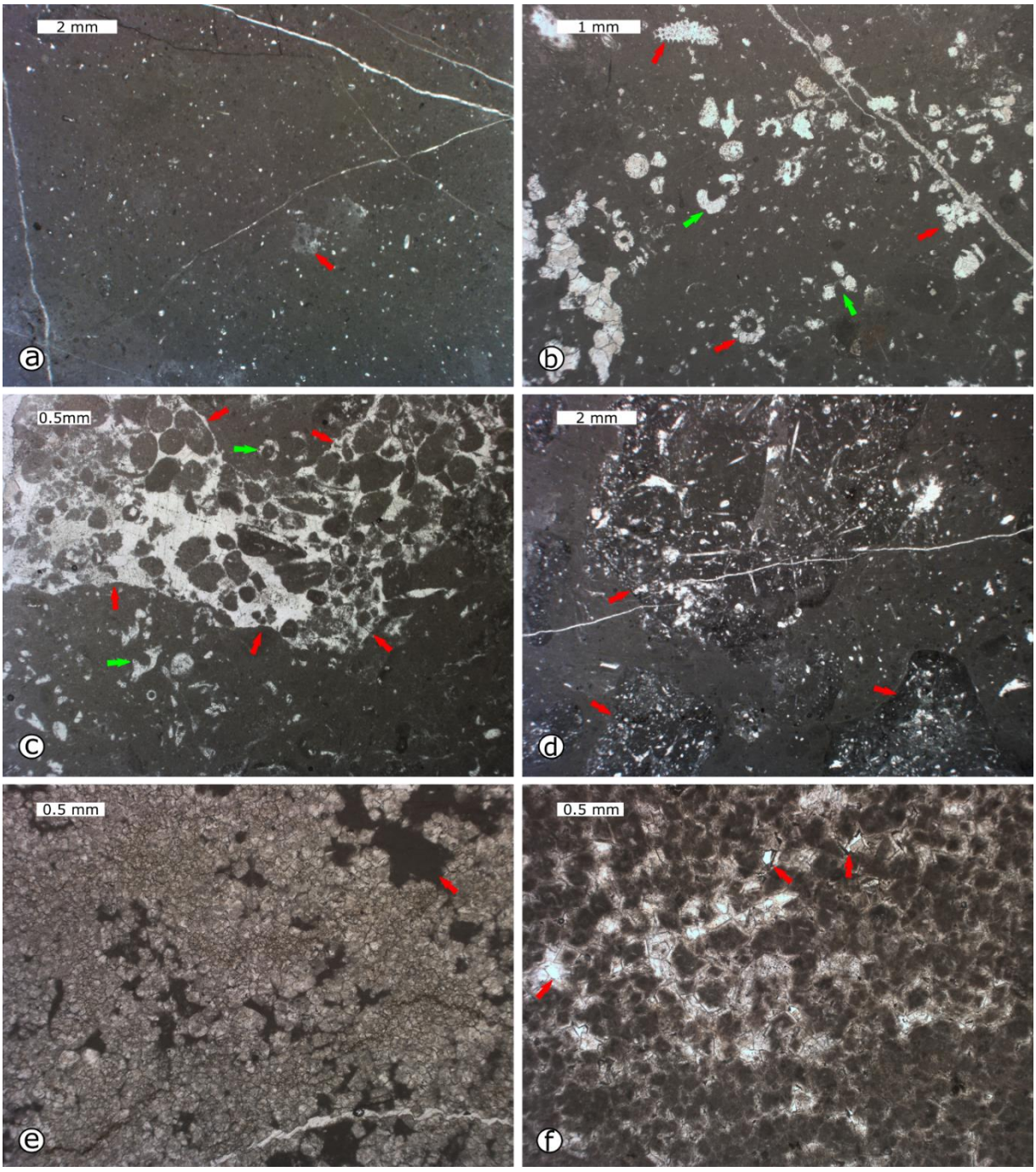

Figure 11 Microfacies of the Lower Cretaceous shallow-water carbonates of the Conocchia cliff: a) mudstone-wackestone with intraclasts and rare skeletal fragments, note some bioturbated area (arrow), thin section cc2/3.76; b) algal-intraclastic wackestone with fragments of Clypeina sp. (green arrows) and Salpingoporella sp. (red arrows), thin section cc2/3.5; c) algal-intraclastic wackestone with Clypeina sp. (green arrows), note the large bioturbation/burrow (red arrows pointing the boundaries) filled with an intraclastic grainstone/packstone, thin-section cc3/3.92; d) oncoidal wackestone with large Lithocodium (arrows) nodules, c1/89.5; e) fine-medium crystalline dolomite mosaic, note some preserved precursor mudstone (arrow), c1/124; f) coarse crystalline dolomite mosaic, note some preserved intercrystalline pores (arrows), thin section LM3.1.

of new taxa (e.g. *Vercorsella sp*.) and, overall, the assemblages of benthic foraminifers show higher diversity compared to the previous interval. All these evidences suggest a depositional environment dominated by a lagoon with semi-restricted to normal marine circulation. The

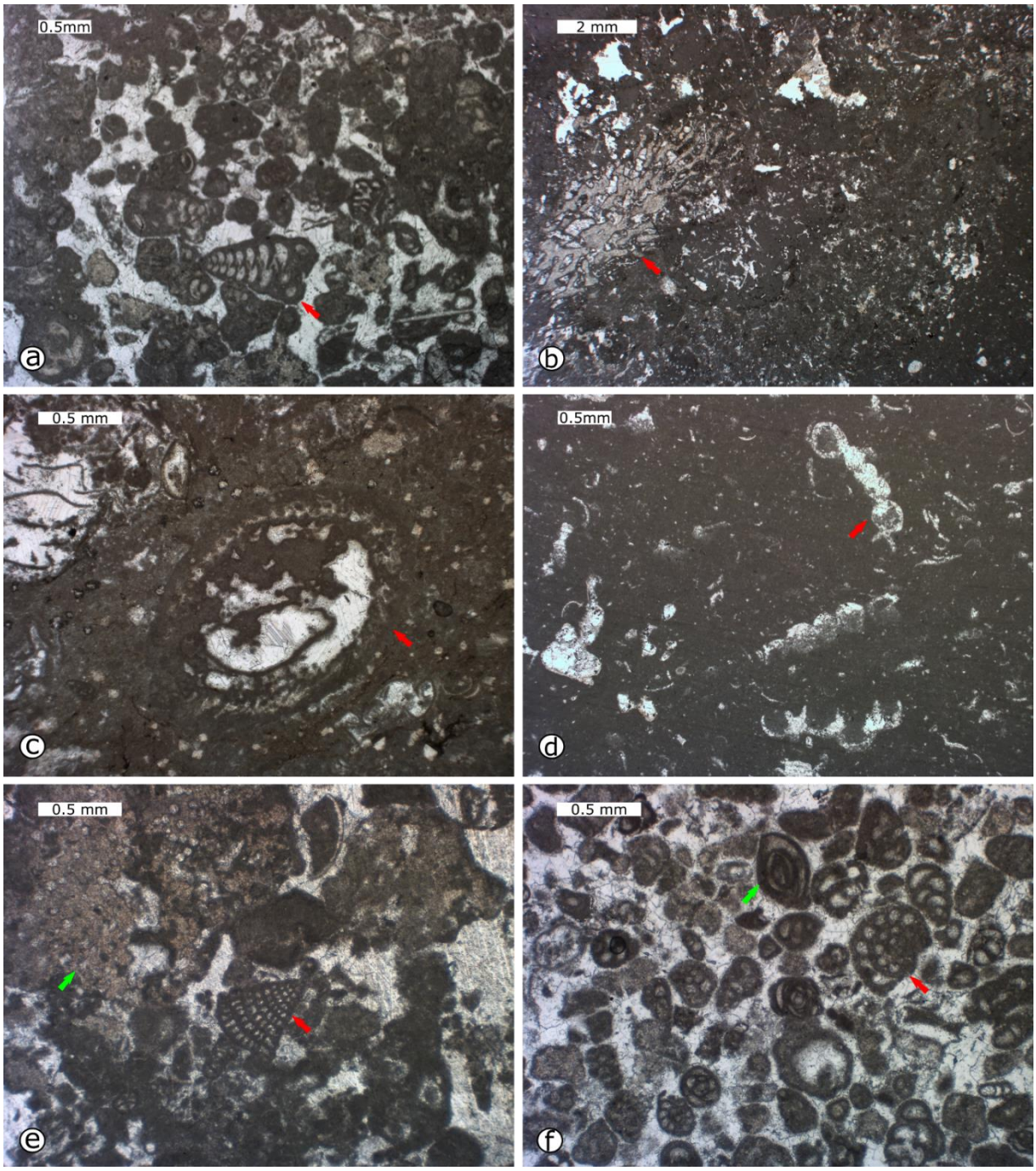

Figure 12 Microfacies of the Lower Cretaceous shallow-water carbonates of the Conocchia cliff: a) foraminiferal grainstone/packstone with Praechrysalidina infracretacea (arrow), thin section cc6/9.54; b) peloidal-intraclastic packstone/wackestone with Sarmentofascis zamparelliae (arrow), thin section cc6/10.72; c) algal wackestone with (?) Epimastopora cekici (arrow), thin section cc6/1.46; d) algal wackestone with Clypeina sp. (arrow), thin section cc6/8.48; e) foraminiferal packstone with Vercorsella sp. (red arrow) and undefined encrusting algae (?) (green arrow), thin section cc7/6.20; f) foraminiferal grainstone with Debarina sp. (red arrow) and miliolids (green arrow), thin section cc7/2.03.

last interval, about 35-m-thick, is mainly calcareous, except for the last few meters which are completely dolomitized. The lithofacies record a further shift toward more open marine circulation (Figures 13e-f), with a significative presence of grain-supported textures and high taxa diversity.

About the fossil content, the presence of *Praechrysalidina infracretacea* (LUPERTO SINNI) (Figure 13a), *Vercorsella scarsellai* (DE CASTRO), *Sabaudia sp*. and *Salpingoporella sp.* (Figure 12b), places the investigated section in the *Salpingoporella dinarica* biozone of De Castro (1991), which is dated as early Barremian to late Aptian. This biozone corresponds to a biostratigraphic interval straddling the *Cuneolina scarsellai* and *Cuneolina camposauri* biozone and the *Salpingoporella dinarica* biozone of Chiocchini et al. (2008). A more precise constraint on the age of the investigated interval can be obtained by estimating its stratigraphic position relative to the Orbitolina level, a well-known biostratigraphic marker of the Apennine Carbonate Platform. The Orbitolina level is exposed in the Mt. Faito ridge, west of the studied area. By graphical interpolation, its position can be projected eastward to a stratigraphic level lying about 50 m above the top of the succession of the Conocchia cliff. Considering that the Orbitolina level has been correlated to the upper part of the late Aptian *E. subnodosumcostatum* ammonite zone by carbon-isotope stratigraphy (Di Lucia et al., 2012), an age not younger than the early Aptian can be inferred for the top of stratigraphic succession outcropping on the Conocchia cliff.

4.1.2 The Basilicata subsurface

[Testo non disponibile in quanto relativo a dati protetti da segreto industriale]

4.2 Cyclostratigraphy and Sequence Stratigraphy

4.2.1 The Conocchia cliff

The analysis of lithofacies and their stacking pattern revealed that the Conocchia cliff succession is characterized by a hierarchy of sedimentary cycles expressed by systematic changes of bed thickness and lithofacies. Following the example of D'Argenio et al. (1997), the sedimentary succession can be then subdivided in elementary cycles, bundles (groups of elementary cycles) and superbundles (groups of bundles) (Figure 11).

The elementary cycle, normally corresponding to a single bed, is a meter-scale unit characterized by a succession of specific lithofacies and is normally bounded by a discontinuity surface, formed when a rapid facies change and/or a diagenetic contrast occurs (Clari et al., 1995; Hillgartner, 1998). In the investigated elementary cycles, discontinuity surfaces usually correspond to subaerial exposure surfaces that were lithified very early in their diagenetic history by interaction with meteoric fluids. Most of the observed cycles are subtidal "diagenetic" cycles, with subaerial exposure surfaces directly overlying subtidal deposits (Hardie et al., 1986). Peritidal cycles, with well-developed intertidal-supratidal facies (Strasser, 1991), are less frequent. In the rare cases when top cycles do not have clear exposure surfaces, but nevertheless show a shallowing upward lithofacies trend, the cycle boundaries are placed at the transition from the shallowing to the deepening shift (Amodio et al., 2013). Finally, if cycles do not exhibit significative lithofacies shift, and/or sedimentary structures and textures are completely obliterated by dolomitization, bed thickness variations are considered as a proxy for depositional settings. Indeed, according to D'Argenio et al. (2008), thicker cycles

implies a greater accommodation space and thus an open marine environment, while thinner cycles are associated with peritidal settings.

The elementary cycles are stacked into bundles, which are defined by the stacking pattern of the lithofacies associations, by the variation in the thickness of the elementary cycles and by the magnitude of the exposure surfaces. Lithofacies variations are usually combined with variation of dolomitization intensity (i.e. calcite/dolomite proportion) and cycle thickness. Thickest cycles at the base of the bundles are generally more calcareous, show normal marine subtidal lithofacies and are capped by poorly developed subaerial exposure surfaces. Thinnest cycles at the top of the bundles show more restricted subtidal facies and can be fully dolomitized (dolomite cap), with more pronounced evidences of subaerial exposure. According to Vinci (2015) and Vinci et al. (2017), who investigated the dolomitized bodies exposed in the Lower Cretaceous carbonates of Mt. Faito, the gradual decrease of dolomitization intensity from the top to the bottom of these cycles is due to a downward flow of dolomitizing fluids linked to the reflux (Adams and Rhodes, 1960) of mesohaline brines. In the Conocchia cliff section (Figure 11) groups of 3 to 8 elementary cycles form 67 bundles with an average thickness of 186 cm. Among these, 1 bundle clearly records a supratidal setting, 6 an intertidal setting and 56 a subtidal setting. The remaining 4 bundles were partially covered by vegetation and therefore was not possible to clearly identify the main depositional setting.

The same criteria have been applied to define sedimentary cyclicity at the superbundle scale. Superbundles are formed by the stacking of two to three bundles. A total of 30 superbundles (Figure 11), with an average thickness of 430 cm were identified in the studied section.

Sequence stratigraphy defines depositional systems and surfaces related to changes of eustatic sea level. The application of its concepts was first based and limited to the

interpretation of depositional geometries at the basin-scale (Van Wagoner et al., 1988; Emery and Myers, 1996) and identification of relative system tracts (Vail, 1987). When sequence stratigraphy is applied to shallow-water carbonate deposits, it must be considered that the typical geometry of system tracts could not develop, because these sediments accumulate mostly through vertical aggradation. However, features such as emersion and transgressive surfaces or facies changes can be recognized as well and be used to identify distinct system tracts (Strasser, 1994; D'Argenio et al., 1997). In particular, transgressive and regressive facies trends may be considered equivalent to transgressive and highstand system tracts (Amodio et al., 2013). Using this approach, it is possible to analyze the three levels in which the cyclicity was recognized (namely the elementary cycles, bundles and superbundles) in terms of sequence stratigraphy and, on the basis of their hierarchical organization, consider elementary cycles equivalent to 6th order cycles, bundles to 5th order cycles and superbundles to 4th order cycles (*sensu* Vail et al., 1991) (Figure 14).

6th order cycles represent the elementary sequences (*sensu* Strasser et al., 1999), and show a facies evolution corresponding to the shortest recognizable cycle of environmental change. 5th and 4th order cycles (respectively equivalent to bundles and superbundles) particularly exhibit clear sequence boundaries, maximum flooding surfaces and system tracts (Goldhammer et al., 1990; Schlager et al., 1994). Relative sequence boundaries (SB) correspond to bundle and superbundle limits, while the maximum flooding surfaces (MFS) may be located where the most open marine lithofacies of each cycle occurs, normally developed within the thickest elementary cycles (D'Argenio et al., 1999). Transgressive system tracts (TST) are characterized by open lagoon lithofacies associated to a thickening upward of stacked cycles. In contrast, the highstand system tracts (HST) are characterized by an increase in dolomitization intensity, shallower depositional settings and thinning upward of stacked

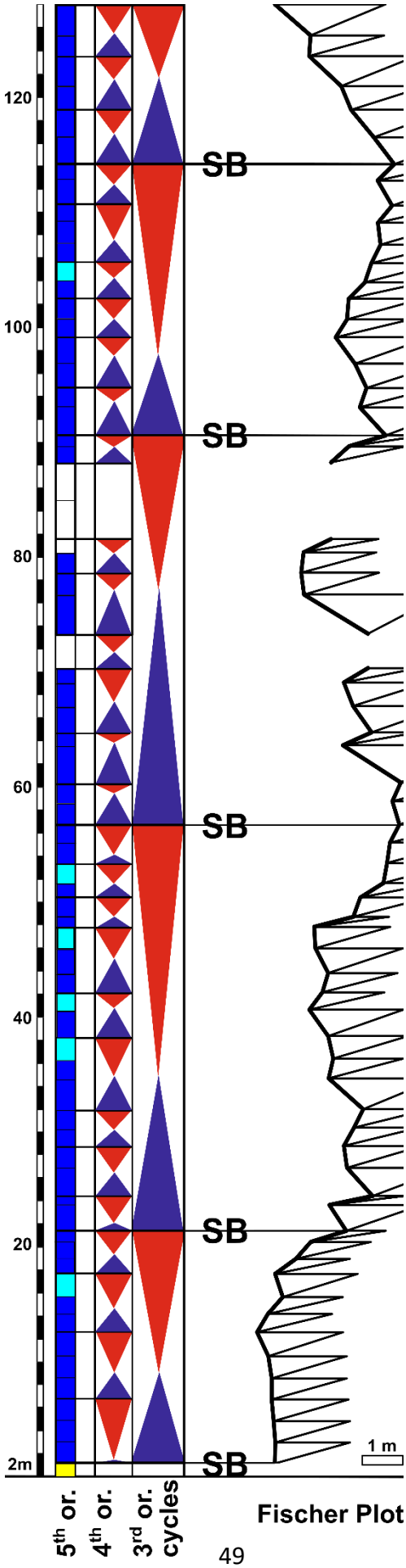

Figure 13 Sequence stratigraphic interpretation of sedimentary cyclicity of the Conocchia cliff and Fischer plot used to extract low-frequency cycles (3rd order sequences). See Figure 4.2 for the legend.

cycles. Lowstand system tracts (LST) are missing, as it commonly occurs in shallow-water carbonate platforms, because the accommodation space is low (Strasser et al., 1999).

Regular changes of facies and thickness of high-frequency cycles superimposed on low-frequency cycles of relative sea-level changes are well known in Mesozoic carbonate platforms (D'Argenio et al., 1999; Strasser et al., 1999). In order to extract these low-frequency cycles (3^{rd} order sequences) from the stratigraphic record and highlight cycle hierarchy, the number and thickness of 5^{th} order cycles have been used to build a Fischer plot (Fischer, 1964) (Figures 14 and 15). Fischer plots are a graphical method to define changes in accommodation space and identify depositional sequences on carbonate platforms, by plotting cumulative departure from mean cycle thickness as a function of time (Read and Goldhammer, 1988) or cumulative stratigraphic thickness (Day, 1997). The resulting plot is a curve that, in peritidal shallow-water carbonates, can be used to evaluate the magnitude of 3^{rd} order sea-level fluctuations and correlate multiple stratigraphic sections (Read and Goldhammer, 1988).

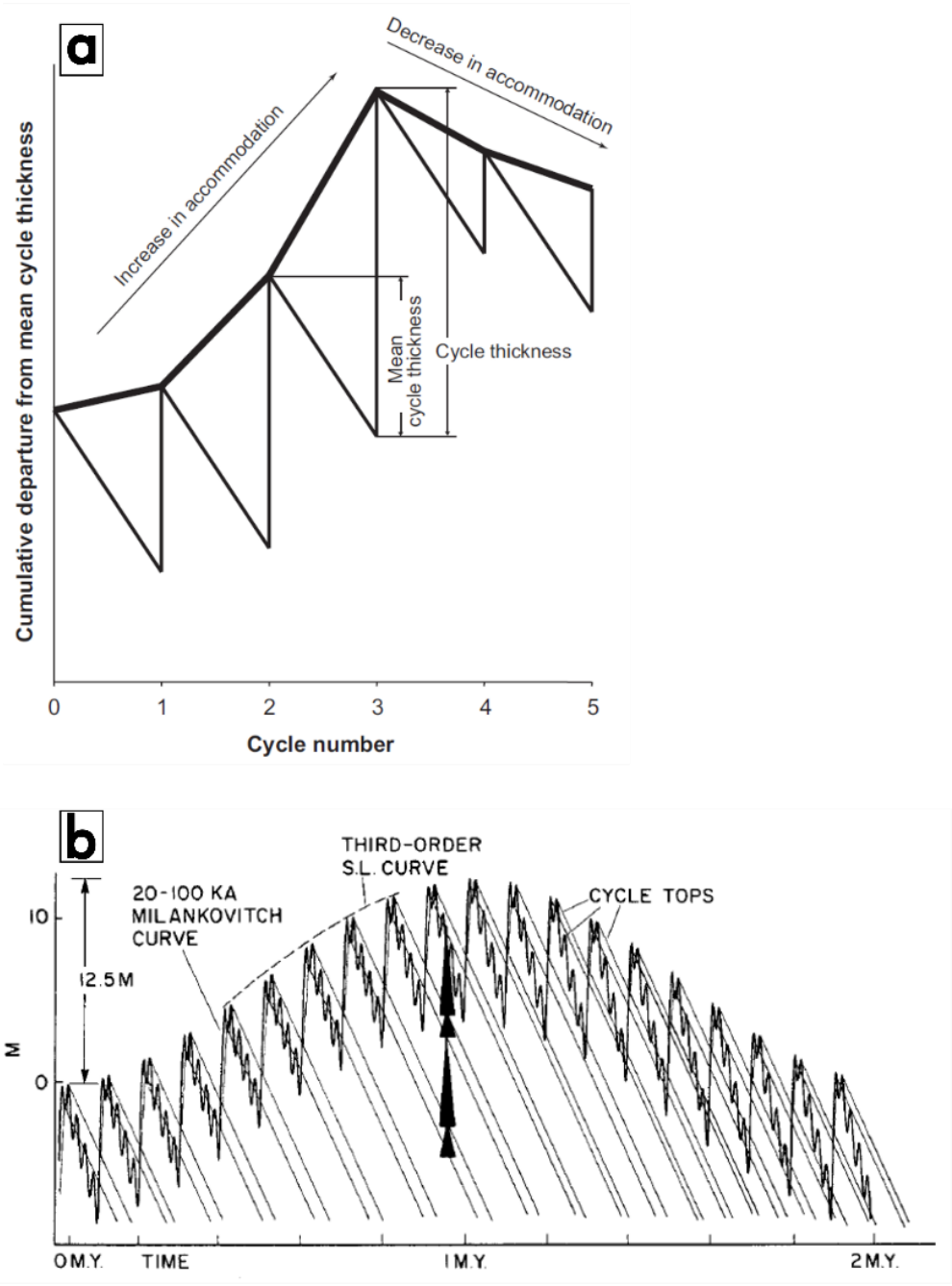

Figure 14 a) Portion of an example of Fischer Plot showing changes in accommodation space (vertical axis) as a function of cycle number (horizontal axis). Thin vertical lines are individual cycle thicknesses. Increase in accommodation is shown by thick line sloping up to the right (from Husinec et al. 2008); b) example of Fischer plot showing the extraction of third-order sea-level curve from the 20-100 ka oscillations (5th order cycles). Changes in accommodation space (vertical axis) are shown as a function of time (horizontal axis) (from Read and Goldhammer, 1988).

The Fischer plots presented in this study have been built using the excel spreadsheet macro "FISCHERPLOTS" published by Husinec et al. (2008). This spreadsheet requires the thickness of each 5th order cycle and the number and thickness of possible gaps in the stratigraphic

section. The output is a computation of the average cycle thickness and a plot of a curve showing the cumulative departure from the average cycle thickness as a function of cycle number or stratigraphic thickness (Figure 15). The cumulative effect of progressive changes in thickness of 5th order cycles allows to identify the 3rd order system tracts of the section (Read and Goldhammer, 1988). The cycles that plot on the rising part of the 3rd order deviation (peaking at maximum positive departure) compose the transgressive system tract. Cycles that plot on the falling limb of the 3rd order deviation constitute the highstand system tract, culminating in a SB.

The Fischer plot curve of the Conocchia cliff, coupled with field observations, allowed to recognize four complete 3rd order sequences bounded by five SBs (Figure 14). Their stratigraphic thickness ranges from 20 m to 36 m, the average value is 27 m. Considering the architecture of the transgressive/highstand system tracts, it appears that the transgressive system tracts are characterized by asymmetric superbundles with more pronounced deepening trends, higher limestone/dolostone ratio, more open marine facies and thicker elementary cycles; while the highstand system tracts are characterized by asymmetric shallowing-upward superbundles with lower limestone/dolostone ratio and thinner elementary cycles.

4.2.2 The Basilicata subsurface

[Testo non disponibile in quanto relativo a dati protetti da segreto industriale]

4.3 Mechanical stratigraphy

4.3.1 The Conocchia cliff

The analysis of fracture distribution within the Conocchia succession is based on the dataset acquired by Corradetti (2016), who performed a structural study of the cliff using a VOM (Conocchia cliff – Old Survey, Table 1) obtained by SfM photogrammetry (see Chapter 3.2 for a detailed description of the used materials and methods). Fracture and bedding attitude extraction was performed using OpenPlot (Tavani et al., 2011, 2014), an open source software for structural analysis in a 3-D environment, by manual digitization of points along the traces of the intersections between outcrop topography and fractures and bedding. 1003 through-going fractures and 20 bedding attitudes were digitized and analyzed (Figure 19). More

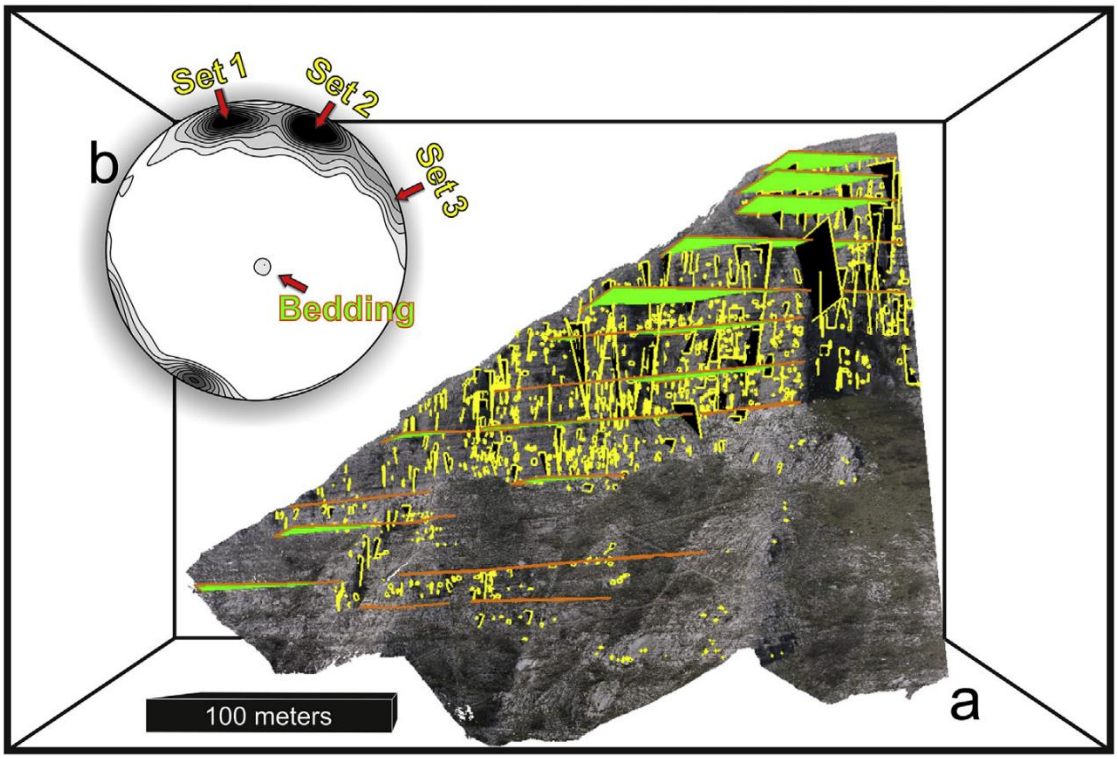

Figure 15 a) Perspective view of the Conocchia virtual outcrop model from the south, showing digitized fractures (black rectangles with yellow borders) and bedding surfaces (green rectangles with orange borders). b) Contour plot showing three sets of fractures and a tight cluster of bedding planes. From Corradetti et al. 2018.

fractures were present along the outcrop, but all fractures smaller than 2 m were filtered and

deleted in OpenPlot before data analysis. This prevented working with a fracture population down-sampled because of the model resolution. The filter was applied to the perimeter of the digitized fractures (which are polygons in 3D), and all fractures owing a perimeter of less than 4 m were removed. Contour plot shows that poles to bedding form a tight cluster indicating gentle dips towards the NW (mean bedding has a strike of 246° and a dip of 9°). Contouring of poles to digitized fracture planes shows that these structures are distributed around three clusters (Figure 19b). The fractures, at high angle to bedding, are oriented mostly ENE-WSW (Set 1), ESE-WNW (Set 2) and NNW-SSE (Set 3). Fractures belonging to Set 3 are oriented at high angle to the cliff and thus are the least affected by biases. For this reason, they have been filtered (Figures 20a-b) and projected independently from the other fracture sets onto an orthorectified panel (Figure 20c), perpendicular to both fracture direction and bedding dip direction. Projected features were saved in *.svg format and hence ready to be opened by

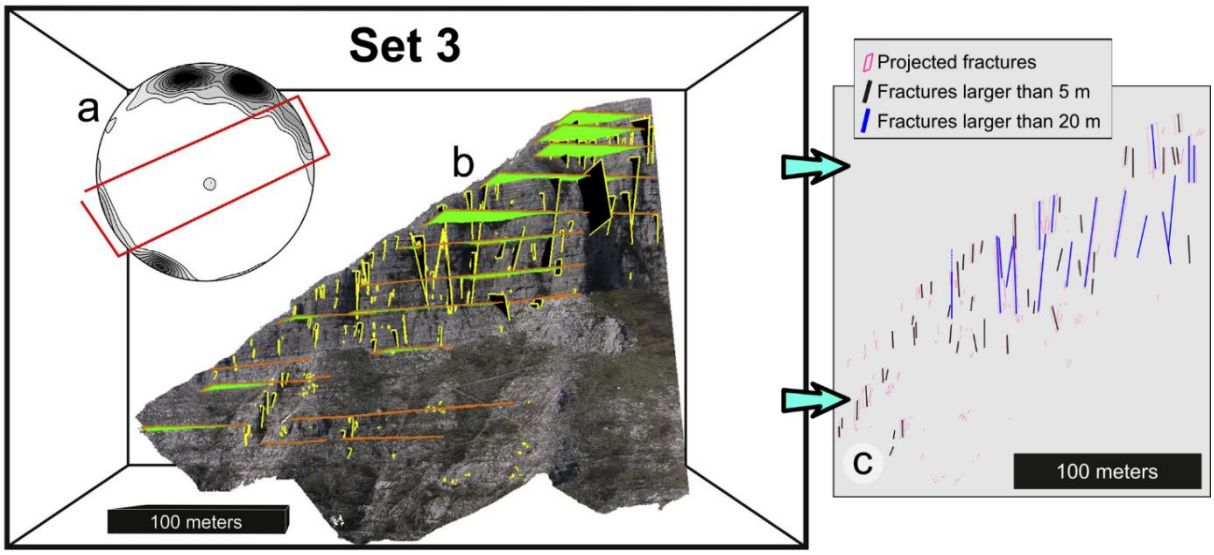

Figure 16 a) Selection of the Set 3 cluster on the stereonet using OpenPlot; b) Visualization of the selected cluster in the 3D environment; c) Projection of the selected cluster on an orthorectified panel (modified from Corradetti et al. 2018).

any vector drawing software. Because not all the joints and bedding surfaces were perfectly oriented with respect to the direction of projection, being distributed around the related maxima, some of the projected planes constituted thin polygons rather than lines. Hence projected joints were manually re-digitized using Inkscape™, a free and open-source vectorial

graphic software. From this perspective it was then possible to identify mechanical boundaries, which are layers where major fractures arrest on, and hence to schematize mechanical units between them. As a final result, Corradetti (2016) identified several boundaries able to arrest the propagation of through-going fractures, two of which were particularly efficient, by ensuring the arrest of 100% of fractures (Figure 21).

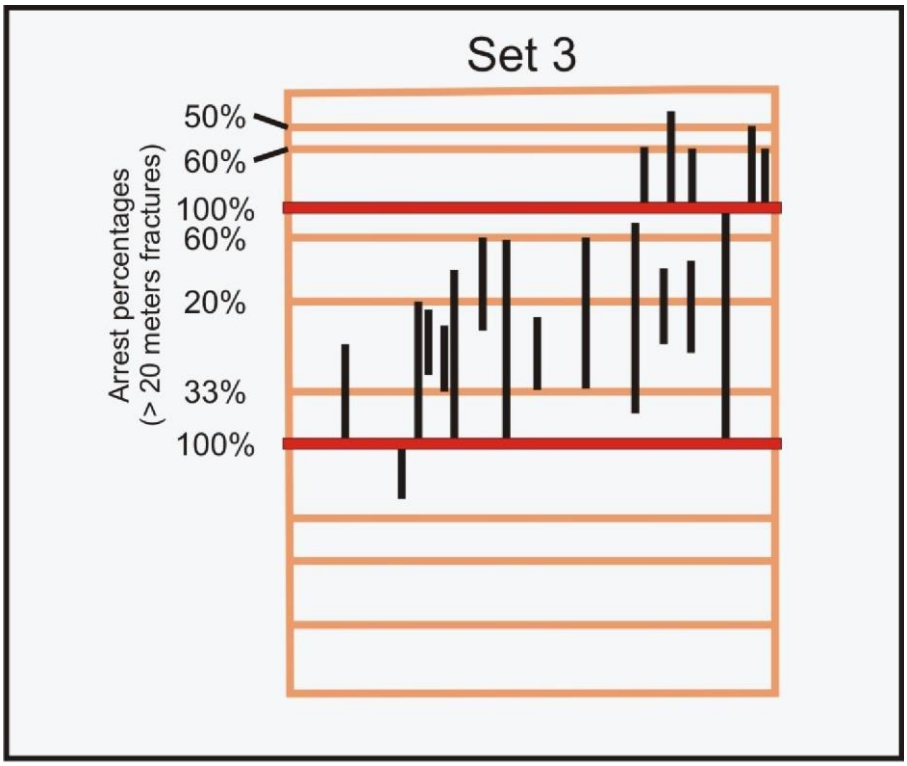

Figure 17 Synthetic representation of the mechanical stratigraphy of the Conocchia cliff for fractures larger than 20 meters belonging to Set 3. Thick red lines highlight the two main boundaries arresting fracture propagation (from Corradetti, 2016).

In order to better understand the role of these boundaries in the mechanical stratigraphy of the cliff and the parameters controlling their effectiveness, during this study was performed a new, high-resolution structural analysis of the two main mechanical boundaries identified by Corradetti (2016). A new VOM of the Conocchia cliff was built, with a resolution considerably higher than the previous one, and two panels were analyzed, corresponding to the upper boundary and to a portion of the lower mechanical boundary (Figure 22). Using

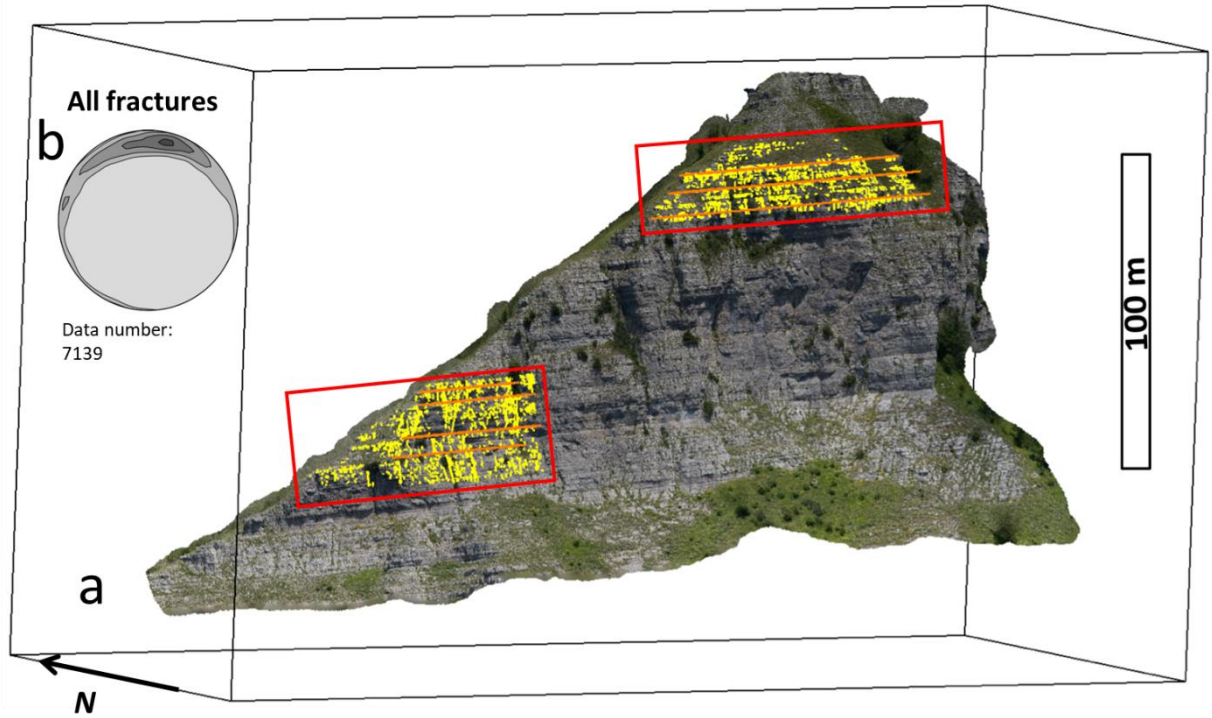

Figure 18 a) VOM of the Conocchia cliff – New Survey: yellow lines represent the digitized fractures, orange lines represent the digitized bedding attitudes, red rectangles indicate the panels analysed during the high-resolution structural analysis.

OpenPlot, were manually acquired 7132 fractures and 7 bedding attitudes. All fractures larger than 1 m were filtered and, as a result, only 683 fractures were considered in the further steps of the analysis (Figure 23c). Contouring of poles to digitized fracture planes shows a distribution consistent with the results of the previous study (Figure 23c). Indeed, can be recognized the same 3 sets, respectively oriented ENE-WSW (Set 1), ESE-WNW (Set 2) and NNW-SSE (Set 3), plus another cluster of fractures oriented NNE-SSW (Set 4). The fracture dataset acquired during this study has been merged with fractures from the previous survey (Corradetti, 2016) in order to perform a multi-scale analysis of the outcrop and evaluate the observation-scale effect on the acquisition of structural data (Figures 23a-b).

For the same purpose were made some field measurements along the slope at the western flank of the Conocchia cliff and in some adjacent exposures of the studied succession (Figures 24 and 25). The collected fractures appear as confined by bedding and by laterally discontinuous, internal bedding-parallel sedimentary or diagenetic discontinuities, such as

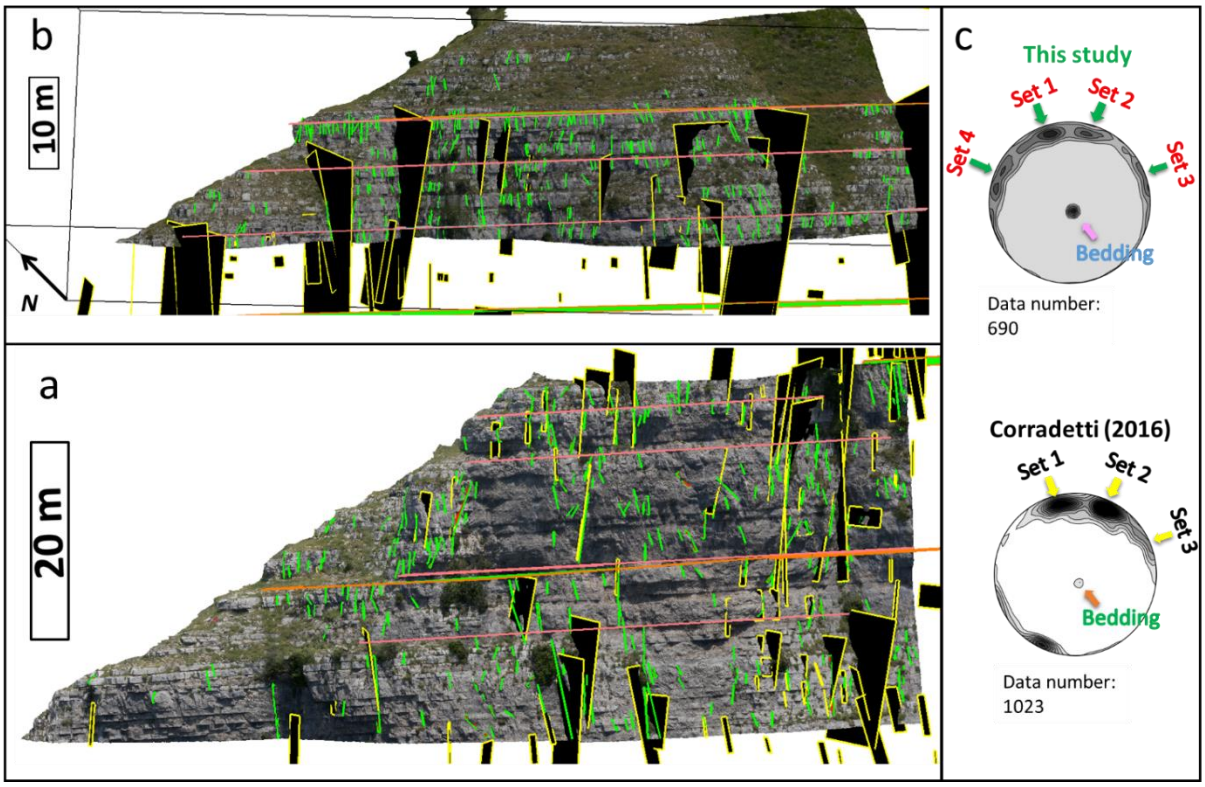

Figure 19 VOM of the Conocchia cliff – New Survey. Fractures (red rectangles with green borders) and bedding attitudes (rectangles with pink borders) acquired on the lower (a) and upper (b) panels of the new VOM were merged with fractures (black rectangles with yellow borders) and bedding attitudes (green rectangles with orange borders) acquired by Corradetti (2016). c) Contour plots showing fracture clusters recognized during this study and by Corradetti (2016).

stromatolitic/microbial planar to wavy laminations, stylolites and dolomite seams (Tavani et al., 2016b).

Digitized fractures from the 2016 survey (Corradetti, 2016) have been used for a spatial distribution analysis at the platform scale. Fractures filtered as Set 1 and Set 2 show parallelism with the outcrop topography. For this reason, only fractures clustered around Set 3 are suited for spacing analysis. The panel oriented perpendicular to this set has been used to evaluate the distribution of fractures over the layers of the outcrop. This step consisted in the collection of fracture spacing values, for fractures higher than 2 m, every 2 m of stratigraphy. In this way, was obtained a panel of fracture number and fracture intensity, which is the number of intersected fractures per unit length (Figure 26a). The average and median of the spacing along the stratigraphy was also obtained (Figure 26b). On the basis of these results, the outcrop stratigraphy was divided in mechanical units (*sensu* Bertotti et al.,

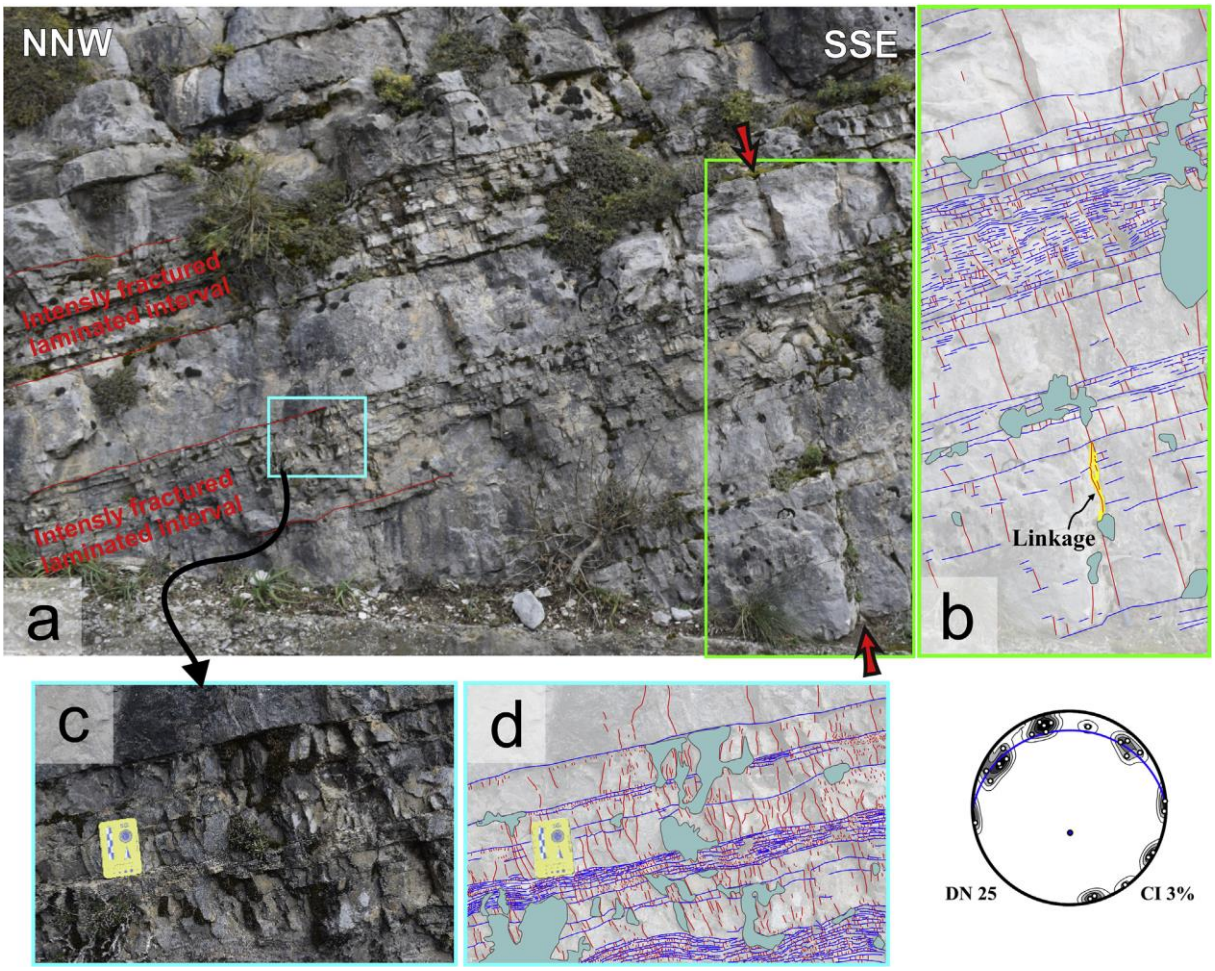

Figure 20 (a) Field example and (b) line-drawing of an incipient through-going fracture formed by linkage of pre-existing layer-bound fractures perpendicular to bedding. This through-going fracture is well defined within thick strata, while it is not visible/recognizable within the thinly layered and intensely fractured strata package. (c) Magnification and line-drawing (d) of one of these intensely fractured packages where major through-going fractures are not able to propagate as single and well-defined elements. These thinly stratified layers are so intensely fractured that most of the fractures are shorter than the thickness of the lines drawn. Orientation data are given in stereographic equal-area projections of frequency contour of poles to planes. Blue great circles are reference bedding. DN and CI refer to data number and contouring interval, respectively. From Corradetti et al. (2017).

2007) based on clear variations of fracture intensity and spacing, as indicated by horizontal green and grey lines in Figure 26. Intervals with low data number are not considered. These lines were drawn with thickness of 1 and 4 m, respectively, to incorporate different sources of error including: (i) the resolution of the mesh, (ii) the uncertainty in positioning the tip of the digitized fractures, and (iii) the uncertainty in assigning the stratigraphic elevation to a given layer.

Finally, to investigate the relationship between lithological properties and fracture distribution, the cumulative stratigraphic thicknesses were calculated for each rock texture

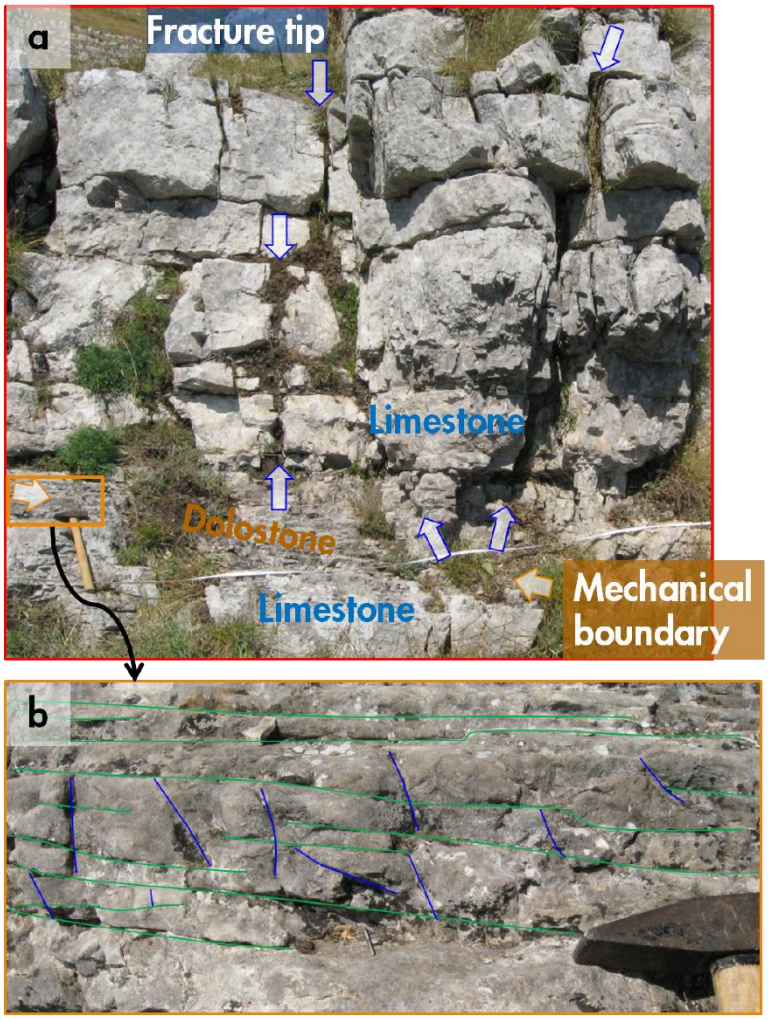

Figure 21 a) Field example of a thinly bedded dolostone level acting as a mechanical boundary. Fractures cross thicker beds and abut against this level; b) close-up of the mechanical boundary. Cm-spaced fractures (blue lines) are confined between bedding surfaces (green lines).

and depositional environment recognized within each mechanical unit. The results are presented as distinct pie charts showing the relative abundance of each texture and facies (Figure 26c).

4.3.2 The Mt. Catiello

In order to verify and compare the results obtained at the Conocchia cliff, the study of reservoir-scale fracture distribution has been extended to a further outcrop exposing the same stratigraphic succession: the Mt. Catiello peak.

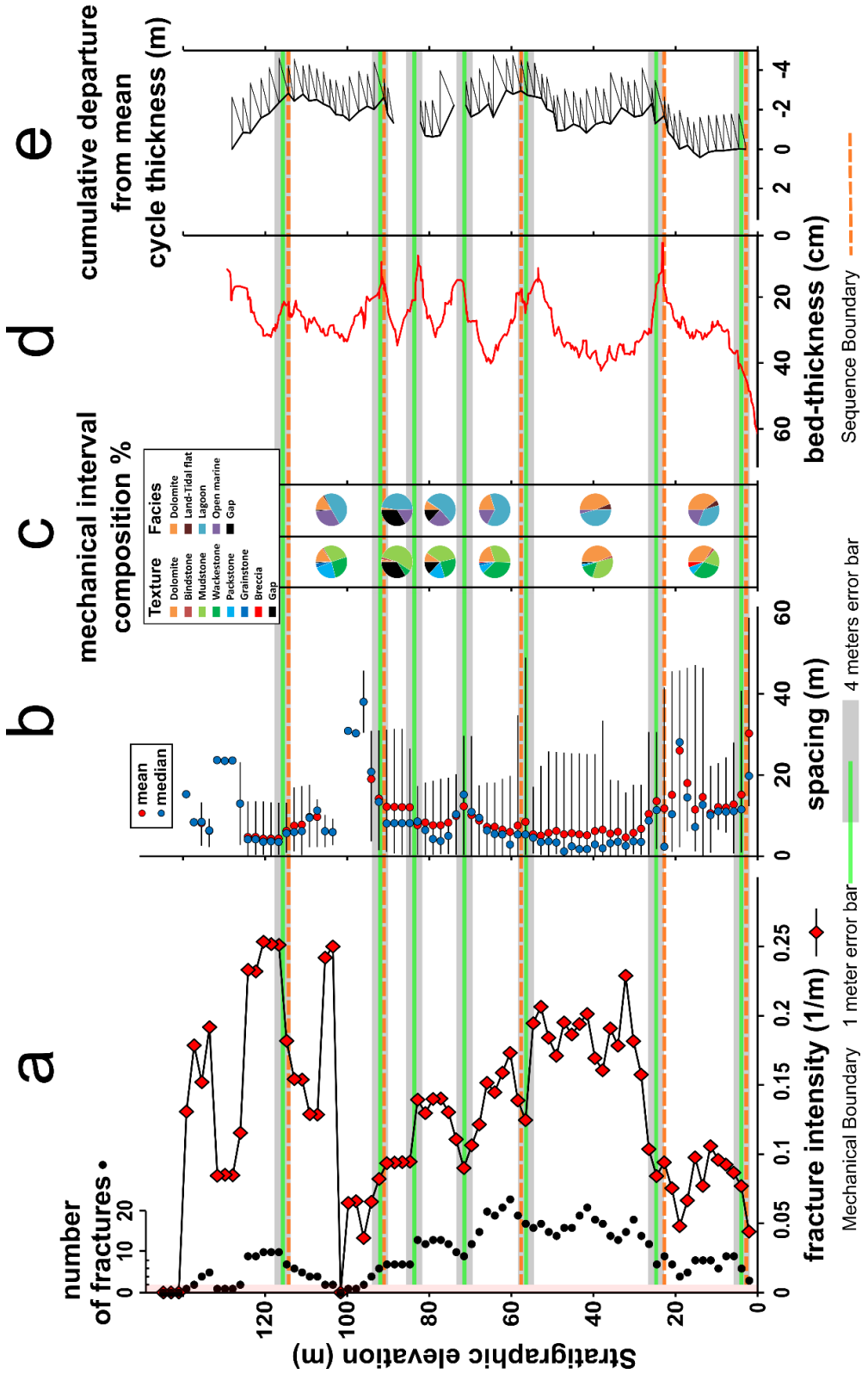

Figure 22 a) Number of fractures and fracture intensity (m^{-1}) for Set 3; b) mean and median spacing. Horizontal green and grey lines correspond to zones of clear variations of fracture intensity and spacing, and separate distinct mechanical units. c) Sedimentary texture and facies relative abundance within the mechanical units; d) bed-thickness variation; e) Fischer plot; orange dashed lines correspond to SBs and are plotted for comparison with mechanical boundaries.

Following the same approach described for the study of the Conocchia cliff, fracture and

bedding attitudes were extracted from a new VOM (Mt. Catiello, Table 1, Figure 27) using OpenPlot (Tavani et al., 2011, 2014). In this way, 9643 georeferenced structural discontinuities

Figure 23 View from SSW of the Mt. Catiello VOM

(meters-long faults, through-going fractures and fractures, collectively named as fractures) and 22 bedding attitudes were digitized and analyzed (Figure 28). More discontinuities were present along the outcrop, but fractures below the meter scale were not considered due to the model resolution.

The analysis highlighted that the structural architecture of the investigated outcrop is characterized by the presence of a fault system consisting of four high-angle faults (Figure 28a), each of them formed by various fault strands, which are roughly oriented N-S. The fault crossing the upper part of the model shows on his plane some dextral slickensides that suggest

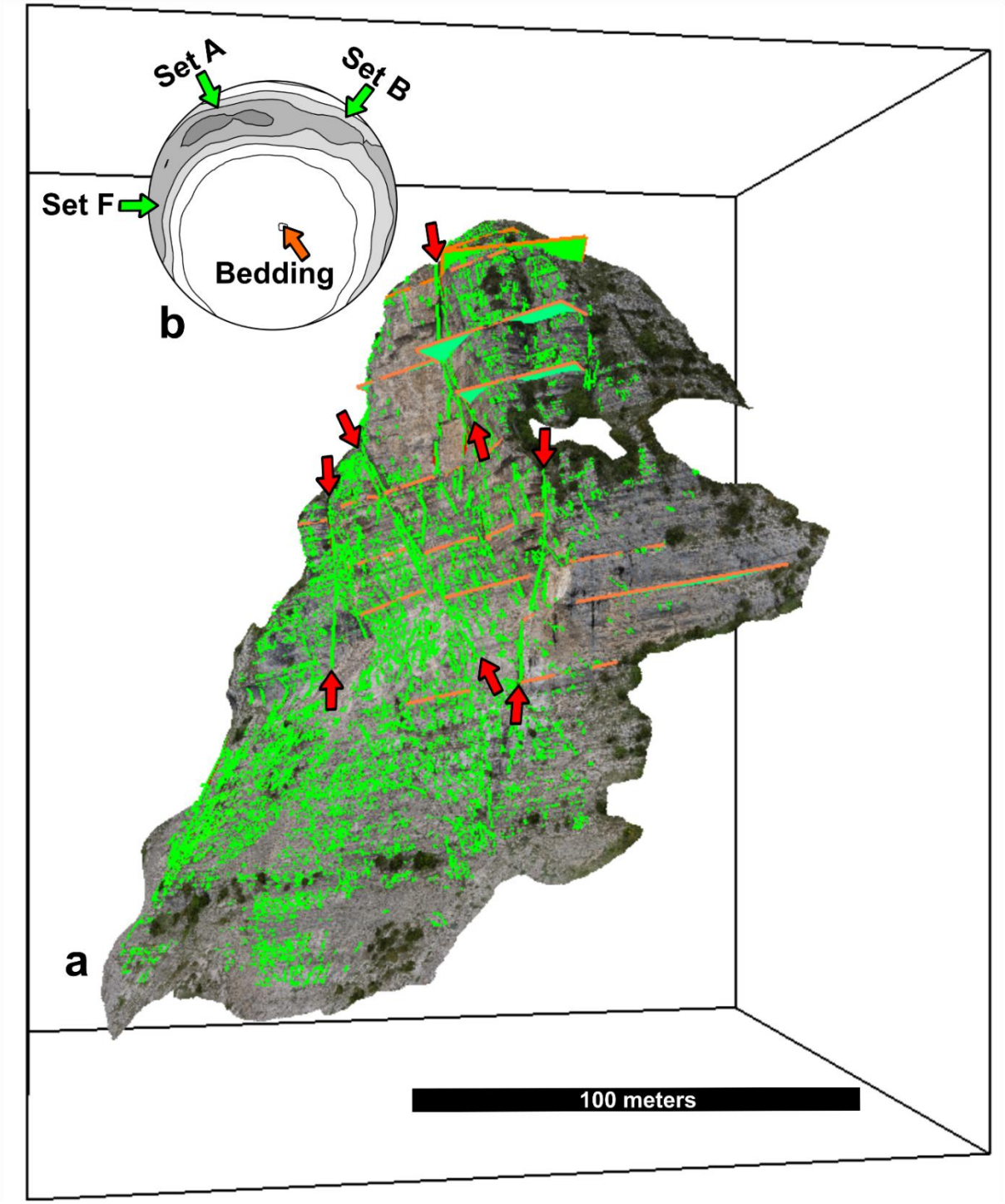

Figure 24 a) Perspective view from SSW of the Mt. Catiello VOM wih digitized fractures (rectangles with green borders) and bedding planes (rectangles with orange borders), red arrows point the tips of the main N-S trending faults; b) contouring plot showing two fracture sets (Set A and B), the trend of the main faults (Set F) and a cluster of bedding planes.

a dominant strike-slip component and a minor dip-slip component. The observed stratigraphic heave, in the various fault strands, ranges from a few centimeters to a few meters. As shown in the contour plot (Figure 28b), in addition to N-S oriented fractures (Set F) – strike-parallel to the main faults – two more cluster of poles to digitized fractures planes are recognized,

both at high angle to bedding, and oriented respectively NE-SW (Set A) and NW-SE (Set B). Poles to bedding, instead, form a cluster indicating dips mostly towards the NW.

The dimensional parameters of these sets were separately analyzed. For this purpose, each fracture set was selected by drawing a polygon directly in the stereonet and was independently visualized in the 3D environment (Figures 29b, 30b and 31b). This procedure allowed to easily and quickly select the fractures of interest and visualize them in 3D, in order the to better understand their orientation with respect to the model. For each fracture set was identified the average direction of intersection between the fractures and the bedding surfaces. These directions were then used to project each fracture set onto a perpendicular plane. The results are three orthorectified panels, which represent the less distorted feasible way to evaluate the distribution of the digitized fractures filtered by orientation. Obviously, not all the discontinuities were perfectly oriented with respect to the direction of projection, but being distributed around the related maxima, some of the projected planes constitute thin polygons rather than lines. To tackle this issue, that would preclude a correct evaluation of the dimensional parameters of discontinuities, a new feature was added to OpenPlot. The upgraded version of the software is now able to automatically draw and show only the major axis of a projected plane, avoiding the need of manual re-digitization of structural discontinuities, a time-consuming step required by the previous workflow (Corradetti, 2016; Corradetti et al., 2018). Once that these new orthorectified panels were obtained, the distribution of fractures has been evaluated by means of linear scan-lines, as done for the Conocchia cliff. However, due to the more complex structural architecture of the outcrop and to its irregular topographic surface (a pyramid-shaped peak), the results of the analysis were neither meaningful nor satisfying.

This first failure pushed to find a different solution and to create a new workflow for the

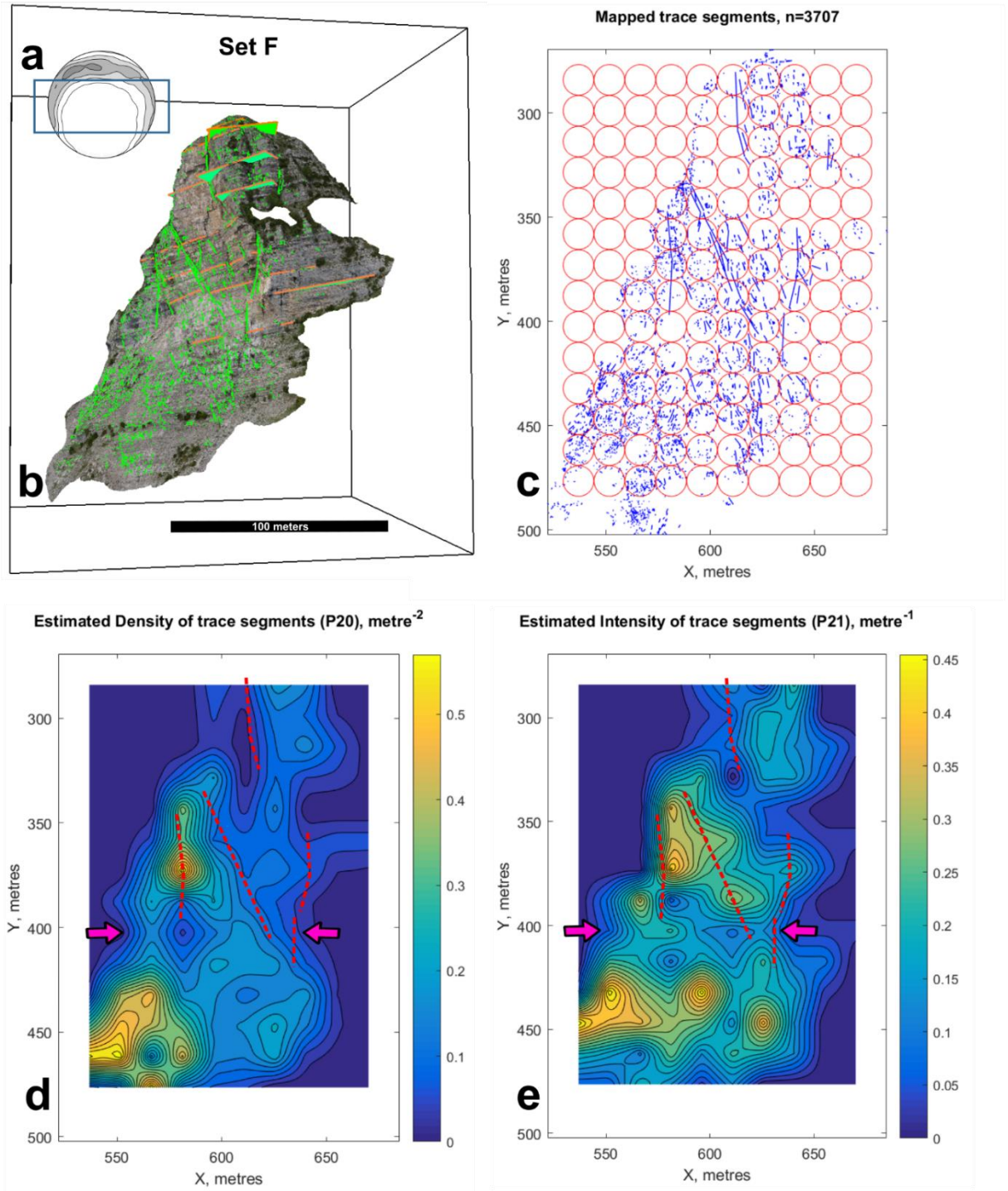

Figure 25 a) Contour plot, the polygon shows the selected fracture set; b) perspective view from SSW of the Mt. Catiello VOM with N-S trending selected fractures (rectangles with green borders) and bedding planes (rectangles with orange borders); c) orthorectified fracture trace map showing the locations of the scan circles used to estimate intensity and density; spatial density maps of estimated density (d) and estimated intensity (e) of fracture traces. Red dashed lines show the main fault traces. Pink arrows point the main mechanical boundary.

quantification of fracture patterns, suited to outcrops with a complex structure and/or topography.

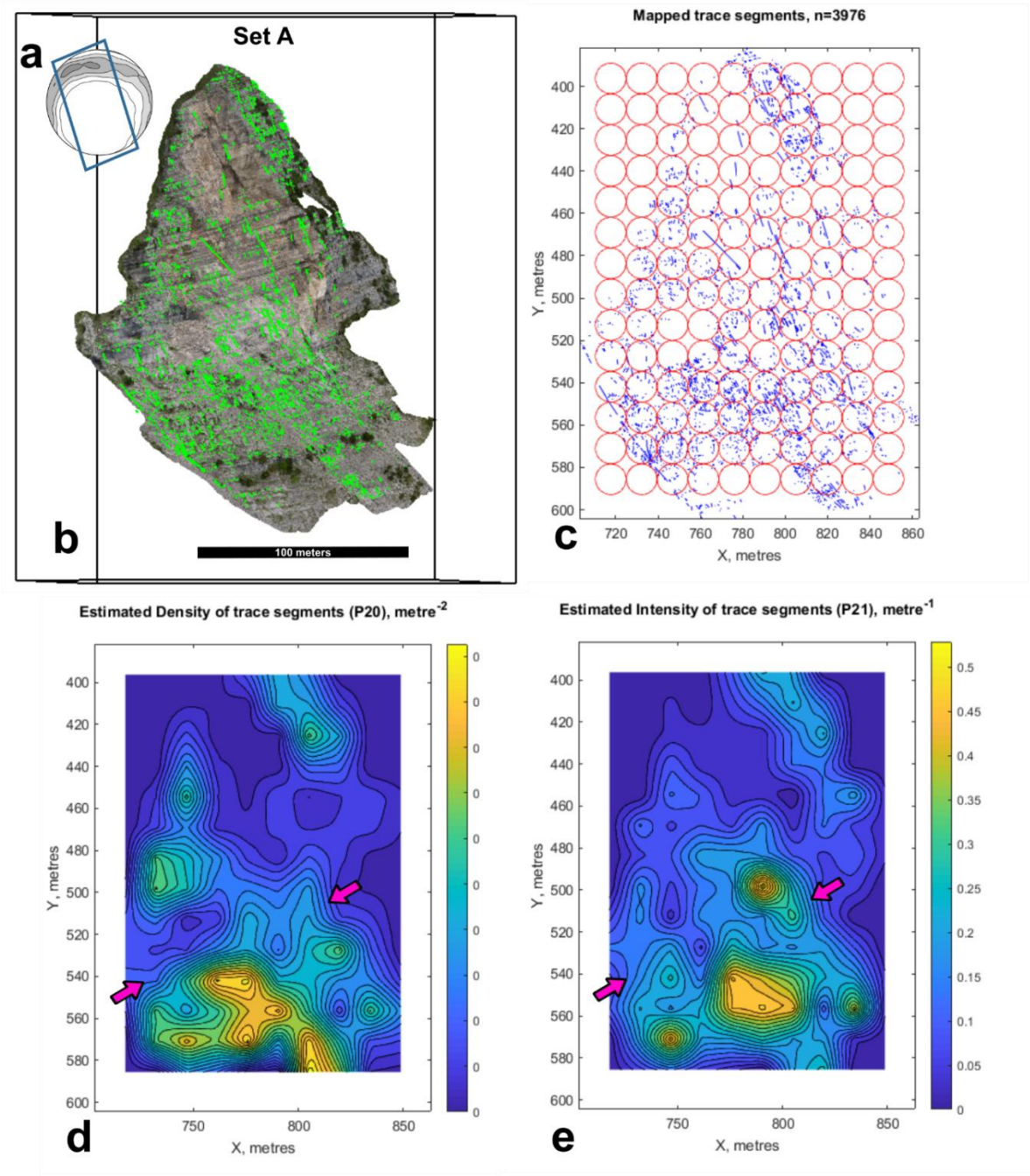

Figure 26 a) Contour plot, the polygon shows the selected fracture set; b) perspective view from WSW of the Mt. Catiello VOM with selected fractures (rectangles with green borders) and bedding planes (rectangles with orange borders); c) orthorectified fracture trace map showing the locations of the scan circles used to estimate intensity and density; spatial density maps of estimated density (d) and estimated intensity (e) of fracture traces. Pink arrows point the main mechanical boundary.

The orthorectified panels showing 2D fracture traces, were exported from OpenPlot as a scalable vector graphics file (.svg) and used as the input file for FracPaQ, an open-source, cross-platform and freely available MATLAB™ toolbox designed to quantify fracture patterns in two dimensions (Healy et al., 2017).

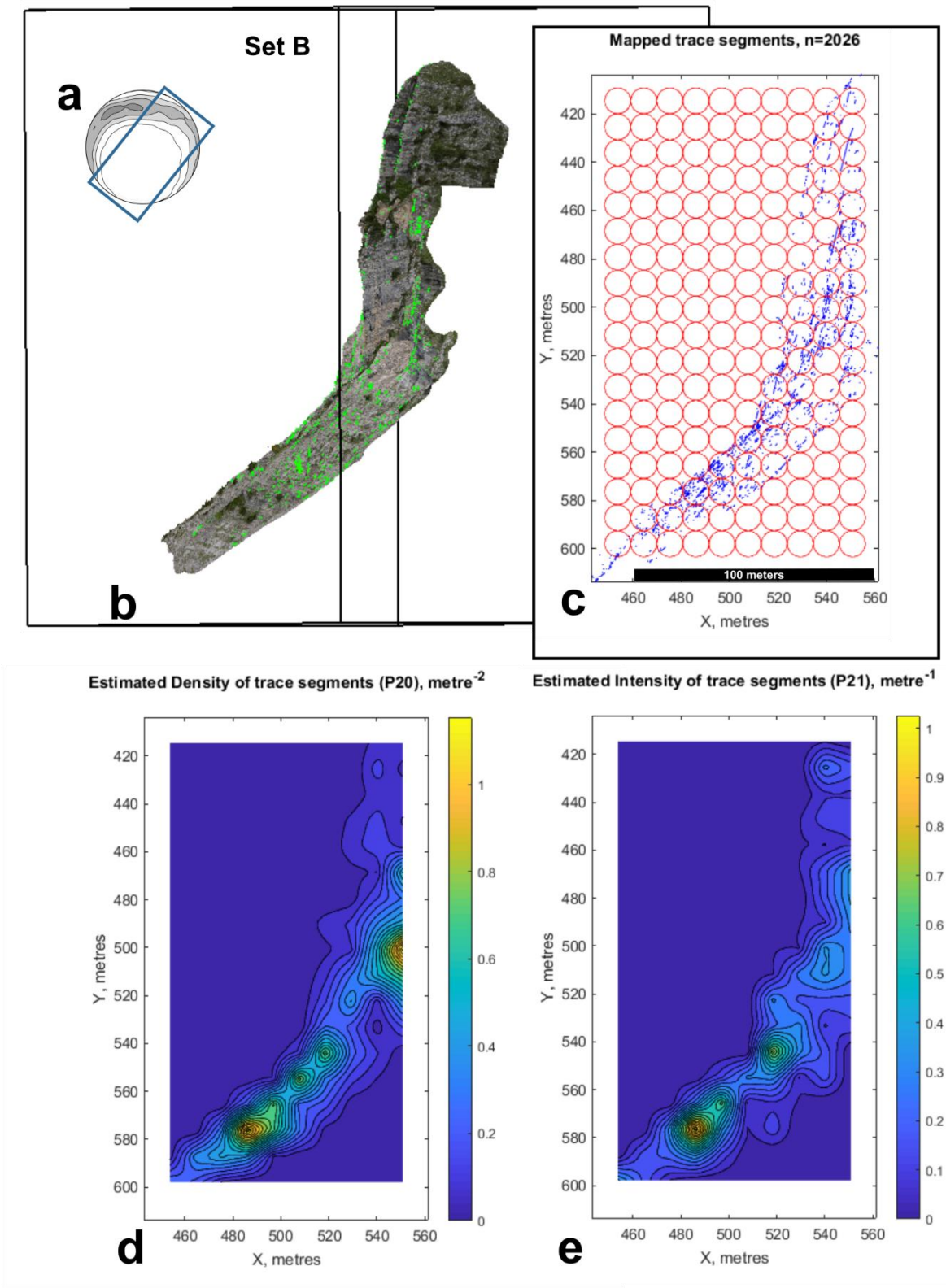

Figure 27 a) Contour plot, the polygon shows the selected fracture set; b) perspective view from SSE of the Mt. Catiello VOM with selected fractures (rectangles with green borders) and bedding planes (rectangles with orange borders); c) orthorectified fracture trace map showing the locations of the scan circles used to estimate intensity and density; spatial density maps of estimated density (d) and estimated intensity (e) of fracture traces.

Density (P20) and intensity (P21) spatial maps of the fracture patterns, as well as fracture trace maps with the location of scan circles used in the calculations, were produced for each orthorectified panel (see Chapter 3.2.3 for detailed information about the used method). The number of circles is set at 10 along the horizontal axis for all the maps. The panel derived from Set F consists of 3707 mapped trace segments, with the scan circles having a radius of 7.34 m (Figure 29c). The estimated fracture density map (Figure 29d) shows two main zones with high density (high number of fractures per square meter), one in the lower half part of the panel and one in the upper, divided by a minimum zone, parallel to the stratification, which is situated at around 100 m from the base of the outcrop. The intensity map shows a similar pattern (Figure 29e), with two wider zones characterized by high intensity (large lengths of fracture per unit area) divided by a minimum zone, parallel to the stratification situated at the same stratigraphic height of the previous one. Overall, the spatial maps suggest that the two zones characterized by higher intensity and density values correspond to two distinct mechanical units separated by a mechanical boundary. Moreover, comparing the maps with the trace of the main faults (dashed red lines, Figures 29d and 29e), which are parallel to the Set F, we can see that three up to four of them have their lower terminations roughly coinciding with the zone considered as a mechanical boundary. The fourth fault, which crosscuts the uppermost portion of the outcrop, could be confined within a third distinct mechanical unit, highlighted by a cluster of relatively higher density and intensity. The mechanical boundary dividing this unit from the lower one could correspond to a minimum zone containing the terminations of the main fault traces. However, care must be taken when interpreting these results, because the quality of the upper part of the Mt. Catiello virtual outcrop could be biased by the presence of some vegetated areas and some altered rock

surfaces that prevent an optimal identification of all existing structural discontinuities and, thus, an optimal characterization of the mechanical units.

The panel derived from Set A consists of 3976 mapped trace segments, with the scan circles having a radius of 7.21 m (Figure 30c). The estimated fracture density map shows a pattern similar to those observed for the Set F, with a well defined high-density zone in the lower part of the panel, characterized by sensitively higher values. This zone is divided by a minimum interval, parallel to the stratification (NW dipping), from the two main clusters of high density observed in the upper portion of the panel. The intensity map shows a more scattered, but still recognizable pattern characterized by higher intensity in the lower half part of the panel and lower intensity in the upper portion of the panel. The overall spatial distribution of fractures resembles those observed for the Set F, with two main mechanical units, lower and upper, divided by a mechanical boundary parallel to the stratification (Figures 29d and 29e). Analyzing the 3D virtual outcrop, can be clearly observed that the identified mechanical units and the main mechanical boundary correspond to the same stratigraphic level in both the investigated panels.

The panel derived from Set B consists of 2026 mapped trace segments, with the scan circles having a radius of 5.34 m (Figure 31c). However, this set shows strong parallelism with the orientation of outcrop topography (Figure 31b). For this reason, the obtained map cannot be confidently used for fracture analysis and will not be discussed in this study.

4.3.3 The Basilicata subsurface

[Testo non disponibile in quanto relativo a dati protetti da segreto industriale]

5 DISCUSSIONS

5.1 Definition of depositional sequences and the use of Fischer Plots

The shallow-water carbonates outcropping at the Conocchia cliff are characterized by a hierarchy of sedimentary cycles expressed by systematic changes of bed thickness and lithofacies that can be grouped in elementary cycles, bundles and superbundles (Figure 11). Previous studies on the cyclostratigraphy of the Apennine Carbonate Platform invoked high-frequency eustatic changes, modulated by the Earth's orbital fluctuations, as the main control on sedimentary cyclicity shown by Lower Cretaceous carbonates of Mt. Faito (D'Argenio et al., 1999, 2004; Raspini, 2001; Amodio et al., 2013). Milankovitch forcing, as the main driving factor of the high-frequency cyclicity of Mt. Faito and other Lower Cretaceous successions of the Apennine Carbonate Platform, is also supported by the spectral analysis of quantitative information about textures, lithofacies, early meteoric fabrics and bed thickness (D'Argenio et al., 2004). On this basis, the Authors attributed elementary cycles to precession cycles (20ky), bundles to short eccentricity cycles (100ky) and superbundles to long eccentricity cycles (400 ky). These high-frequency cycles are superimposed on low-frequency environmental oscillations, with a prevailing eustatic origin that reflects third-order sea-level oscillations (D'Argenio et al., 1999). The eustatic origin of the low-frequency oscillations is confirmed by the possibility of correlating the third-order SBs at supra-regional scale (D'Argenio et al., 2004, 2008; Amodio and Weissert, 2017). The stacking pattern, facies and average thickness of elementary cycles, bundles and superbundles described by Amodio et al. (2013), who investigated the Barremian-Aptian interval of Mt. Faito, are perfectly comparable with those observed at the Conocchia cliff section. Therefore, their conclusions can be extended to the stratigraphic succession presented in this work and, in particular, third-order SBs identified at the Conocchia cliff (Figure 14) can be used for regional and supra-regional correlations.

The third-order depositional sequences of the investigated section were defined using a Fischer plot curve calibrated with field observations (Figure 14). The use of Fischer plot for the analysis of cyclic carbonate platform has attracted some criticism since it was first introduced (Drummond and Wilkinson, 1993; Boss and Rasmussen, 1995; Burgess et al., 2001; Bosence et al., 2009), on the basis of the assumption required for its correct application and the subjectivity of the cycle picking process. Indeed, it is necessary to assume a constant subsidence rate and that during each sea-level fluctuations the accommodation space was always filled up to the intertidal zone, which implies that the thickness of a sedimentary cycle correspond to the accommodation created during a sea-level fluctuation.

In the Early Cretaceous, the Apennine Carbonate Platform was part of the Adria passive continental margin and was in the late stage of its thermal cooling (Channell et al., 1979). It was then characterized by a constant subsidence until the Albian-Cenomanian boundary, when started the first Cretaceous extensional stage affecting the Adria margin (Tavani et al., 2013; Vitale et al., 2017). This event is well-documented in the Sorrento Peninsula by Tavani et al. (2013) and Iannace et al. (2014), who found evidences of syn-sedimentary extension and soft-sediment deformation.

Considering that only a part of the cycles observed at the Conocchia cliff clearly show intertidal lithofacies (Figures 11 and 14), the use of the Fischer plot for the stratigraphic analysis could be questionable. However, even if the intertidal zone is not always recorded in the cycles, the investigated shallow-water carbonates still belong to an aggrading greenhouse platform, where high-frequency changes in sea level are small and the top of each cycle is a subaerial exposure surface. For this reason, the curve obtained from the Fischer plot could not be used to calculate the exact magnitude of sea-level change, but can be still used to qualitatively

estimate sea-level rises and falls in an efficient way and, in particular, to define sequences on a cyclic carbonate platform, which would otherwise be difficult to pick given the subtle facies change within the succession (Husinec et al., 2008). In this regard, the Fischer plots have the advantage of being an objective representation of a measured stratigraphic section (Sadler et al., 1993), particularly useful to detect the overall trend of third-order sea-level fluctuations (Read and Goldhammer, 1988). Moreover, it has been shown that even if the picking of a few input cycles is affected by a subjectivity bias, this make relatively difference in the general form of the output curve (Sadler et al., 1993).

[Testo non disponibile in quanto relativo a dati protetti da segreto industriale]

5.2 Quantitative analysis of fracture patter from VOMs

The possibility of looking at a photorealistic virtual outcrop in orthographic projection mode represents one of the most important applications offered by the digital outcrops for geosciences, and in particular for structural geology (Tavani et al., 2016a). That is because it allows to obtain true measurements of geological structures for optimally oriented and undistorted cross-sections. In this way, it is possible to switch from a strictly qualitative to quantitative analysis of outcrops (Corradetti et al., 2017b). However, as shown by the structural analysis of the Conocchia cliff and of the Mt. Catiello, choosing the optimal method for quantitatively analyze fracture patterns is essential to achieve a meaningful result.

The two most common measurement methods used for quantitatively estimating fracture parameters are straight scan lines and scan area (La Pointe and Hudson, 1985; Priest, 1993; Wu and Pollard, 1995; Guerriero et al., 2010, 2011), which respectively consist in a sampling of all fractures and associated parameters intersecting a straight line, and in a mapping of fracture traces and associated parameters at locations in the map area (Rohrbaugh et al., 2002). The data obtained through these methods, however, can be subjected to orientation bias, length bias, censoring and are particularly prone to disguise pattern heterogeneities (Terzaghi, 1965; Priest and Hudson, 1981; La Pointe and Hudson, 1985; Priest, 1993; Kulatilake et al., 1997). Especially this latter type of bias can critically affect the results of an analysis, as highlighted during the study of the Mt. Catiello fracture distribution, which aims to identify distinct mechanical units in a faulted outcrop with an irregular topography.

These problems can be addressed using an alternative type of estimator, namely the circular scan lines and windows, which do not require knowledge of fracture spacing or orientation

and, therefore, are distribution independent (Mauldon et al., 2001; Rohrbaugh et al., 2002). Circular estimators are part of the tools available in FracPaQ (Healy et al., 2017), which combines the circular estimators in a regular grid of equiareal circles, and allows to easily identify vertical and lateral variations of fracture distribution.

Using a software such as FracPaQ to estimate these parameters represent a further benefit for a fracture quantification workflow, since it allows to sensitively reduce the time required for calculations and offers the possibility to quickly visualize the results as maps of fracture spatial distribution. In this regard, is important to stress that to achieve a geologically sounded result, the extraction and selection of the input data is a crucial step. The software, indeed, was originally developed to perform structural analysis assuming that the input fracture traces lie on a statistically flat 2D surface, where topography does not affect the appearance of any fracture trajectories (Healy et al., 2017). Consequently, its application to the study of dataset derived from 3D VOMs is possible only using a workflow that implies the production of orthorectified cross-sections, such as the one presented in this study.

This new workflow, therefore, expands the scope of OpenPlot and FracPaQ, allowing the extraction of quantitative information from 3D datasets, improving our ability to quantify structural data in a quick and robust way. The implementation of these results offers a new tool for the study of fractured reservoirs, and further increases the range of application of remote sensing for geosciences.

5.3 Mechanical stratigraphy

5.3.1 The Conocchia cliff

The structural analysis of Lower Cretaceous shallow-water carbonates exposed at the Conocchia cliff was performed integrating field-based investigations with remote sensing techniques, allowing multi-scale approach.

Field investigations revealed the occurrence of abundant fractures at the bed scale and highlighted that the rock mass is often subdivided into laterally discontinuous layers by sedimentary laminations and diagenetic features like microbial mats, bedding-parallel stylolites and dolomite seams (Tavani et al., 2016b) (Figures 24 and 25). These features acted as weak mechanical layers on which bed-scale fractures arrested. This observation is consistent with previous studies in similar carbonate multilayers (Underwood et al., 2003; Di Naccio et al., 2005; Larsen et al., 2010), which detected the role of laminated and thin-bedded facies in arresting fracture propagation. These discontinuities can be considered, for mechanical purposes, equivalent to bedding surfaces. In the field, was also recognized the occurrence of through-going fractures (Figure 24), which are well evident in the 3D digital model. Field observations indicate that these fractures can be considered as resulting from the connection of vertically aligned, precursory (e.g. Crider and Peacock, 2004) strata-bound fractures. For example, trough-going fractures may appear as single straight segments in the VOM used for the 2016 survey (Figure 19). However, observation at a more detailed scale and the use of a VOM with higher resolution (Figures 22 and 23), reveals that they are segmented and formed by various strands arranged in a quasi-aligned fashion, with the single strands being isolated by sedimentary features. The fact that, almost regardless of their height,

trough-going fractures are segmented and formed by isolated strands - the strands being bounded by sedimentary structures - and that trough-going joints look straight only when zooming out, can be explained by assuming that these fractures result from the linkage of precursory bed-confined joints. In fact, trough-going fractures that developed before or together with strata-bound fractures should appear as single planar features, which is not the case. All these observations are consistent with similar ones made by other authors in various regions (e.g. Finn et al., 2003; Gross and Eyal, 2007), who documented the coalescence and linkage of vertically aligned, pre-existing, bed-confined joints, to form large through-going fractures. These through-going fractures are well defined and hence recognizable within thicker, less intensely fractured beds, while they seem to arrest, or at least they are no more recognizable, in correspondence of relatively thinner, and more intensely fractured, beds (Figures 24 and 25). This behavior may be interpreted as mimicking the arrest of strata-bound fractures into mechanically weak bed interfaces (e.g. Pollard and Aydin, 1988; Gross et al., 1995).

Fracture data acquired by Corradetti (2016) from the digital outcrop model have been used for a spatial distribution analysis at the platform scale. These digitized fractures display no evidence of shearing. The three identified orientation sets (ENE-WSW, ESE-WNW, and NNW-SSE trending sets) were checked in the field and recognized as joints. Joints were filtered in OpenPlot based on their orientation (Figure 20). Only joints belonging to Set 3 (NNW-SSE) were used to perform the spatial distribution analysis, while Set 1 and Set 2 were discarded because oriented in parallel with outcrop topography. Set 3 joints were then projected onto a plane perpendicular to their intersection with bedding and analyzed in 2D, as generally done with photo panels (Figure 20c). From this panel, were identified several horizontal boundaries that inhibited the propagation of through-going joints, on the basis of fracture intensity and

spacing variations. These variations were analyzed with respect to the thickness of beds, the lithological variations and the sequence stratigraphic organization of the succession (Figure 26).

Comparing the results obtained from the digitized fracture analysis with a stratimetric log showing mean bed thickness variations (Figure 26d), it is clear that the position of the six boundaries identified as changes in fracture intensity and spacing roughly coincide with the six main peaks associated with a decrease in bed thickness. This match is coherent with field observations that showed more prominent cliff-forming rocks, also observed from the weathering profile, corresponding to packages of more calcareous and thicker beds, while thinly bedded bed-packages are associated to dolomitic intervals. It is worth noting that in identifying these horizontal boundaries, were not considered scan-lines with very sparse data (i.e. with less than 2 fractures sampled). To further explore the relationship between lithological properties and fracture distribution, for each mechanical unit (bounded by horizontal green and grey lines in Figure 26) was calculated the relative abundance of distinct rock texture and facies, here presented as pie charts (Figure 26c). The comparison of the lithological properties with fracture intensity shows a positive correlation with the relative abundance of dolomite. Indeed, the distribution of fracture intensity observed at the Conocchia cliff records a first increment corresponding to the transition between the first, basal mechanical unit and the next one, followed by a gradual decrease up to the last mechanical unit, which shows a marked increase of fracture intensity values. The same trend is shown by the relative abundance of dolomite in the mechanical units. It is often assumed that dolostone has higher fracture intensity than limestone because of a more brittle behavior (Nelson, 2001), and this assumption has been confirmed by several studies of fracture stratigraphy that reported an increase in fracture intensity in dolostones adjacent to

limestones (Ortega et al., 2010; Lapponi et al., 2011; Barbier et al., 2012). On the other hand, other studies did not found an increase specifically associated with dolomitization (Wennberg et al., 2006). As more recent studies have highlighted, dolomitization can have a dual effect in modulating fracture intensity, depending not only on dolomite crystal size, but also on bed thickness and textures of precursor limestones (Rustichelli et al., 2015; Giorgioni et al., 2016; Korneva et al., 2018). The results presented in this study show that at the scale of these mechanical units (identified on the basis of the distribution of through-going fractures), the relative amount of dolostone can be critical to control fracture intensity. However, the influence of other structural and lithological factors (i.e. texture, porosity, etc.) cannot be entirely ruled out.

Overall, the presented data suggest that the key control on the distribution of large-scale fractures in this >200 m thick carbonate succession is bed thickness. Trough-going fractures arrest where a package of very thin layers is sandwiched between packages of much thicker beds (Figure 25). In particular, the most evident arresting level is located at about 22 m of stratigraphic elevation from the base of the succession. It corresponds to a 43-cm-thick dolomitic level, thinly subdivided into sub-levels, each one no more than a few cm thick, holding cm-spaced strata-bound joints. This package of very thin beds is sandwiched between thicker calcareous strata (i.e. >20 cm thick). As it is showed and discussed by Corradetti et al. (2018), the effectiveness of this thinly bedded levels in arresting the propagation of fractures is due to the peculiar growth model of through-going joints at the Conocchia cliff, occurred by linkage of previous stratabound joints, suggested by evidence collected both in the field and on the 3D models (Figure 32). According to this kind of growth mode, also reported by previous studies (e.g. Gross and Eyal, 2007), the network of stratabound joints plays a key role in the vertical connection of major through-going joints. In fact, due to the well-known

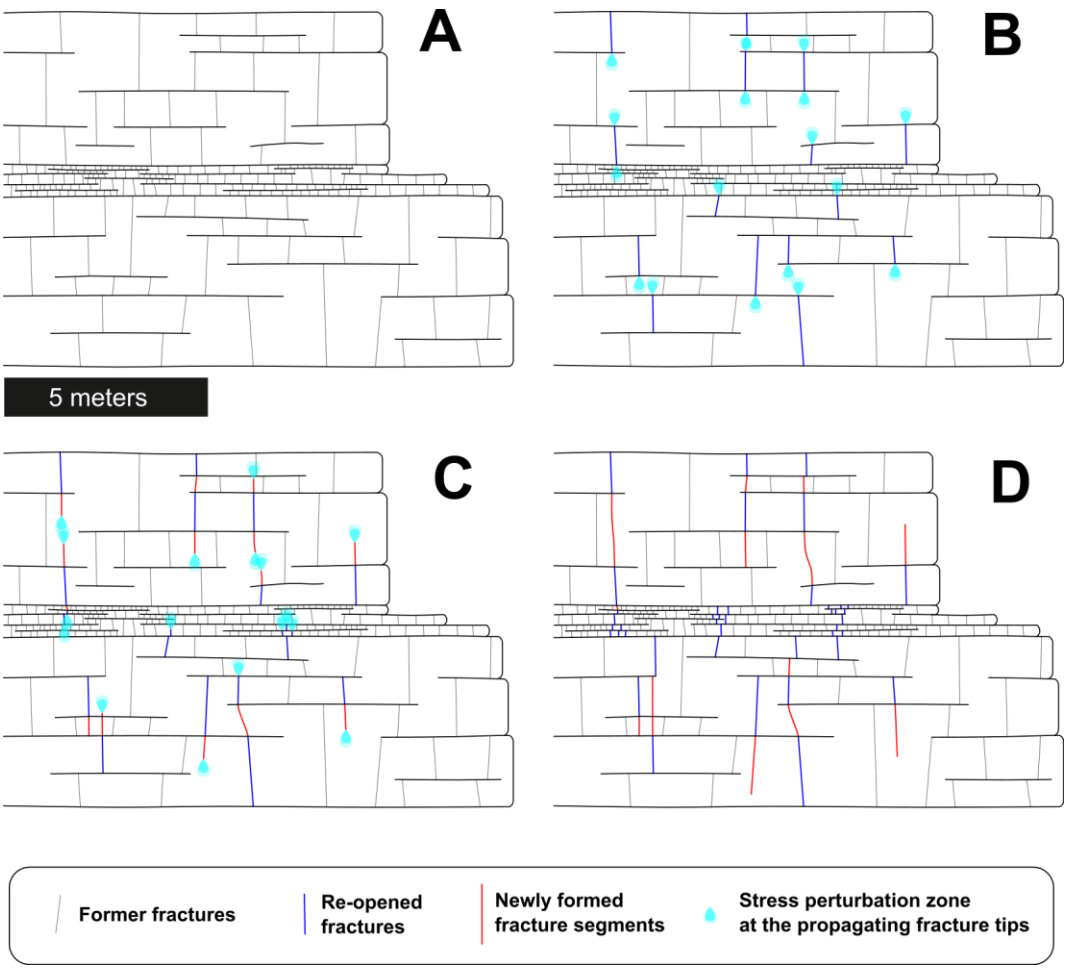

Figure 28 a) Schematic distribution of strata-bound joints. Once a strata-bound fracture network has developed, further re-opening (b) can lead to both development of new segments linking pre-existing joints or the re-opening of joints within the stress perturbation areas (c). As a consequence, joints are expected to create new segments within thick-bedded packages, while where they cross-cut thinly bedded packages, they produce the re-opening of widespread strata-bound joints (d). From Corradetti et al. 2018.

dependence between bed thickness and strata-bound joint spacing, thin mechanical units - independently from the origin of the anisotropy, being either real bedding or pseudo-bedding produced by (incomplete) parting along lamination surfaces and/or dolomite seams - are characterized by a substantially higher bed-scale fracture density. Therefore, once the stratabound fracture network has developed, further extension leads to the connection of previous joints (Becker and Gross, 1996). During this connection stage, further opening of pre-existing joints creates a stress perturbation area at the tips of opening joints (Gross et al., 1995) (Figure 32b). This can lead to both development of new segments linking previous joints and the reopening of joints within the stress perturbation areas (Figure 32c). It is intuitive that

the probability for a perturbation area to include a pre-existing joint is higher for thinly-bedded strata, where closely spaced strata-bound joints are available to be reopened. On the other hand, when the stress perturbation area migrates throughout a thick-bedded package, where joints are more widely spaced, the probability of intersecting these joints decreases. As a consequence, through-going joints during their propagation are expected to create new segments within thick bedded packages, while where they cross-cut thinly bedded packages, they produce the reopening of widespread strata-bound joints (Figure 32d). In this latter case, the result is that the through-going joint splays into numerous small joints, and it is no longer able to propagate as a single and well-defined nearly-straight joint. This mechanism of reopening vs. linkage of joints implies a scale-dependent switch in the behavior of mechanical units made of thinly stratified dolostones, from a highly brittle one at the bed scale to a fracture inhibited zone at the seismic-scale, thus resulting in a mechanical boundary behavior for large joints. In essence, similarly to strata-bound joints, which arrest at the ductile bed interface (Becker and Gross, 1996), through-going joints mostly terminate at layers made of thinly-bedded and highly fractured strata.

The connectivity of this fracture system has been analyzed by Massaro et al. (2018), who performed a multi-scale study integrating fracture data acquired from the 3D model by Corradetti (2016) with new measures obtained from a dedicated field survey. From this dataset was derived a stochastic distribution of joints, which was used to build a discrete fracture network (DFN) model (see Lei et al., 2017 for a review). The DFN model shows that through-going fractures guarantee vertical connectivity through the reservoir, playing a primary role in terms of permeability. On the other hand, the thinly stratified “weak” levels, which arrest the propagation of through-going fractures, act both as mechanical barrier and

low permeability zones, and can therefore cause a vertical compartmentalization of the reservoir.

Comparing the sequence stratigraphic organization with the mechanical stratigraphy of these shallow-water carbonates, it is clear that the intervals with thinly-bedded levels – which are able to arrest the propagation of through-going fractures – correspond to the main SBs, and that each 3rd order SB corresponds to one of the mechanical boundaries previously identified (Figure 26). Conversely, two out of the six mechanical boundaries (situated around 70 m and 84 m of stratigraphic elevation respectively) do not coincide with a 3rd order SB but, as the Figure 26 is showing, nonetheless they correspond to some pronounced 4th order cycle boundaries, highlighted also by two minor deviation of the Fischer plot curve. Overall, these results show that sequence stratigraphic analysis can be used to identify the main mechanical units and mechanical boundaries of a carbonate platform exposure. Indeed, in these carbonates, when a 3rd order SB is found, a mechanical boundary is found too (Figure 33).

The Fischer plot diagram has proven to be a valuable tool for SB identification. This is because in these shallow-water successions the sedimentary cyclicity is mainly expressed through variations of elementary cycle and bundle thickness. The Fischer plot curve highlights exactly these variations and, therefore, can be used to identify objectively the position of 3rd order SBs, which correspond to intervals where bundles, and then also elementary cycles, averagely have a reduced thickness.

The role of 3rd order sedimentary sequences in defining the main mechanical units of shallow-water carbonates was highlighted also by previous works (Morettini et al., 2005; Barbier et al., 2012). In particular, Morettini et al. (2005) investigated the sequence and mechanical stratigraphy of the Fahud field of Oman and found that the clay-rich maximum flooding

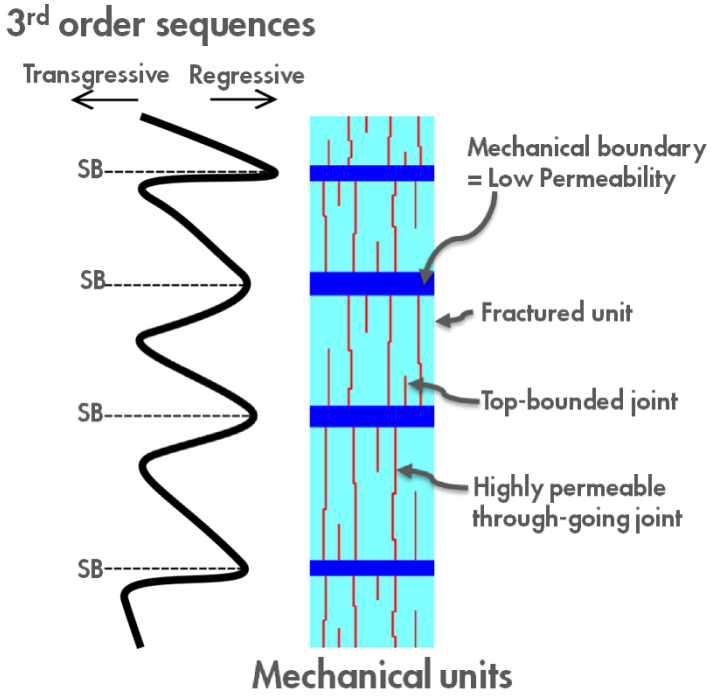

Figure 29 Cartoon showing the control of 3rd order sedimentary sequences on mechanical stratigraphy. Sequence boundaries (SB) correspond to Mechanical boundaries.

surfaces of 3rd order sequences act as a mechanical barrier for fracture propagation; while Barbier et al. (2012) studied the fracturing pattern of the Madison Formation (Wyoming, USA) and found that the interfaces of large-scale mechanical units can be correlated with the SBs of 3rd order depositional sequences, which are characterized by the presence of evaporite solution collapse breccias. If the presented case-study is compared with these two examples, it is obvious that none of the proposed solution for the identification of the mechanical units can be fully applied to the others. This consideration cannot be surprising, since one of the paradigms in the study of carbonate rocks is that because of their intrinsic heterogeneities – due to differences in terms of carbonate factories, depositional settings, diagenesis, burial and deformation histories – conceptual models cannot be applied indiscriminately, and each case-study requires ad-hoc solutions. On the other hand, the consistence shown in identifying 3rd order depositional sequences as a critical element for the definition of mechanical units in such different case-studies, suggests that the identification of 3rd order sedimentary

sequences is essential during reservoir characterization studies, not only to assess sedimentological properties, but also to predict large-scale fracture distribution.

5.3.2 The Mt. Catiello

The information extracted from the quantitative analysis of fracture patterns at Mt. Catiello, allows to test the observations made at the Conocchia cliff on an outcrop exposing the same stratigraphic succession but characterized by a different structural architecture. Morevor, allows to compare the two different workflows applied for the quantification of fracture patterns.

Overall, from the analysis of spatial density maps of fracture patterns, two main mechanical units can be identified at Mt. Catiello, Upper and Lower, separated by a main mechanical boundary (Figures 29d and 29e). Even if the two units show comparable average values in terms of estimated fracture intensity and density, they exhibit distinct fracture patterns, with the Upper Unit more prone to the development of less numerous but higher discrete fractures and the Lower Unit characterized by smaller but more abundant discrete fractures (Figures 30d and 30e). In order to unravel the potential stratigraphic controls on fracture distribution, the results obtained from remote sensing observations were combined with field investigations. The field survey showed that the two mechanical units are characterized by distinct stratigraphic features: the Upper Unit consists of a cyclic succession of shallowing-upward peritidal limestones and dolomitic limestones, while the Lower Unit consists of dolostones with common stromatolitic laminae at the top of the strata. Even if these differences could explain the distinct mechanical behavior of the two units, care must be taken when interpreting these results. Decades of research and debate on the role of lithological

parameters and associated petrophysical attributes in controlling fracture development in carbonates have shown that, in this field, interpretation of results rarely is straightforward and an acritical application of a rule of the thumb can be misleading (see Giorgioni et al. 2016 for a review). Regarding the Lower Cretaceous dolomitized carbonates of Mt. Faito area, Giorgioni et al. (2016) showed that rock texture (crystal/grain size) is more important than lithology (dolostone vs. limestone) in regulating the background fracture pattern.

Comparing the Mt. Catiello with the Conocchia cliff it appears that, even if characterized by a slightly different structural style, their mechanical stratigraphy has some remarkable similarities. The correlation of the two outcrops shows that the most effective mechanical boundary identified at the Conocchia is situated at the same stratigraphic height of the main mechanical boundary identified at Mt. Catiello, and that they are both consisting of a thinly-bedded dolomitic interval. The two boundaries, therefore, can be considered as the same stratigraphic level which act as a laterally-persistent mechanical boundary. The absence of other clear mechanical boundaries affecting the Upper Unit of Mt Catiello, as was instead shown at the Conocchia cliff, suggest a hierarchy of these boundaries. We can then suppose that in two carbonate multilayers of same thickness and stratigraphy, one crossed by through-going fracture and one crossed by faults, should be expected more effective mechanical boundaries in the multilayer affected by through-going fractures and less effective boundaries in the multilayer affected by faults. Such a phenomenon could be due to the impact of different effective displacement for the involved structural discontinuities.

Recognizing the persistent stratigraphic features that act as mechanical barriers and control the fracture pattern distribution in shallow-water carbonates of the Sorrento Peninsula has a wide applicative impact, since they host important fractured aquifers (De Vita et al., 2018) and

are the outcrop analogues of the fractured reservoirs hosting huge hydrocarbon accumulations in the subsurface of Basilicata, Southern Italy (Iannace et al., 2014). Considering that these mechanical barriers are also low-permeability zones that can cause a vertical compartmentalization of the reservoirs (Massaro et al., 2018), linking their position to specific stratigraphic intervals can substantially help to understand the reservoir architecture and build a realistic model of fluid circulation. Moreover, the mechanical barrier dividing the two mechanical units of Mt. Catiello, correspond to a stratigraphic interval that, combined with the fracture pattern developed in the Upper Unit, represent the pre-conditional factors that caused a huge rock fall along the southwestern slope of Mt. Catiello (Perriello Zampelli et al., 2015). Therefore, recognizing the persistent nature of this mechanical barrier in the Mt. Faito area could also help to predict the potential occurrence of hazardous mass movements.

5.3.3 The Basilicata subsurface

[Testo non disponibile in quanto relativo a dati protetti da segreto industriale]

6 CONCLUSIONS AND PERSPECTIVES

In the present thesis an integrated study of the mechanical stratigraphy of two Lower Cretaceous reservoir analogues exposed in the Sorrento peninsula (southern Italy) has been carried out.

The aim was to understand the role of sedimentary controls on fracture distribution in shallow water carbonates and test the applicability of the outcrop-based concepts developed in the first part of the study on a subsurface dataset from the subsurface of the Basilicata region (southern Italy). The study was performed integrating field measurements and remote sensing of Virtual Outcrop Models (VOMs) of the reservoir analogues with the analysis of borehole image log and core data from selected wells.

The key point of the study is that 3rd order sedimentary sequences play a primary control on the thickness of mechanical units and on the distribution of large-scale fractures. Therefore, sequence stratigraphy can be successfully used to predict the distribution of large-scale fractures in shallow-water carbonate platforms.

The main results can be summarized as follows:

- The outcrop studies revealed that major through-going fractures that cross the investigated exposures generally cross-cut thick beds (bed thickness > 30 cm), whereas they tend to abut against packages made of thinly stratified layers, in the same manner as bed-confined fractures abut against less competent interlayers.

- Sequence stratigraphic analysis allowed to identify the key control exerted by 3rd order sedimentary sequences on the formation of the thinly bedded levels. Therefore, 3rd order sedimentary sequences control the thickness of mechanical units and the

position of their boundaries, which implies that sequence stratigraphy can be used to predict height and distribution of through-going fractures.

- Testing these outcrop-based insights in the subsurface showed that potential mechanical boundaries can be identified through a sequence stratigraphic analysis performed on FMI logs of vertical wells. The correlation observed between the mean thickness of mechanical units and the mean spacing of large scale faults and fracture corridor occurring in the same mechanical units confirms the key control exerted by the stratigraphic architecture of these carbonates on their mechanical stratigraphy.
- Following these outcomes, is proposed a new approach to estimate large-scale fracture intensity in carbonate reservoirs, based on the evaluation of the thickness of mechanical units through a sequence stratigraphic analysis.

The presented thesis offers new ideas and new tools for the study of fractured shallow-water carbonates.

Future perspectives for this study could be to further explore the possible applications of the most promising result, the prediction of large-scale fracture intensity using sequence stratigraphy, on other fractured reservoirs characterized by comparable geological conditions. The full application of this workflow would provide a valuable tool for reservoir quality prediction.

Considering the positive results achieved with the integration of structural data extracted from VOMs with fieldwork, continuing further this approach could lead to significative results when a multi-scale integrated analysis of geological bodies is required.

Finally, considering the persistent link between stratigraphy and fracture pattern distribution shown by the shallow-water carbonates of the Sorrento Peninsula, the results of this study could be extended and applied to other fields, such as the management of fractured aquifers or the evaluation of slope stability, that could substantially benefit from the predictive-concept developed and from the large amount of acquired data.

Acknowledgments

I hope that the wide audience of international readers will excuse me but, as provided by the Regulation of Academic Acknowledgments, I will switch to my mother tongue to celebrate the Ritual Credits. However, if you are really curious to know what is hidden in the next lines, feel free to contact me. I will be happy to let you know.

Lavorare ad un progetto di ricerca così trasversale non sarebbe stato possibile senza il supporto di un Team di alto livello e dalle competenze eterogenee. Il primo ringraziamento va quindi a tutto il Gruppo di Ricerca. Grazie per la formazione e le opportunità che mi avete offerto durante gli anni di studio e di dottorato. È stato un piacere collaborare con tutti Voi.

Dopo questa doverosa premessa, nel momento in cui vanno fatti i nomi ed i cognomi, non posso che iniziare con il ringraziare colui che è stato il mio Tutor in questi anni di dolomia e di fratture, il Prof. Alessandro Iannace. Grazie per la stima dimostrata nei confronti del mio lavoro e per avermi affidato ancora una volta un progetto stimolante e dal grande potenziale. L'unico rammarico è quello di non aver ancora incrociato le chitarre per una suonata…cerchiamo di rimediare!

E dopo il Tutor, il Tutor-Ombra: Grazie al Prof. Stefano Tavani. Come ben sai grandi sono i tuoi meriti e le tue colpe, ma soprattutto Grazie per…no! Non si può dire, l'intero manoscritto andrebbe in contro alla più feroce censura.

Ancor più che per i suoi tanti contributi scientifici, un Grazie va al Prof. Mariano Parente per le tante esperienze di formazione internazionale a cui ho avuto accesso in questi anni. Senza i

suoi suggerimenti mi sarei perso alcuni dei momenti migliori del dottorato, e forse oggi non sarei un felice migrante economico.

Passando al reparto giovani un meritatissimo Grazie va al Dott. Amerigo Corradetti, pioniere dei VOM ed esperto di Conocchie. Avendomi sempre preparato al peggio, le cose non sono mai andate troppo male.

Un Grazie anche a tutti gli altri giovani del gruppo, compagni di (dis)avventure e vittime del dottorato, vi auguro la salvezza. In ordine di apparizione Ernesto Prinzi, Francesco Puzone, Mariarosaria Martino, Monia Sabbatino e Lorenzo Consorti.

Il progetto di ricerca presentato in questa tesi ha beneficiato del supporto di Shell Italia E&P, a cui vanno i miei sentiti ringraziamenti.

Nel ringraziare anche il personale Shell con il quale ho avuto il piacere di collaborare, non posso che iniziare da Carlos Pirmez, che ha creduto nel progetto con grande entusiasmo ed energia, ed ha contribuito al manoscritto in qualità di referee. Grazie anche a Stefano Torrieri, Maurizio Giorgioni e Martin Eriksson per aver sponsorizzato, seguito e supportato tutte le fasi del mio internship nei Paesi Bassi con il Carbonate Research Team di Shell Global Solutions International.

Un grande Grazie va poi al Carbonate Research Team stesso, per la grande occasione di crescita che mi ha offerto e per avermi fatto sentire davvero parte del gruppo di ricerca. Un ringraziamento davvero speciale va però ai miei due tutor Michele Claps e Nino Cilona. Grazie per la fiducia mostrata nel progetto di ricerca, per il grandissimo supporto e per la vostra amicizia. Spero di avere anche in futuro la fortuna di lavorare con voi.

È doveroso un ringraziamento particolare al Prof. Giovanni Bertotti (Università di Delft, Paesi Bassi), per aver dedicato il suo tempo alla valutazione di questa tesi e per i suoi suggerimenti, che hanno permesso di migliorare la qualità di questo manoscritto.

Impossibile ringraziare uno ad uno i tanti amici e colleghi - vecchi, nuovi, ritrovati - con cui ho condiviso questo percorso. Un'eccezione però va fatta per i futuri PhD di Casa Tripodi, Niccolò e Leonardo, per aver reso speciale il mio breve ritorno in patria, e per gli amici che nelle vite precedenti c'erano già, Gesù e Luca, anche loro futuri PhD. A tutti Voi auguro il meglio.

Infine, l'ultimo grande Grazie va alla mia Famiglia. Tre anni di grandi cambiamenti, partenze e arrivi. I chilometri aumentano, ma non le distanze. Grazie a tutti Voi.

References

Adams, J., Chandler, J., 2002. Evaluation of lidar and medium scale photogrammetry for detecting soft-cliff coastal change. Photogrammetric Record 17, 405–418. https://doi.org/10.1111/0031-868X.00195

Adams, J.E., Rhodes, M.L., 1960. Dolomitization by seepage refluxion. AAPG Bulletin 44, 1912–1920.

Agosta, F., Alessandroni, M., Antonellini, M., Tondi, E., Giorgioni, M., 2010. From fractures to flow: A field-based quantitative analysis of an outcropping carbonate reservoir. Tectonophysics 490, 197–213. https://doi.org/10.1016/j.tecto.2010.05.005

Amodio, S., Ferreri, V., D'Argenio, B., 2013. Cyclostratigraphic and chronostratigraphic correlations in the Barremian-Aptian shallow-marine carbonates of the central-southern Apennines (Italy). Cretaceous Research 44, 132–156. https://doi.org/10.1016/j.cretres.2013.04.003

Amodio, S., Weissert, H., 2017. Palaeoenvironment and palaeoecology before and at the onset of Oceanic Anoxic Event (OAE) 1a : Reconstructions from Central Tethyan archives. Palaeogeography, Palaeoclimatology, Palaeoecology 479, 71–89. https://doi.org/10.1016/j.palaeo.2017.04.018

Angerer, E., Lanfranchi, P., Rogers, S.F., 2003. Fractured reservoir modeling from seismic to simulator: A reality? The Leading Edge 22, 684. https://doi.org/10.1190/1.1599697

Antonellini, M., Mollema, P.N., 2000. A natural analog for a fractured and faulted reservoir in dolomite: Triassic Sella Group, northern Italy. AAPG Bulletin 84, 314–344. https://doi.org/10.1306/c9ebcddd-1735-11d7-8645000102c1865d

Assereto, R.L.A.M., Kendall, C.G.S.C., 1977. Nature, origin and classification of peritidal tepee structures and related breccias. Sedimentology 24, 153–210. https://doi.org/10.1111/j.1365-3091.1977.tb00254.x

Aydin, A., 2000. Fractures, faults, and hydrocarbon entrapment, migration and flow. Marine and Petroleum Geology 17, 797–814. https://doi.org/10.1016/S0264-8172(00)00020-9

Bai, T., Pollard, D.D., Gao, H., 2000. Explanation for fracture spacing in layered materials. Nature 403, 753–756.

Barbier, M., Hamon, Y., Callot, J.P., Floquet, M., Daniel, J.M., 2012. Sedimentary and diagenetic controls on the multiscale fracturing pattern of a carbonate reservoir: The Madison Formation (Sheep Mountain, Wyoming, USA). Marine and Petroleum Geology 29, 50–67. https://doi.org/10.1016/j.marpetgeo.2011.08.009

Becker, A., Gross, M.R., 1996. Mechanism for joint saturation in mechanically layered rocks: an example from southern Israel., Tectonophysics. https://doi.org/10.1016/0040-1951(95)00142-5

Bemis, S.P., Micklethwaite, S., Turner, D., James, M.R., Akciz, S., T. Thiele, S., Bangash, H.A.,

2014. Ground-based and UAV-Based photogrammetry: A multi-scale, high-resolution mapping tool for structural geology and paleoseismology. Journal of Structural Geology 69, 163–178. https://doi.org/10.1016/j.jsg.2014.10.007

Bertello, F., Fantoni, R., Franciosi, R., Gatti, V., Ghielmi, M., Pugliese, A., 2010. From thrust-and-fold belt to foreland: hydrocarbon occurrences in Italy. In: Vining, B.A., Pickering, S.C. (Eds.), Petroleum Geology: From Mature Basins to New Frontiers—Proceedings of the 7th Petroleum Geology Conference. Geological Society, London., 113–126. https://doi.org/10.1144/0070823

Bertotti, G., Hardebol, N., Taal-van Kroppen, J.K., Luthi, S.M., 2007. Toward a quantitative definition of mechanical units: New techniques and results from an outcropping deep-water turbidite succession (Tanqua-Karoo Basin, South Africa). AAPG Bulletin 91, 1085–1098. https://doi.org/10.1306/03060706074

Bisdom, K., Bertotti, G., Bezerra, F.H., 2017a. Inter-well scale natural fracture geometry and permeability variations in low-deformation carbonate rocks. Journal of Structural Geology 97, 23–36. https://doi.org/10.1016/j.jsg.2017.02.011

Bisdom, K., Bertotti, G., Nick, H.M., 2016. The impact of in-situ stress and outcrop-based fracture geometry on hydraulic aperture and upscaled permeability in fractured reservoirs. Tectonophysics 690, 63–75. https://doi.org/10.1016/j.tecto.2016.04.006

Bisdom, K., Gauthier, B.D.M., Bertotti, G., Hardebol, N.J., 2014. Calibrating discrete fracture-network models with a carbonate three-dimensional outcrop fracture network: Implications for naturally fractured reservoir modeling. AAPG Bulletin 98, 1351–1376. https://doi.org/10.1306/02031413060

Bisdom, K., Nick, H.M., Bertotti, G., 2017b. An integrated workflow for stress and flow modelling using outcrop-derived discrete fracture networks. Computers and Geosciences 103, 21–35. https://doi.org/10.1016/j.cageo.2017.02.019

Bistacchi, A., Ashley Griffith, W., Smith, S.A.F., di Toro, G., Jones, R., Nielsen, S., 2011. Fault Roughness at Seismogenic Depths from LIDAR and Photogrammetric Analysis. Pure and Applied Geophysics 168, 2345–2363. https://doi.org/10.1007/s00024-011-0301-7

Bistacchi, A., Balsamo, F., Storti, F., Mozafari, M., Swennen, R., Solum, J., Tueckmantel, C., Taberner, C., 2015. Photogrammetric digital outcrop reconstruction, visualization with textured surfaces, and three-dimensional structural analysis and modeling: Innovative methodologies applied to fault-related dolomitization (Vajont Limestone, Southern Alps, Italy). Geosphere 11, 2031–2048. https://doi.org/10.1130/GES01005.1

Bosellini, A., 2004. The western passive margin of Adria and its carbonates platforms. Special Volume of the Italian Geological Society for the IGC 32 Florence 79–92.

Bosence, D., Procter, E., Aurell, M., Bel Kahla, A., Boudagher-Fadel, M., Casaglia, F., Cirilli, S., Mehdie, M., Nieto, L., Rey, J., Scherreiks, R., Soussi, M., Waltham, D., 2009. A Dominant Tectonic Signal in High-Frequency, Peritidal Carbonate Cycles? A Regional Analysis of Liassic Platforms from Western Tethys. Journal of Sedimentary Research 79, 389–415. https://doi.org/10.2110/jsr.2009.038

Boss, S.K., Rasmussen, K.A., 1995. Misuse of Fischer plots as sea-level curves. Geology 23, 221–

224. https://doi.org/10.1130/0091-7613(1995)023<0221:MOFPAS>2.3.CO;2

Bourne, S.J., Rijkels, L., Stephenson, B.J., Willemse, E.J.M., 2001. Predictive Modelling of Naturally Fractured Reservoirs Using Geomechanics and Flow Simulation. GeoArabia 6, 27–42.

Bratton, T., Gillespie, P., Li, B., Marcinew, R., Ray, S., Nelson, R., Schoderbek, D., Sonneland, L., 2006. The Nature of Naturally Fractured Reservoirs. Oilfield Review 18, 4–23.

Bravi, S., De Castro, P., 1995. The Cretaceous fossil fishes level of Capo d'Orlando, near Castellammare di Stabia (NA): biostratigraphy and depositional environment. Sciences Géologiques - Memoires 47, 45–72.

Buckley, S.J., Schwarz, E., Terlaky, V., Howell, J.A., Arnott, R.W., 2010. Combining aerial photogrammetry and terrestrial lidar for reservoir analog modeling. Photogrammetric Engineering and Remote Sensing 76, 953–963. https://doi.org/10.14358/PERS.76.8.953

Burgess, P.M., Wright, V.P., Emery, D., 2001. Numerical forward modelling of peritidal carbonate parasequence development: Implications for outcrop interpretation. Basin Research 13, 1–16. https://doi.org/10.1046/j.1365-2117.2001.00130.x

Carannante, G., Pugliese, A., Ruberti, D., Simone, L., Vigliotti, M., Vigorito, M., 2009. Evoluzione cretacica di un settore della piattaforma apula da dati di sottosuolo e di affioramento (Appennino campano-molisano). Italian Journal of Geosciences 128, 3–31.

Carannante, G., Ruberti, D., Sirna, M., 2000. Upper Cretaceous ramp limestones from the Sorrento Peninsula (southern Apennines, Italy): micro- and macrofossil associations and their significance in the depositional sequences. Sedimentary Geology 132, 89–123.

Casini, G., Hunt, D.W., Monsen, E., Bounaim, A., 2016. Fracture characterization and modeling from virtual outcrops. AAPG Bulletin 100, 41–61. https://doi.org/10.1306/09141514228

Cawood, A.J., Bond, C.E., Howell, J.A., Butler, R.W.H., Totake, Y., 2017. LiDAR, UAV or compass-clinometer? Accuracy, coverage and the effects on structural models. Journal of Structural Geology 98, 67–82. https://doi.org/10.1016/j.jsg.2017.04.004

Cello, G., Mazzoli, S., 1999. Apennine tectonics in southern Italy: a review. Journal of Geodynamics 27, 191–211.

Chafetz, H.S., Zhang, J., 1998. Authigenic euhedral megaquartz crystals in a Quaternary dolomite. Journal of Sedimentary Research 68, 994–1000.

Channell, J.E.T., D'Argenio, B., Horvath, F., 1979. Adria, the African promontory, in mesozoic Mediterranean palaeogeography. Earth-Science Reviews 15, 213–292. https://doi.org/10.1016/0012-8252(79)90083-7

Chesley, J.T., Leier, A.L., White, S., Torres, R., 2017. Using unmanned aerial vehicles and structure-from-motion photogrammetry to characterize sedimentary outcrops: An example from the Morrison Formation, Utah, USA. Sedimentary Geology 354, 1–8. https://doi.org/10.1016/j.sedgeo.2017.03.013

Chiocchini, M., Chiocchini, R.A., Didaskalou, P., Potetti, M., 2008. Ricerche micropaleontologiche e biostratigrafiche sul Mesozoico della piattaforma carbonatica laziale-abruzzese (Italia centrale). Memorie Descrittive Della Carta Geologica d'Italia

LXXXIV.

Ciarcia, S., Mazzoli, S., Vitale, S., Zattin, M., 2011. On the tectonic evolution of the Ligurian accretionary complex in southern Italy. Geological Society of America Bulletin 124, 463–483. https://doi.org/10.1130/B30437.1

Cilona, A., Aydin, A., Likerman, J., Parker, B., Cherry, J., 2016. Structural and statistical characterization of joints and multi-scale faults in an alternating sandstone and shale turbidite sequence at the Santa Susana Field Laboratory: Implications for their effects on groundwater flow and contaminant transport. Journal of Structural Geology 85, 95–114. https://doi.org/10.1016/j.jsg.2016.02.003

Clapuyt, F., Vanacker, V., Van Oost, K., 2016. Reproducibility of UAV-based earth topography reconstructions based on Structure-from-Motion algorithms. Geomorphology 260, 4–15. https://doi.org/10.1016/j.geomorph.2015.05.011

Clari, P.A., Dela Pierre, F., Martire, L., 1995. Discontinuities in carbonate successions: identification, interpretation and classification of some Italian examples. Sedimentary Geology 100, 97–121. https://doi.org/10.1016/0037-0738(95)00113-1

Cooke, M.L., Simo, J.A., Underwood, C.A., Rijken, P., 2006. Mechanical stratigraphic controls on fracture patterns within carbonates and implications for groundwater flow. Sedimentary Geology 184, 225–239. https://doi.org/10.1016/j.sedgeo.2005.11.004

Corbett, K., Friedman, M., Spang, J., 1987. Fracture development and mechanical stratigraphy of Austin Chalk, Texas. AAPG Bulletin 71, 17–28.

Corradetti, A., 2016. 3D structural characterization of outcrops by means of close-range multi-view stereo-photogrammetry. PhD Thesis - Università degli Studi di Napoli Federico II.

Corradetti, A., McCaffrey, K., De Paola, N., Tavani, S., 2017a. Evaluating roughness scaling properties of natural active fault surfaces by means of multi-view photogrammetry. Tectonophysics 717, 599–606. https://doi.org/10.1016/j.tecto.2017.08.023

Corradetti, A., Tavani, S., Parente, M., Iannace, A., Vinci, F., Pirmez, C., Torrieri, S., Giorgioni, M., Pignalosa, A., Mazzoli, S., 2018. Distribution and arrest of vertical through-going joints in a seismic-scale carbonate platform exposure (Sorrento peninsula, Italy): Insights from integrating field survey and digital outcrop model. Journal of Structural Geology 108, 121–136. https://doi.org/10.1016/j.jsg.2017.09.009

Corradetti, A., Tavani, S., Russo, M., Arbués, P.C., Granado, P., 2017b. Quantitative analysis of folds by means of orthorectified photogrammetric 3D models: a case study from Mt. Catria, Northern Apennines, Italy. Photogrammetric Record 32, 480–496. https://doi.org/10.1111/phor.12212

Crider, J.G., Peacock, D.C.P., 2004. Initiation of brittle faults in the upper crust: A review of field observations. Journal of Structural Geology 26, 691–707. https://doi.org/10.1016/j.jsg.2003.07.007

D'Argenio, B., De Castro, P., Emiliani, C., Simone, L., 1975. Bahamian and Apenninic Limestones of Identical Lithofacies and Age: GEOLOGIC NOTES. AAPG Bulletin 59, 524–530.

D'Argenio, B., Ferreri, V., Amodio, S., 2008. Sequence stratigraphy of Cretaceous carbonate

platforms: A cyclostratigraphic approach. In: Amorosi, A., Haq, B.U., Sabato, L. (Eds.), Advances in Application of Sequence Stratigraphy in Italy. 157–171.

D'Argenio, B., Ferreri, V., Amodio, S., Pelosi, N., 1997. Hierarchy of high-frequency orbital cycles in Cretaceous carbonate platform strata. Sedimentary Geology 113, 169–193. https://doi.org/10.1016/S0037-0738(97)00076-6

D'Argenio, B., Ferreri, V., Raspini, A., Amodio, S., Buonocunto, F.P., 1999. Cyclostratigraphy of a carbonate platform as a tool for highprecision correlation. Tectonophysics 315, 357–385.

D'Argenio, B., Ferreri, V., Weissert, H., Amodio, S., Buonocunto, F.P., Wissler, L., 2004. A multidisciplinary approach to global correlation and geochronology: the Cretaceous shallow-water carbonates of southern Apennines, Italy. In: D'Argenio, B., Fischer, A.G., Premoli Silva, I., Weissert, H., Ferreri, V. (Eds.), Cyclostratigraphy: Approaches and Case Histories. SEPM Special Pubicationl 81, 103–122.

Day, P.I., 1997. The Fischer diagram in the depth domain: a tool for sequence stratigraphy. Journal of Sedimentary Research 67, 982–984.

De Castro, P., 1991. Mesozoic. In: Barattolo, F., De Castro, P., Parente, M. (Eds.), Field Trip Guide-Book, '"5th International Symposium on Fossil Algae"'. 21–38.

De Castro, P., 1962. Il Giura-Lias dei Monti Lattari e dei rilievi ad ovest della Valle dell'Irno e della Piana di Montoro. Bollettino Della Societa Dei Naturalisti in Napoli 71, 3–34.

De Vita, P., Allocca, V., Celico, F., Fabbrocino, S., Mattia, C., Monacelli, G., Musilli, I., Piscopo, V., Scalise, A.R., Gianpietro, S., Tranfaglia, G., Celico, P., 2018. Hydrogeology of continental southern Italy. Journal of Maps 14, 230–241. https://doi.org/10.1080/17445647.2018.1454352

Dean, R.H., Lo, L.L., 1988. Simulations of Naturally Fractured Reservoirs. SPE Reservoir Engineering 3. https://doi.org/10.2118/14110-PA

Demicco, R. V., Hardie, L.A. (Eds.), 1995. Sedimentary Structures and Early Diagenetic Features of Shallow Marine Carbonate Deposits. SEPM (Society for Sedimentary Geology).

Dershowitz, W.S., Herda, H.H., 1992. Interpretation of fracture spacing and intensity. The 33th US Symposium on Rock Mechanics (USRMS). American Rock Mechanics Association.

Dewey, J.F., Helman, M.L., Knott, S.D., Turco, E., Hutton, D.H.W., 1989. Kinematics of the western Mediterranean. Geological Society, London, Special Publications 45, 265–283. https://doi.org/10.1144/GSL.SP.1989.045.01.15

"Di Naccio," D., Boncio, P., Cirilli, S., Casaglia, F., Morettini, E., Lavecchia, G., Brozzetti, F., 2005. Role of mechanical stratigraphy on fracture development in carbonate reservoirs: Insights from outcropping shallow water carbonates in the Umbria-Marche Apennines, Italy. Journal of Volcanology and Geothermal Research 148, 98–115. https://doi.org/10.1016/j.jvolgeores.2005.03.016

Donselaar, M.E., Schmidt, J.M., 2005. Integration of outcrop and borehole image logs for high-resolution facies interpretation: Example from a fluvial fan in the Ebro Basin, Spain. Sedimentology 52, 1021–1042. https://doi.org/10.1111/j.1365-3091.2005.00737.x

Drummond, C.N., Wilkinson, B.H., 1993. Aperiodic accumulation of cyclic peritidal carbonate. Geology 21, 1023–1026. https://doi.org/10.1130/0091-7613(1993)021<1023:AAOCPC>2.3.CO;2

Ekstrom, M.P., Dahanl, C.A., Chen, M., Lloyd, P.M., Rossil, D.J., 1986. Formation Imaging With Scanning Arrays. Society of Petrophysicists & Well Log Analysts 27th Annual Logging Symposium. Houston, Texas.

Eliassen, A., Talbot, M.R., 2005. Solution-collapse breccias of the Minkinfjellet and Wordiekammen Formations, Central Spitsbergen, Svalbard: A large gypsum palaeokarst system. Sedimentology 52, 775–794. https://doi.org/10.1111/j.1365-3091.2005.00731.x

Emery, D., Myers, K., 1996. Sequence Stratigraphy. Blackwell Science, Oxford.

Favalli, M., Fornaciai, A., Isola, I., Tarquini, S., Nannipieri, L., 2012. Multiview 3D reconstruction in geosciences. Computers and Geosciences 44, 168–176. https://doi.org/10.1016/j.cageo.2011.09.012

Fernández, O., 2005. Obtaining a best fitting plane through 3D georeferenced data. Journal of Structural Geology 27, 855–858. https://doi.org/10.1016/j.jsg.2004.12.004

Finn, M.D., Gross, M.R., Eyal, Y., Draper, G., 2003. Kinematics of throughgoing fractures in jointed rocks. Tectonophysics 376, 151–166. https://doi.org/10.1016/j.tecto.2003.10.001

Firpo, G., Salvini, R., Francioni, M., Ranjith, P.G., 2011. Use of Digital Terrestrial Photogrammetry in rocky slope stability analysis by Distinct Elements Numerical Methods. International Journal of Rock Mechanics and Mining Sciences 48, 1045–1054. https://doi.org/10.1016/j.ijrmms.2011.07.007

Fischer, A.G., 1964. The Lofer cyclothems of the Alpine Triassic. Kansas Geological Survey Bulletin 169, 107–149.

Florez-Nino, J.M., Aydin, A., Mavko, G., Antonellini, M., Ayaviri, A., 2005. Fault and fracture systems in a fold and thrust belt: An example from Bolivia. AAPG Bulletin 89, 471–493. https://doi.org/10.1306/11120404032

Flügel, E., 2004. Microfacies of Carbonate Rocks: Analysis, Interpretation and Application, Springer-Verlag Berlin Heidelberg. https://doi.org/10.1007/978-3-642-03796-2

Folk, R.L., Pittman, J.S., 1971. Length-slow chalcedony: a new testament for vanished evaporites. Journal of Sedimentary Petrology 41, 1045–1058.

Folkestad, A., Veselovsky, Z., Roberts, P., 2012. Utilising borehole image logs to interpret delta to estuarine system: A case study of the subsurface Lower Jurassic Cook Formation in the Norwegian northern North Sea. Marine and Petroleum Geology 29, 255–275. https://doi.org/10.1016/j.marpetgeo.2011.07.008

Gao, M., Xu, X., Klinger, Y., Van Der Woerd, J., Tapponnier, P., 2017. High-resolution mapping based on an Unmanned Aerial Vehicle (UAV) to capture paleoseismic offsets along the Altyn-Tagh fault, China. Scientific Reports 7, 1–11. https://doi.org/10.1038/s41598-017-08119-2

Gauthier, B.D.M., Garcia, M., Daniel, J.-M.J., Zellou, A.M., Toublanc, A., Garcia, M., Daniel, J.-

M.J., 2002. Integrated Fractured Reservoir Characterization: A Case Study in a North Africa Field. SPE Reservoir Evaluation & Engineering 5, 24–25. https://doi.org/10.2118/79105-PA

Giorgioni, M., Iannace, A., D'Amore, M., Dati, F., Galluccio, L., Guerriero, V., Mazzoli, S., Parente, M., Strauss, C., Vitale, S., 2016. Impact of early dolomitization on multi-scale petrophysical heterogeneities and fracture intensity of low-porosity platform carbonates (Albian-Cenomanian, southern Apennines, Italy). Marine and Petroleum Geology 73, 462–478. https://doi.org/10.1016/j.marpetgeo.2016.03.011

Goldhammer, R.K., Dunn, P.A., Hardie, L.A., 1990. Depositional cycles, composite sea-level changes, cycle stacking patterns, and the hierarchy of stratigraphic forcing: examples from Alpine Triassic platform carbonates. Geol. Soc. Am. Bull. 102, 535–562.

Graziano, R., Raspini, A., 2015. Long- and short-term hydroclimatic variabilities in the Aptian Tethys : Clues from the orbital chronostratigraphy of evaporite-rich beds in the Apennine carbonate platform (Mt. Faito, southern Italy). Palaeogeography, Palaeoclimatology, Palaeoecology 418, 319–343. https://doi.org/10.1016/j.palaeo.2014.11.021

Gross, M.R., 1993. The origin and spacing of cross joints; examples from the Monterey Formation, Santa Barbara coastline, California. Journal of Structural Geology 15, 737–751.

Gross, M.R., Eyal, Y., 2007. Throughgoing fractures in layered carbonate rocks. Bulletin of the Geological Society of America 119, 1387–1404. https://doi.org/10.1130/0016-7606(2007)119[1387:TFILCR]2.0.CO

Gross, M.R., Fischer, M.P., Engelder, T., Greenfield, R.J., 1995. Factors controlling joint spacing in interbedded sedimentary rocks: integrating numerical models with field observations from the Monterey Formation, USA. In: Ameen, M.S. (Ed.), Fractography: Fracture Topography as a Tool in Fracture Mechanics and Stress Analysis. Geological Society, London, Special Publications, 215–233. https://doi.org/10.1144/GSL.SP.1995.092.01.12

Grün, A., Remondino, F., Zhang, L.I., 2004. Photogrammetric reconstruction of the great buddha of Bamiyan, Afghanistan. Photogrammetric Record 19, 177–199. https://doi.org/10.1111/j.0031-868X.2004.00278.x

Guerriero, V., Dati, F., Giorgioni, M., Iannace, A., Mazzoli, S., Vitale, S., 2015. The role of stratabound fractures for fluid migration pathways and storage in well-bedded carbonates. Italian Journal of Geosciences 134, 383–395. https://doi.org/10.3301/IJG.2014.27

Guerriero, V., Iannace, A., Mazzoli, S., Parente, M., Vitale, S., Giorgioni, M., 2010. Quantifying uncertainties in multi-scale studies of fractured reservoir analogues : Implemented statistical analysis of scan line data from carbonate rocks. Journal of Structural Geology 32, 1271–1278. https://doi.org/10.1016/j.jsg.2009.04.016

Guerriero, V., Mazzoli, S., Iannace, A., Vitale, S., Carravetta, A., Strauss, C., 2013. A permeability model for naturally fractured carbonate reservoirs. Marine and Petroleum Geology 40, 115–134. https://doi.org/10.1016/j.marpetgeo.2012.11.002

Guerriero, V., Vitale, S., Ciarcia, S., Mazzoli, S., 2011. Improved statistical multi-scale analysis

of fractured reservoir analogues. Tectonophysics 504, 14–24. https://doi.org/10.1016/j.tecto.2011.01.003

Haneberg, W.C., 2008. Using close range terrestrial digital photogrammetry for 3-D rock slope modeling and discontinuity mapping in the United States. Bulletin of Engineering Geology and the Environment 67, 457–469. https://doi.org/10.1007/s10064-008-0157-y

Hardebol, N.J., Bertotti, G., 2013. DigiFract: A software and data model implementation for flexible acquisition and processing of fracture data from outcrops. Computers and Geosciences 54, 326–336. https://doi.org/10.1016/j.cageo.2012.10.021

Hardebol, N.J., Maier, C., Nick, H., Geiger, S., Bertotti, G., Boro, H., 2015. Multiscale fracture network characterization and impact on flow: A case study on the Latemar carbonate platform. Journal of Geophysical Research: Solid Earth 120, 8197–8222. https://doi.org/10.1002/2015JB011879

Hardie, L.A., Bosellini, A., Goldhammer, R.K., 1986. Repeated subaerial exposure of subtidal carbonate platforms, Triassic, Northern Italy: evidence for high frequency sea-level oscillations on a 104 year scale. Paleoceanography 1, 447–457.

Harwin, S., Lucieer, A., 2012. Assessing the accuracy of georeferenced point clouds produced via multi-view stereopsis from Unmanned Aerial Vehicle (UAV) imagery. Remote Sensing 4, 1573–1599. https://doi.org/10.3390/rs4061573

Healy, D., Rizzo, R.E., Cornwell, D.G., Farrell, N.J.C., Watkins, H., Timms, N.E., Gomez-Rivas, E., Smith, M., 2017. FracPaQ: A MATLAB^{TM} toolbox for the quantification of fracture patterns. Journal of Structural Geology 95, 1–16. https://doi.org/10.1016/j.jsg.2016.12.003

Heaney, P.J., 1995. Moganite as an indicator for vanished evaporites: a testament reborn? Journal of Sedimentary Research 65, 633–638.

Hencher, S.R., 2014. Characterizing discontinuities in naturally fractured outcrop analogues and rock core: the need to consider fracture development over geological time. In: Spence, G.H., Redfern, J., Aguilera, R., Bevan, T.G., Cosgrove, J.W., Couples, G.D., Daniel, J.-M. (Eds.), Advances in the Study of Fractured Reservoirs. Geological Society, London, Special Publications, 113–123. https://doi.org/10.1144/SP374.15

Hillgartner, H., 1998. Discontinuity surfaces on a shallow-marine carbonate platform (Berriasian, Valanginian, France and Switzerland). Journal of Sedimentary Research 68, 1093–1108.

Hodgetts, D., Drinkwater, N.J., Hodgson, J., Kavanagh, J., Flint, S.S., Keogh, K.J., Howell, J.A., 2004. Three-dimensional geological models from outcrop data using digital data collection techniques: an example from the Tanqua Karoo depocentre, South Africa. Geological Society, London, Special Publications 239, 57–75. https://doi.org/10.1144/GSL.SP.2004.239.01.05

Howell, J.A., Martinius, A.W., Good, T.R., 2014. The application of outcrop analogues in geological modelling: a review, present status and future outlook. Geological Society, London, Special Publications 387, 1–25. https://doi.org/10.1144/SP387.12

Huang, Q., Angelier, J., 1989. Fracture spacing and its relation to bed thickness., Geological

Magazine. https://doi.org/10.1017/S0016756800006555

Husinec, A., Basch, D., Rose, B., Read, J.F., 2008. FISCHERPLOTS: An Excel spreadsheet for computing Fischer plots of accommodation change in cyclic carbonate successions in both the time and depth domains. Computers and Geosciences 34, 269–277. https://doi.org/10.1016/j.cageo.2007.02.004

Iannace, A., 1993. Caratteri diagenetici dei carbonati di Piattaforma dell'Appennino Meridionale e loro implicazioni paleogeografiche. Rivista Italiana Di Paleontologia e Stratigrafia 99, 57–80.

Iannace, A., Capuano, M., Galluccio, L., 2011. "Dolomites and dolomites" in Mesozoic platform carbonates of the Southern Apennines: Geometric distribution, petrography and geochemistry. Palaeogeography, Palaeoclimatology, Palaeoecology 310, 324–339. https://doi.org/10.1016/j.palaeo.2011.07.025

Iannace, A., Frijia, G., Galluccio, L., Parente, M., 2014. Facies and early dolomitization in Upper Albian shallow-water carbonates of the southern Apennines (Italy): paleotectonic and paleoclimatic implications. Facies 60, 169–194. https://doi.org/10.1007/s10347-013-0362-4

ISPRA, 2016. Carta Geologica d'Italia alla scala 1:50.000, foglio 466 "Sorrento".

James, M.R., Robson, S., 2012. Straightforward reconstruction of 3D surfaces and topography with a camera: Accuracy and geoscience application. Journal of Geophysical Research: Earth Surface 117, 17. https://doi.org/10.1029/2011JF002289

Korneva, I., Bastesen, E., Corlett, H., Eker, A., Hirani, J., Hollis, C., Gawthorpe, R.L., Rotevatn, A., Taylor, R., 2018. The effects of dolomitization on petrophysical properties and fracture distribution within rift-related carbonates (Hammam Faraun Fault Block, Suez Rift, Egypt). Journal of Structural Geology 108, 108–120. https://doi.org/10.1016/j.jsg.2017.06.005

Kulatilake, P.H.S.W., Fiedler, R., Panda, B.B., 1997. Box fractal dimension as a measure of statistical homogeneity of jointed rock masses. Engineering Geology 48, 217–229.

La Pointe, P.R., Hudson, J.A., 1985. Characterization and interpretation of rock mass joint patterns. Geological Society of America Special Papers 199, 37. https://doi.org/10.1130/SPE199-p1

Ladeira, F.L., Price, N.J., 1981. Relationship between fracture spacing and bed thickness. Journal of Structural Geology 3, 179–183.

Lai, J., Wang, G., Wang, S., Cao, J., Li, M., Pang, X., Han, C., Fan, X., Yang, L., He, Z., Qin, Z., 2018. A review on the applications of image logs in structural analysis and sedimentary characterization. Marine and Petroleum Geology 95, 139–166. https://doi.org/10.1016/j.marpetgeo.2018.04.020

Lapponi, F., Casini, G., Sharp, I., Blendinger, W., Fernandez, N., Romaire, I., Hunt, D., 2011. From outcrop to 3D modeling; a case study of a dolomitized carbonate reservoir, Zagros Mountains, Iran. In: Hollis, C., Sharp, I. (Eds.), Albian-Cenomanian-Turonian Carbonate-Siliciclastic Systems of the Arabian Plate; Advances in Diagnosis, Structure and Reservoir Modeling: Petroleum Geoscience, Vol. 17. 283–307.

Larsen, B., Gudmundsson, A., Grunnaleite, I., Sælen, G., Talbot, M.R., Buckley, S.J., 2010. Effects of sedimentary interfaces on fracture pattern, linkage, and cluster formation in peritidal carbonate rocks. Marine and Petroleum Geology 27, 1531–1550. https://doi.org/10.1016/j.marpetgeo.2010.03.011

Lato, M.J., Vöge, M., 2012. Automated mapping of rock discontinuities in 3D lidar and photogrammetry models. International Journal of Rock Mechanics and Mining Sciences 54, 150–158. https://doi.org/10.1016/j.ijrmms.2012.06.003

Laubach, S.E., Olson, J.E., Gross, M.R., 2009. Mechanical and fracture stratigraphy. AAPG Bulletin 93, 1413–1426. https://doi.org/10.1306/07270909094

Lavenu, A.P.C., Lamarche, J., Salardon, R., Gallois, A., Marié, L., Gauthier, B.D.M., 2014. Relating background fractures to diagenesis and rock physical properties in a platform-slope transect. Example of the Maiella Mountain (central Italy). Marine and Petroleum Geology 51, 2–19. https://doi.org/10.1016/j.marpetgeo.2013.11.012

Lei, Q., Latham, J.P., Tsang, C.F., 2017. The use of discrete fracture networks for modelling coupled geomechanical and hydrological behaviour of fractured rocks. Computers and Geotechnics 85, 151–176. https://doi.org/10.1016/j.compgeo.2016.12.024

Lézin, C., Odonne, F., Massonnat, G.J., Escadeillas, G., 2009. Dependence of joint spacing on rock properties in carbonate strata. AAPG Bulletin 93, 271–290. https://doi.org/10.1306/09150808023

Li, J.Z., Laubach, S.E., Gale, J.F.W., Marrett, R.A., 2018. Quantifying opening-mode fracture spatial organization in horizontal wellbore image logs, core and outcrop: Application to Upper Cretaceous Frontier Formation tight gas sandstones, USA. Journal of Structural Geology 108, 137–156. https://doi.org/10.1016/j.jsg.2017.07.005

Lofts, J.C., Bourke, L.T., 1999. The recognition of artefacts from acoustic and resistivity borehole imaging devices. In: Lovell, M., Williamson, G., Harvey, P. (Eds.), Borehole Imaging: Applications and Case Histories. Geological Society of London Special Publications, 59–76. https://doi.org/10.1144/GSL.SP.1999.159.01.03

Lucia, J.F., 1995. Rock-Fabric/petrophysical Classification of Carbonate Pore Space for Reservoir Characterization. AAPG Bulletin 79, 1275–1300. https://doi.org/10.1306/7834D4A4-1721-11D7-8645000102C1865D

Malinverno, A., Ryan, W.B.F., 1986. Extension in the Tyrrhenian Sea and shortening in the Apennines as result of arc migration driven by sinking of the lithosphere. Tectonics 5, 227–245. https://doi.org/10.1029/TC005i002p00227

Mancini, F., Dubbini, M., Gattelli, M., Stecchi, F., Fabbri, S., Gabbianelli, G., 2013. Using unmanned aerial vehicles (UAV) for high-resolution reconstruction of topography: The structure from motion approach on coastal environments. Remote Sensing 5, 6880–6898. https://doi.org/10.3390/rs5126880

Massaro, L., Corradetti, A., Vinci, F., Tavani, S., Iannace, A., Parente, M., Mazzoli, S., 2018. Multiscale Fracture Analysis in a Reservoir-Scale Carbonate Platform Exposure (Sorrento Peninsula, Italy): Implications for Fluid Flow. Geofluids 10. https://doi.org/10.1155/2018/7526425

Massironi, M., Zampieri, D., Superchi, L., Bistacchi, A., Ravagnan, R., Bergamo, A., Ghirotti, M., Genevois, R., 2013. Geological structures of the vajont landslide. Italian Journal of Engineering Geology and Environment - Book Series 6, 573–582. https://doi.org/10.4408/IJEGE.2013-06.B-55

Mauldon, M., Dunne, W.M., Rohrbaugh, M.B.J., 2001. Circular scanlines and circular windows: new tools for characterizing the geometry of fracture traces. Journal of Structural Geology 23, 247–258.

Mazzoli, S., Helman, M., 1994. Neogene patterns of relative motion for Africa-Europe: some implications for recent central Mediterranean tectonics. Geologische Rundschau 84, 277–291.

McGinnis, R.N., Ferrill, D.A., Morris, A.P., Smart, K.J., Lehrmann, D., 2017. Mechanical stratigraphic controls on natural fracture spacing and penetration. Journal of Structural Geology 95, 160–170. https://doi.org/10.1021/acsami.5b06699

McGinnis, R.N., Ferrill, D.A., Smart, K.J., Morris, A.P., Higuera-Diaz, C., Prawica, D., 2015. Pitfalls of using entrenched fracture relationships: Fractures in bedded carbonates of the hidden valley fault zone, Canyon Lake Gorge, Comal County, Texas. AAPG Bulletin 99, 2221–2245. https://doi.org/10.1306/07061513012

McQuillan, H., 1973. Small-scale fracture density in Asmari Formation of southwest Iran and its relation to bed thickness and structural setting. AAPG Bulletin 57, 2367–2385.

Menegoni, N., Meisina, C., Perotti, C., Crozi, M., 2018. Analysis by UAV Digital Photogrammetry of Folds and Related Fractures in the Monte Antola Flysch Formation (Ponte Organasco, Italy). Gesosciences 8, 299.

Minisini, D., Wang, M., Bergman, S.C., Aiken, C., 2014. Geological data extraction from lidar 3-D photorealistic models: A case study in an organic-rich mudstone, Eagle Ford Formation, Texas. Geosphere. https://doi.org/10.1130/GES00937.1

Monsen, E., Hunt, D.W., Bounaim, A., Savary-Sismondini, B., Brenna, T., Nickel, M., Sonneland, L., Thurmond, J.B., Gillespie, P.A., 2011. The automated interpretation of photorealistic outcrop models. In: Martinsen, O.J., Pulham, A.J., Haughton, D.W., Sullivan, M.D. (Eds.), Outcrops Revitalized—Tools, Techniques and Applications. SEPM Concepts in Sedimentology and Paleontology 10, Tulsa, Oklahoma, 107–136.

Morellato, C., Redini, F., Doglioni, C., 2003. On the number and spacing of faults. Terra Nova 15, 315–321. https://doi.org/10.1046/j.1365-3121.2003.00501.x

Morettini, E., Thompson, A., Eberli, G., Rawnsley, K., Roeterdink, R., Asyee, W., Christman, P., Cortis, A., Foster, K., Hitchings, V., Kolkman, W., van Konijnenburg, J.H., 2005. Combining high-resolution sequence stratigraphy and mechanical stratigraphy for improved reservoir characterisation in the Fahud field of Oman. GeoArabia 10, 17–44. https://doi.org/10.1306/8626DB99-173B-11D7-8645000102C1865D

Mostardini, F., Merlini, S., 1986. L' Appennino centro-meridionale. Sezioni geologiche e proposta di modello strutturale. Memorie Della Società Geologica Italiana 35, 177–202.

Muniz, M.C., Bosence, D.W.J., 2015. Pre-salt microbialites from the Campos Basin (offshore Brazil): image log facies, facies model and cyclicity in lacustrine carbonates. In: Bosence,

D.W.J., Gibbons, K.A., Le Heron, D.P., A., M.W., Pritchard, T., Vining, B.A. (Eds.), Microbial Carbonates in Space and Time: Implications for Global Exploration and Production. Geological Society, London, Special Publications. 221–242. https://doi.org/10.1144/SP418.10

Narr, W., 1996. Estimating average fracture spacing in subsurface rock. AAPG Bulletin 80, 1565–1586. https://doi.org/10.1306/64EDA0B4-1724-11D7-8645000102C1865D

Narr, W., Schechter, D.W., Thompson, L.B., 2006. Naturally Fractured Reservoir Characterization. Society of Petroleum Engineers, Ricardson, TX.

Narr, W., Suppe, J., 1991. Joint spacing in sedimentary rocks. Journal of Structural Geology 13, 1037–1048.

Nelson, R.A., 2001. Geologic Analysis of Naturally Fractured Reservoirs, Geologic Analysis of Naturally Fractured Reservoirs. Gulf Professional Publishing, Houston. https://doi.org/10.1016/B978-088415317-7/50005-1

Odling, N.E., Gillespie, P., Bourgine, B., Castaing, C., Chiles, J.P., Christensen, N.P., Fillion, E., Genter, A., Olsen, C., Thrane, L., Trice, R., Aarseth, E., Walsh, J.J., Watterson, J., 1999. Variations in fracture system geometry and their implications for fluid flow in fractures hydrocarbon reservoirs., Petroleum Geoscience. https://doi.org/10.1144/petgeo.5.4.373

Ogniben, L., 1969. Schema introduttivo alla geologia del confine Calabro Lucano. Memorie Della Società Geologica Italiana 8, 453–763.

Oldow, J.S., D'Argenio, B., Ferranti, L., Pappone, G., Marsella, E., Sacchi, M., 1993. Large-scale longitudinal extension in the southern Apennines contractional belt, Italy. Geology 21, 1123–1126. https://doi.org/10.1130/0091-7613(1993)021

Ortega, O.J., Gale, J.F.W., Marrett, R., 2010. Quantifying diagenetic and stratigraphic controls on fracture intensity in platform carbonates: An example from the Sierra Madre Oriental, northeast Mexico. Journal of Structural Geology 32, 1943–1959. https://doi.org/10.1016/j.jsg.2010.07.004

Ortega, O.J., Marrett, R.A., Laubach, S.E., 2006. A scale-independent approach to fracture intensity and average spacing measurement. AAPG Bulletin 90, 193–208. https://doi.org/10.1306/08250505059

Panza, E., Agosta, F., Rustichelli, A., Zambrano, M., Tondi, E., Prosser, G., Giorgioni, M., Janiseck, J.M., 2016. Fracture stratigraphy and fluid flow properties of shallow-water, tight carbonates: The case study of the Murge Plateau (southern Italy). Marine and Petroleum Geology 73, 350–370. https://doi.org/10.1016/j.marpetgeo.2016.03.022

Patacca, E., Scandone, P., 2007. Geology of the Southern Apennines. Bollettino Della Società Geologica Italiana. Volume Speciale 75–119.

Patacca, E., Scandone, P., 1989. Post-Tortonian mountain building in the Apennines. The role of the passive sinking of a relic lithospheric slab. In: Hiraki, A., Boriani, A., Bonafede, M., Piccardo, G.B., Vai, G.B. (Eds.), The Lithosphere in Italy: Advances in Earth Science Research, Vol. 80. Accademia Nazionale dei Lincei, Rome, 157–176.

Peacock, D.C.P., 2006. Predicting variability in joint frequencies from boreholes. Journal of Structural Geology 28, 353–361. https://doi.org/10.1016/j.jsg.2005.10.007

Perriello Zampelli, S., De Vita, P., Imbriaco, D., Calcaterra, D., 2015. Engineering geology for society and territory – Volume 2: Landslide processes. In: Lollino, G., Giordan, D., Crosta, G.B., Corominas, J., Azzam, R., Wasowski, J., Sciarra, N. (Eds.), Engineering Geology for Society and Territory - Volume 2: Landslide Processes. 813–816. https://doi.org/10.1007/978-3-319-09057-3

Pollard, D.D., Aydin, A., 1988. Progress in understanding jointing over the past century. Geological Society of America Bulletin 100, 1181–1204. https://doi.org/10.1130/0016-7606(1988)100<1181

Pöppelreiter, M., García-Carballido, C., Kraaijveld, M., 2010. Borehole image log technology: Application across the exploration and production life cycle. In: Pöppelreiter, M., García-Carballido, C., Kraaijveld, M. (Eds.), Dipmeter and Borehole Image Log Technology - AAPG Memoir 92. 1–13.

Price, N.J., 1966. Fault and Joint Development in Brittle and Semi-brittle Rocks. Pergamon.

Priest, S.D., 1993. Discontinuity analysis for rock engineering. Chapman and Hall, New York.

Priest, S.D., Hudson, J.A., 1981. Estimation of discontinuity spacing and trace length using scanline surveys. International Journal of Rock Mechanics and Mining Sciences and Geomechanics Abstracts 18, 183–197. https://doi.org/10.1016/0148-9062(81)90973-6

Pringle, J.K., Clark, J.D., Westerman, A.R., Stanbrook, D.A., Gardiner, A.R., Morgan, B.E.F., 2001. Virtual outcrops: 3-D reservoir analogues. Journal of the Virtual Explorer 4, 51–55. https://doi.org/10.3809/jvirtex.2001.00036

Raspini, A., 2012. Shallow water carbonate platforms (Late Aptian-Early Albian, Southern Apennines) in the context of supraregional to global changes: Re-appraisal of palaeoecological events as reflectors of carbonate factory response. Solid Earth 3, 225–249. https://doi.org/10.5194/se-3-225-2012

Raspini, A., 2001. Stacking pattern of cyclic carbonate platform strata : Lower Cretaceous of southern Apennines , Italy. Journal of the Geological Society, London 158, 353–366.

Read, J.F., Goldhammer, R.K., 1988. Use of Fischer plots to define third-order sea-level curves in Ordovician peritidal cyclic carbonates, Appalachians. Geology 16, 895–899.

Reitman, N.G., Bennett, S.E.K., Gold, R.D., Briggs, R.W., DuRoss, C.B., 2015. High-resolution trench photomosaics from image-based modeling: Workflow and error analysis. Bulletin of the Seismological Society of America 105, 2354–2366. https://doi.org/10.1785/0120150041

Remondino, F., El-Hakim, S., 2006. Image-based 3D modelling: A review. Photogrammetric Record 21, 269–291. https://doi.org/10.1111/j.1477-9730.2006.00383.x

Richard, P., Bazalgette, L., Al-Kindi, M., 2014. North Oman fault geometries in outcrops, analogues and subsurface. Geological Society, London, Special Publications 392, 447–460. https://doi.org/10.1144/SP392.21

Richet, R., Borgomano, J., Adams, E.W., Masse, J.P., Viseur, S., 2011. Numerical Outcrop

Geology Applied to Stratigraphical Modeling of Ancient Carbonate Platforms: The Lower Cretaceous Vercors Carbonate Platform (Se France). In: Martinsen, O.J., Pulham, A.J., Haughton, P., Sullivan, M.D. (Eds.), Outcrops Revitalized: Tools, Techniques and Applications. SEPM Concepts in Sedimentology and Paleontology. 195–210.

Robson, J., 1987. Depositional models for some Cretaceous carbonates from the Sorrento Peninsula, Italy. Memorie Della Società Geologica Italiana 40, 251–257.

Rohrbaugh, M.B.J., Dunne, W.M., Mauldon, M., 2002. Estimating fracture trace intensity, density, and mean length using circular scan lines and windows. AAPG Bulletin 86, 2089–2104. https://doi.org/10.1306/61EEDE0E-173E-11D7-8645000102C1865D

Rustichelli, A., Agosta, F., Tondi, E., Spina, V., 2013. Spacing and distribution of bed-perpendicular joints throughout layered, shallow-marine carbonates (Granada Basin, southern Spain). Tectonophysics 582, 188–204. https://doi.org/10.1016/j.tecto.2012.10.007

Rustichelli, A., Iannace, A., Girundo, M., 2015. Dolomitization impact on fracture density in pelagic carbonates: Contrasting case studies from the Gargano Promontory and the Southern Apennines (Italy). Italian Journal of Geosciences 134, 556–575. https://doi.org/10.3301/IJG.2014.43

Sadler, P.M., Osleger, D.A., Montanez, I.P., 1993. On the Labeling, Length, and Objective Basis of Fischer Plots. Journal of Sedimentary Research Vol. 63, 360–368. https://doi.org/10.1306/D4267AFF-2B26-11D7-8648000102C1865D

Schlager, W., Reijmer, J.J.G., Droxler, A., 1994. Highstand Shedding of Carbonate Platforms. Journal of Sedimentary Research B64, 270–281. https://doi.org/10.1306/D4267FAA-2B26-11D7-8648000102C1865D

Schlumberger, 2002. FMI: Borehole geology, geomechanics and 3D reservoir modelling.

Seers, T.D., Hodgetts, D., 2016. Extraction of three-dimensional fracture trace maps from calibrated image sequences. Geosphere 12, 1323–1340. https://doi.org/10.1130/GES01276.1

Sharp, I., Gillespie, P., Lønøy, A., Horn, S., Morsalnezhad, D., 2006. Outcrop Characterisation of Fractured Cretaceous Carbonate Reservoirs , Zagros Mts , Iran. First International Oil Conference and Exhibition in Mexico Held in Cancun, Mexico, 31 August–2 September 2006. SPE.

Shiner, P., Beccacini, A., Mazzoli, S., 2004. Thin-skinned versus thick-skinned structural models for Apulian carbonate reservoirs: constraints from the Val d'Agri Fields, S Apennines, Italy. Marine and Petroleum Geology 21, 805–827. https://doi.org/10.1016/j.marpetgeo.2003.11.020

Sibley, D.F., Gregg, J.M., 1987. Classification of dolomite rock texitures. Journal of Sedimentary Petrology 57, 967–975.

Spence, G.H., Couples, G.D., Bevan, T.G., Aguilera, R., Cosgrove, J.W., Daniel, J.-M., Redfern, J., 2014. Advances in the study of naturally fractured hydrocarbon reservoirs: a broad integrated interdisciplinary applied topic. In: Spence, G.H., Redfern, J., Aguilera, R., Bevan, T.G., Cosgrove, J.W., Couples, G.D., Daniel, J.-M. (Eds.), Advances in the Study of

Fractured Reservoirs. Geological Society, London, Special Publications, 1–22. https://doi.org/10.1144/SP374.19

Storti, F., Balsamo, F., Cappanera, F., Tosi, G., 2011. Sub-seismic scale fracture pattern and in situ permeability data in the chalk atop of the Krempe salt ridge at Lägerdorf, NW Germany: Inferences on synfolding stress field evolution and its impact on fracture connectivity. Marine and Petroleum Geology 28, 1315–1332. https://doi.org/10.1016/j.marpetgeo.2011.03.014

Strasser, A., 1994. Milankovitch Cyclicity and High-Resolution Sequence Stratigraphy in Lagoonal-Peritidal Carbonates (Upper Tithonian-Lower Berriasian, French Jura Mountains). In: de Boer, P.L., Smith, D.G. (Eds.), Orbital Forcing and Cyclic Sequences. Special Publications International Association of Sedimentologists, vol 19, 285–301. https://doi.org/10.1002/9781444304039.ch19

Strasser, A., 1991. Lagoonal-peritidal sequences in carbonate environments: auto- cyclic and allocyclic processes. In: Einsele, G., Ricken, W., Seilacher, A. (Eds.), Cycles and Events in Stratigraphy. Springer-Verlag, Berlin, 709–721.

Strasser, A., Pittet, B., Hillgartner, H., Pasquier, J.-B., 1999. Depositional sequences in shallow carbonate-dominated sedimentary systems : concepts for a high-resolution analysis. Sedimentary Geology 128, 201–221.

Sturzenegger, M., Stead, D., 2009. Quantifying discontinuity orientation and persistence on high mountain rock slopes and large landslides using terrestrial remote sensing techniques. Natural Hazards and Earth System Science 9, 267–287. https://doi.org/10.5194/nhess-9-267-2009

Szeliski, R., 2010. Computer Vision : Algorithms and Applications. Springer-Verlag, London. https://doi.org/10.1007/978-1-84882-935-0

Tavani, S., Arbues, P., Snidero, M., Carrera, N., Muñoz, J.A., 2011. Open Plot Project: An open-source toolkit for 3-D structural data analysis. Solid Earth 2, 53–63. https://doi.org/10.5194/se-2-53-2011

Tavani, S., Corradetti, A., Billi, A., 2016a. High precision analysis of an embryonic extensional fault-related fold using 3D orthorectified virtual outcrops: The viewpoint importance in structural geology. Journal of Structural Geology 86, 200–210. https://doi.org/10.1016/j.jsg.2016.03.009

Tavani, S., Granado, P., Corradetti, A., Girundo, M., Iannace, A., Arbués, P., 2014. Building a virtual outcrop, extracting geological information from it, and sharing the results in Google Earth via OpenPlot and Photoscan: An example from the Khaviz Anticline (Iran). Computers and Geosciences 63, 44–53. https://doi.org/10.1016/j.cageo.2013.10.013

Tavani, S., Iannace, A., Mazzoli, S., Vitale, S., Parente, M., 2013. Late Cretaceous extensional tectonics in Adria: Insights from soft-sediment deformation in the Sorrento Peninsula (southern Apennines). Journal of Geodynamics 68, 49–59. https://doi.org/10.1016/j.jog.2013.03.005

Tavani, S., Vitale, S., Grifa, C., Iannace, A., Parente, M., Mazzoli, S., 2016b. Introducing dolomite seams : hybrid compaction – solution bands in dolomitic limestones. Terra Nova

1–7. https://doi.org/10.1111/ter.12210

Terzaghi, R.D., 1965. Sources of Error in Joint Surveys. Géotechnique 15, 287–304. https://doi.org/10.1680/geot.1965.15.3.287

Thiele, S.T., Micklethwaite, S., Bourke, P., Verrall, M., Kovesi, P., 2015. Insights into the mechanics of en-échelon sigmoidal vein formation using ultra-high resolution photogrammetry and computed tomography. Journal of Structural Geology 77, 27–44. https://doi.org/10.1016/j.jsg.2015.05.006

Ullman, S., 1979. The interpretation of structure from motion. Proceedings of the Royal Society of London. Series B, Containing Papers of a Biological Character. 203, 405–426. https://doi.org/10.1098/rspb.1979.0006

Underwood, C.A., Cooke, M.L., Simo, J.A., Muldoon, M.A., 2003. Stratigraphic controls on vertical fracture patterns in Silurian dolomite, northeastern Wisconsin. AAPG Bulletin 87, 121–142.

Vail, P.R., 1987. Seismic Stratigraphy Interpretation Using Sequence Stratigraphy: Part 1: Seismic Stratigraphy Interpretation Procedure. In: Bally, A.W. (Ed.), Atlas of Seismic Stratigraphy. AAPG Studies in Geology #27, 1–10. https://doi.org/-

Vail, P.R., Audemard, F., Bowman, S.A., Eisner, P.N., Perez-Cruz, C., 1991. The stratigraphic signatures of tectonics, eustasy and sedimentology - an overview. In: Einsele, G., Ricken, W., Seilacher, A. (Eds.), Cycles and Events in Stratigraphy. Springer-Verlag, 617–659.

Van Wagoner, J., Posamentier, H.W., Mitchum, R.M., Vail, P.R., Sarg, J.F., Loutit, T.S., Hardenbol, J., 1988. An overview of the fundamentals of sequence stratigraphy and key definitions. In: Wilgus, C.K., Hastings, B.S., Kendall, C.G.S.C., Posamentier, H.W., Ross, C.A., Van Wagoner, J.C. (Eds.), Sea-Level Changes. An Integrated Approach. Society of Economic Paleontologists and Mineralogists, Special Publications, vol 42, 39–45. https://doi.org/10.2110/pec.88.01.0039

Vasuki, Y., Holden, E.J., Kovesi, P., Micklethwaite, S., 2014. Semi-automatic mapping of geological Structures using UAV-based photogrammetric data: An image analysis approach. Computers and Geosciences 69, 22–32. https://doi.org/10.1016/j.cageo.2014.04.012

Vinci, F., 2015. Analisi di facies e diagenesi di una successione carbonatica del Cretacico Inferiore - Monti Lattari. MS Thesis - Università degli Studi di Napoli Federico II.

Vinci, F., Iannace, A., Parente, M., Pirmez, C., Torrieri, S., Giorgioni, M., 2017. Early dolomitization in the Lower Cretaceous shallow-water carbonates of Southern Apennines (Italy): Clues about palaeoclimatic fluctuations in western Tethys. Sedimentary Geology 362, 17–36. https://doi.org/10.1016/j.sedgeo.2017.10.007

Vitale, S., Amore, O.F., Ciarcia, S., Fedele, L., Grifa, C., Prinzi, E.P., Tavani, S., Tramparulo, F.D., 2017. Structural, stratigraphic, and petrological clues for a Cretaceous–Paleogene abortive rift in the southern Adria domain (southern Apennines, Italy). Geological Journal 53, 660–681. https://doi.org/10.1002/gj.2919

Vitale, S., Ciarcia, S., 2013. Tectono-stratigraphic and kinematic evolution of the southern Apennines/Calabria–Peloritani Terrane system (Italy). Tectonophysics 583, 164–182.

https://doi.org/10.1016/j.tecto.2012.11.004

Vitale, S., Ciarcia, S., Mazzoli, S., Zaghloul, M.N., 2011. Tectonic evolution of the 'Liguride' accretionary wedge in the Cilento area, southern Italy: A record of early Apennine geodynamics. Journal of Geodynamics 51, 25–36. https://doi.org/10.1016/j.jog.2010.06.002

Vitale, S., Dati, F., Mazzoli, S., Ciarcia, S., Guerriero, V., Iannace, A., 2012. Modes and timing of fracture network development in poly-deformed carbonate reservoir analogues , Mt . Chianello , southern Italy. Journal of Structural Geology 37, 223–235. https://doi.org/10.1016/j.jsg.2012.01.005

Volatili, T., Zambrano, M., Cilona, A., Huisman, B.A.H., Rustichelli, A., Giorgioni, M., Vittori, S., Tondi, E., 2019. From fracture analysis to flow simulations in fractured carbonates: The case study of the Roman Valley Quarry (Majella Mountain, Italy). Marine and Petroleum Geology 100, 95–110. https://doi.org/10.1016/j.marpetgeo.2018.10.040

Vollgger, S.A., Cruden, A.R., 2016. Mapping folds and fractures in basement and cover rocks using UAV photogrammetry, Cape Liptrap and Cape Paterson, Victoria, Australia. Journal of Structural Geology 85, 168–187. https://doi.org/10.1016/j.jsg.2016.02.012

Warren, J., 2000. Dolomite: Occurence, evolution and economically important associations. Earth Science Reviews 52, 1–81. https://doi.org/10.1016/S0012-8252(00)00022-2

Wennberg, O.P., Casini, G., Jonoud, S., Peacock, D.C.P., 2016. The characteristics of open fractures in carbonate reservoirs and their impact on fluid flow: a discussion. Petroleum Geoscience 22, 91–104. https://doi.org/10.1144/petgeo2015-003

Wennberg, O.P., Svana, T., Azizzadeh, M., Aqrawi, A.M.M., Brockbank, P., Lyslo, K.B., Ogilvie, S., 2006. Fracture intensity vs. mechanical stratigraphy in platform top carbonates: the Aquitanian of the Asmari Formation, Khaviz Anticline, Zagros, SW Iran., Petroleum Geoscience. https://doi.org/10.1144/1354-079305-675

Westoby, M.J., Brasington, J., Glasser, N.F., Hambrey, M.J., Reynolds, J.M., 2012. "Structure-from-Motion" photogrammetry: A low-cost, effective tool for geoscience applications. Geomorphology 179, 300–314. https://doi.org/10.1016/j.geomorph.2012.08.021

Wilkinson, M.W., Jones, R.R., Woods, C.E., Gilment, S.R., McCaffrey, K.J.W., Kokkalas, S., Long, J.J., 2016. A comparison of terrestrial laser scanning and structure-frommotion photogrammetry as methods for digital outcrop acquisition. Geosphere 12, 1865–1880. https://doi.org/10.1130/GES01342.1

Wu, H., Pollard, D., 1995. An experimental study of the relationship between joint spacing and layer thickness. Journal of Structural Geology 17, 887–905. https://doi.org/10.1016/0191-8141(94)00099-L

Zahm, C.K., Zahm, L.C., Bellian, J. a., 2010. Integrated fracture prediction using sequence stratigraphy within a carbonate fault damage zone, Texas, USA. Journal of Structural Geology 32, 1363–1374. https://doi.org/10.1016/j.jsg.2009.05.012

Zambrano, M., Tondi, E., Korneva, I., Panza, E., Agosta, F., Janiseck, J.M., Giorgioni, M., 2016. Fracture properties analysis and discrete fracture network modelling of faulted tight limestones, Murge Plateau, Italy. Italian Journal of Geosciences 135, 55–67.

https://doi.org/10.3301/IJG.2014.42

Zappaterra, E., 1994. Source-rock distribution model of the Periadriatic region. AAPG Bulletin 78, 333–354.

Zeeb, C., Gomez-Rivas, E., Bons, P.D., Virgo, S., Blum, P., 2013. Fracture network evaluation program (FraNEP): A software for analyzing 2D fracture trace-line maps. Computers and Geosciences 60, 11–22. https://doi.org/10.1016/j.cageo.2013.04.027